UNIVERSITY OF CALIFORNIA SAN DIEGO

Regulation and Function of SALL1 in Mouse Microglia

A dissertation submitted in partial satisfaction of the
requirements for the degree Doctor of Philosophy

in

Biomedical Sciences

by

Bethany Rose Fixsen

Committee in Charge:

Professor Christopher K. Glass, Chair
Professor Christian Achim
Professor Nicole Coufal
Professor Emma Farley
Professor Anjana Rao
Professor Bing Ren

2022

The dissertation of Bethany Rose Fixsen is approved, and it is acceptable in quality and form for publication on microfilm and electronically.

University of California San Diego

2022

DEDICATION

This work is dedicated to my family.

EPIGRAPH

“Eventually, all things merge into one, and a river runs through it.”

Normal Maclean, *A River Runs Through It*

TABLE OF CONTENTS

LIST OF ABBREVIATIONS

TRM	Tissue-resident macrophage
CNS	Central nervous system
YS	Yolk Sac
EMP	Erythromyeloid Progenitor
TF	Transcription factor
TGF-beta	Tumor growth factor beta
HSC	Hematopoietic stem cell
RNA-seq	RNA-sequencing
H3K27ac	Histone 3 Lysine 27 acetylation
LDTF	Lineage determining transcription factor
SDTF	Signal dependent transcription factor
SE	Super-enhancer
ChIP-seq	Chromatin immunoprecipitation followed by sequencing
iPSC	Induced pluripotent stem cell
LPS	Lipopolysaccharide
AD	Alzheimer's disease
GWAS	Genome wide association study
SNP	Single nucleotide polymorphism
LAM	Lipid-accumulating microglia
SALL1	Spalt-like transcription factor 1
TBS	Townes-Brocks Syndrome
ESC	Embryonic stem cell
EKO	Enhancer knockout

LIST OF FIGURES

ACKNOWLEDGEMENTS

I would like to acknowledge Professor Christopher K. Glass for his mentorship over the last five years, for the engaging scientific discussions, and for giving me the opportunity to work creatively and independently during my graduate years.

I would also like to thank my first undergraduate mentors, Dr. Leslie Kay and Dr. Donald Frederick for giving me a chance to begin my research career at UChicago. I am incredibly grateful for the mentorship of Dr. Anne Sperling and Dr. Jesse Williams during my last two years at UChicago and for their support as I moved on to postbaccalaureate research and graduate school. Many thanks go to Dr. John Tsang, Dr. Andrew Martins and Cindi Pfannkoch at the NIAID Lab of Systems Biology; you sparked my interest in genomics and macrophages, which led me to my current studies as a graduate student.

A special thank you goes to the members of the Glass Lab I have been fortunate to call my colleagues and friends; with your support, my scientific and personal growth was greatly bolstered over the last five years. I'd first like to thank Mashito Sakai, whose thoughtful input and patience was key to the success of my project. Claudia Han and Alexi Nott were instrumental in helping me learn bread and butter protocols, planning experiments, and talking me through times both bad and good. My eternal thanks go to Martina Pasillas for her expertise and support during countless hours of sorting nuclei and live cells. Isidoro Cobo provided kind friendship and a critical eye during the formative stages of my manuscript writing and the final years of my PhD studies. I am also grateful for the companionship and insights of my MSTP colleague, Hunter Bennett. Lindsay Milich and Chris Balak were incredible colleagues and excellent friends during the short time that we overlapped. I will never forget the other members

of the Glass Lab (past and present) who made my PhD an amazing experience: Leslie Van Ael, Yohei Abe, Ty Troutman, Thomas Prohaska, Christian Nickl, Yi Zhou, Nathan Spann, Jana Collier, Marten Hoeksema, Sydney O'Brien, Johannes Schlachetzki, and Enchen Zhou.

Finally, I would like to give thanks to my non-scientific family and friends for their undying support throughout my training. Thank you to my mom and dad, Molly and Paul Fixsen, for providing unconditional love and unwavering belief in my abilities throughout my formative years and during the long years of my graduate studies. Thank you to my sister, Anna, and my brother, Joseph, for being amazing siblings—I couldn't have asked for a better family. Many thanks go to my Irish dance and Highland dance family; it has been an honor to learn from and dance with the best for the last eight years.

My graduate research was made possible in part by funding from the following grant: F30AG062159-01.

Chapter 2, in full, is a reprint of material submitted for publication as: Fixsen, Bethany R.; Sakai, Mashito; Zhou, Yi; Han, Claudia Z.; Cobo, Isidoro; Holtman, Inge R.; Warden, Anna S.; Ramirez, Gabriela; Collier, Jana G.; Pasillas, Martina P.; Shen, Zeyang; Yu, Miao; Hu, Rong; Li, Bin; Belhocine, Sarah; Gosselin, David; Coufal, Nicole G.; Ren, Bing; Glass, Christopher K. "SALL1 enforces microglia-specific DNA binding and function of SMADs to establish microglia identity". The dissertation author was one of the primary investigators and authors of this paper.

VITA

Education

2022 Ph.D., Biomedical Sciences	University of California San Diego
2013 B.A., Biological Sciences	University of Chicago

Publications

Nott A, Schlachetzki JCM, Fixsen BR, Glass CK. Nuclei isolation of multiple brain cell types for omics interrogation. Nature Protoc. 2021 Mar; 16(3):1629-1646. doi: 10.1038/s41596-020-00472-3

Han, CZ, Li RZ, Hansen E, Bennett H, Poirion O, Buchanan J, Challacombe JF, Fixsen BR, Trescott S, Schlachetzki JCM, Preissl S, Wang A, O'Connor C, Warden AS, Shriram S, Kim R, Nguyen CT, Schafer D, Ramirez G, Anavim SA, Johnson A, Sajti E, Gupta M, Levy ML, Ben-Haim S, Gonda DD, Laurent L, Glass CK, Coufal NG. Gene regulatorynetworks underlying human microglia maturation. bioRxiv. (2021). doi:10.1101/2021.06.02.446636.

Fong SH, Carlin DE Ozturk K; 2018 UCSD Network Biology Class, Ideker T. Strategies for Network GWAS Evaluated Using Classroom Crowd Science. Cell Syst. 2019 April 24; 8(4):275-280. doi: 10.1016/j.cels.2019.03.013.

Martins AJ, Narayanan M, Prüstel T, Fixsen B, Park K, Gottschalk RA, Lu Y, Andrews-Pfannkoch C, Lau WW, Wendelsdorf KV, Tsang JS. Environment Tunes Propagation of Cell-toCell Variation in the Human Macrophage Gene Network. Cell Syst. 2017 Apr 26;4(4):379-392.e12. ` doi:10.1016/j.cels.2017.03.002.

Williams JW, Tjota MY, Clay BS, Vander Lugt B, Bandukwala HS, Hrusch CL, Decker DC, Blaine KM, Fixsen BR, Singh H, Sciammas R, Sperling AI. Transcription factor IRF4 drives dendritic cells to promote Th2 differentiation. Nat Commun. 2013;4:2990. doi: 10.1038/ncomms3990.

Frederick DE, Brown A, Tacopina S, Mehta N, Vujovic M, Brim E, Amina T, Fixsen B, Kay LM. Task-Dependent Behavioral Dynamics Make the Case for Temporal Integration in Multiple Strategies during Odor Processing. J Neurosci. 2017 Apr 19;37(16):4416-4426. doi: 10.1523/JNEUROSCI.1797-16.2017.

Conference Presentations

Keystone: NeuroImmune Interactions in Health and Disease, First Author Poster (2021)

UCSD MSTP Research Symposium, First Author Poster (2019)
Gordon Research Conference: Neuroimmune Communications in Health and Disease, First Author Poster (2019)
NIH Postbaccalaureate Poster Day, First Author Poster (2014, 2015)
Autumn Immunology Conference, First Author Poster (2013)

Oral Presentations

Nebraska Wesleyan University, Tri-Beta MSTP Pathway Information Session (2020)
UCSD MSTP Journal Club Speaker (2020,2021)
UCSD Biomedical Sciences Immunology Track Interest Group (2020,2021)
Texas A&M HLTH 335 Human Diseases Guest Speaker (2020,2021)
Broad Institute Cell Circuits and Epigenetics Seminar Guest Speaker (2021)
UCSD Biomedical Sciences Lunch Talk (2022)
UCSD BSSA Career talk “What I wish I had done” (2022)
UCSD BMS Annual Spring Retreat Invited Speaker (2022)

Awards

NIH Postbaccalaureate Fellowship Award (2013-15)
Best Honors Thesis Award: Biological Sciences Collegiate Division (2013)
Shirley J. Ilagan Odyssey Scholarship Award (2010-13)
Biological Sciences Collegiate Division Fellowship Award (2012)
University of Chicago Dean’s List (2009-13)
William C. and Corinne J. Dietrich Scholarship Award (2009)
Le Sueur-Henderson High School Valedictorian (2009)

Research Experience

Ph.D. Candidate (2017-present)
Advisor: Christopher K. Glass, M.D. Ph.D., Department of Cellular and Molecular Medicine, University of California San Diego

Post-Baccalaureate Researcher (2013-2015)
Supervisor: John Tsang, Ph.D., Laboratory of Systems Biology, National Institute of Allergy and Infectious Diseases, National Institutes of Health

Undergraduate Researcher (2011-2013)
Supervisor: Anne I. Sperling, Ph.D., Department of Pulmonary Medicine, University of Chicago

Undergraduate Researcher (2011)
Supervisor: Leslie M. Kay, Ph.D., Department of Psychology, University of Chicago

Volunteering Experience

UCSD School of Medicine Student-Run Free Clinic (2015-2017)
UCSD SOM Student-Run Free Clinic: Pulmonology Clinic Manager (2016-2017)
UCSD SOM Student-Run Free Clinic: Rheumatology Clinic Manager (2016-2017)
UCSD SOM Body Donor Memorial Committee (2016)
Microbiology Course Representative (2016)
Arthritis, Rheumatology, and Dermatology Course Representative (2016)
Mentor for UCSD Pre-medical Students (2016-Present)
UCSD MSTP Admissions: Interviewer, Application Screener, Grad School Fair Representative (2018-Present)
UCSD MSTP Women's Advocacy Group (2018-Present)
Del Lago Academy eMentor Program (2018-2019)
UCSD Summer Undergraduate Research Fellowship: Graduate Student Representative (2020-2021)
UCSD Covid19 Vaccination Super Station: Volunteer Vaccinator and Scribe (2021)

Fields of Study

Major Field: Biomedical Sciences

Studies in Genomics and Neuroimmune System
Professor Christopher K. Glass

ABSTRACT OF THE DISSERTATION

Regulation and Function of SALL1 in Mouse Microglia

by

Bethany Rose Fixsen

Doctor of Philosophy in Biomedical Sciences

University of California San Diego, 2022

Professor Christopher K. Glass

Spalt-Like Transcription Factor 1 (*Sall1*) is a critical regulator of microglia identity. Despite its importance, the transcriptional function of SALL1 and mechanisms regulating its expression are not fully understood. Here, we demonstrate that *Sall1* is physically connected to a microglia-specific, environment-dependent super enhancer (SE) containing conserved binding sites for SMAD TFs downstream of TGF-beta signaling. Deletion of the SE in mice (EKO) led to selective loss of *Sall1* transcript and SALL1 protein in microglia, resulting in downregulation of microglial identity genes and activation of inflammation- and aging-associated genes. Using ChIP-seq, we defined binding sites of SALL1 and leveraged EKO mice to probe how SALL1 shapes the regulatory landscape of microglia. We found thousands of putative enhancers whose

activity was increased or abrogated by loss of SALL1; we further classified these enhancers as being ‘directly’ or ‘indirectly’ regulated by SALL1 based on overlap with SALL1 binding sites. Unexpectedly, motifs for SMADs are enriched within enhancers predicted to be directly activated by SALL1, suggesting that collaborative interactions between SALL1 and SMADs are required to establish microglia-specific gene expression. To test this hypothesis, we generated a conditional KO of the common co-SMAD *Smad4* and determined the binding sites of SMAD4 in WT and EKO microglia. These studies demonstrated that SMAD4 binds to the *Sall1* SE and controls *Sall1* expression, and that its ability to activate other major microglia genes is dependent on co-binding with SALL1. Collectively, these results suggest a molecular basis for many of the transcriptional characteristics of yolk sac-derived microglia.

Chapter 1: Background

1A. Discovery of Macrophages and Microglia

Tissue resident macrophages (TRMs) comprise a group of heterogeneous, multifunctional myeloid cells that dwell within almost every tissue of the body. Macrophages are most well-known as phagocytic immune sentinels that quickly mobilize to sites of injury/infection and mount inflammatory responses against invading pathogens [1]. However, it is now appreciated that TRMs exist in equilibrium with their surrounding tissue microenvironment, playing vital roles as mediators of tissue development and repair, and that dysregulation of these processes may lead to the development or progression of a variety of diseases [2-6].

Macrophages were first described by Elie Metchnikoff, a comparative embryologist, in the late 1800s [7, 8]. Through his work examining the structure and development of simple marine organisms, he observed a migratory mesoderm-derived cell subset which ingested extracellular dyes, nutrients, and bacteria, and mobilized to sites of injury. Metchnikoff hypothesized that these cells, which he named “phagocytes”, were playing a role in host response against bacterial infection. Eventually, he identified these cells in a variety of organisms, which laid the foundations for the study of innate immunity [7].

Santiago Ramón y Cajal, a Spanish contemporary of Metchnikoff, leveraged his expertise in art, microscopy, and histology to elucidate neural structures and cellular circuitry within the brain. Ramón y Cajal’s observations of cellular organization and morphology made a lasting impact on the field of neuroscience through his discovery that the nervous system is made up of independent, individual nerve cells [9]. These

studies also described a nebulous group of poorly staining, adendritic cells which he termed the “third element”; this subset of cells is now understood to be the glial cells of the central nervous system [10]. Pío del Río Hortega, another prominent Spanish neuroscientist, optimized silver staining methods to study this class of cells and resolved two distinct cell types, which he called microglia and oligodendroglia [11]. More than 100 years after Pío del Río Hortega ’s observations, microglia are now known as the main tissue resident macrophage population of the central nervous system (CNS).

1B. Microglia Function at Steady State

Under homeostatic conditions, microglia, like other TRMs, dynamically interact with neighboring cells and survey the tissue micro-environment, allowing for rapid activation and mobilization of microglia to sites of injury or inflammation [12-14]. The ability of microglia to phagocytose a variety of materials plays a critical role in brain development and maintenance of brain homeostasis. For example, microglia utilize complement proteins to prune synapses via phagocytosis in the developing and postnatal mouse brain, allowing for the formation and maintenance of proper neural circuitry [15-17]. Microglia also phagocytose neural progenitors and dead cells, promote myelination, and secrete trophic factors guiding cellular genesis and maintenance [18-21]. Overall, microglial functions are essential for promoting brain development and health; perturbation of these processes has the potential to lead to brain pathology and dysfunction [22].

1C. Microglia in Disease

For many years, macrophage polarization was broadly characterized as a binary response including 1) inflammatory “classical” activation associated with stimuli such as lipopolysaccharide (LPS) or interferon gamma (IFN-y) or 2) “alternative” activation associated with resolution of inflammation after stimulation with the cytokines interleukin (IL)-4 and IL-13 [23-25]. However, it is now understood that macrophage activation states exist along a phenotypic spectrum associated with distinct transcriptional profiles [3, 26].

Microglia assume a wide variety of phenotypes when faced with environmental perturbations or inflammatory challenges. Several lines of evidence point towards microglial dysfunction as a factor underlying the development and progression of neurodegenerative, neurodevelopmental, and psychiatric conditions [27]. For example, in Alzheimer’s disease (AD), microglia can secrete inflammatory factors that are harmful to neurons, promote the loss of synapses, and contribute to tau pathology [28-30]. The pathophysiology of brain-related disorders is thought to be controlled by a combination of genetic and environmental influences. Genome wide association studies (GWAS) have uncovered many single nucleotide polymorphisms (SNPs) associated with neurological and psychiatric disorders; the precise contribution of these SNPs to disease have not been completely elucidated. Interestingly, many of these GWAS hits are localized to gene regulatory regions [31]. Studies of the microglial transcriptome and epigenome have revealed that a high proportion of expressed genes and active gene regulatory elements associated with disease risk loci are enriched in microglia compared to other brain cell types [32-36], further strengthening the link between microglia and brain-related diseases.

Altered microglial transcriptomes have been identified in several mouse models. Recent work identified a subset of microglia known as disease-associated microglia (DAMs) in mouse models of neurodegeneration and demyelination [37-39]. These microglia are defined by expression of *Triggering Receptor Expressed on Myeloid Cells 2* (*Trem2), Cd9, Apolipoprotein E (Apoe*), *Cystatin F* (*Cst7),* and *Secreted Phosphoprotein 1* (*Spp1)*. It is still unclear whether this microglia subset is causal for disease, promotes disease pathogenesis, or performs neuroprotective functions. Microglial transcriptomes even shift during non-pathogenic conditions, such as during aging. Throughout aging, microglia gene signatures begin changing, and the appearance of lipid droplet accumulating microglia (LDAM) is associated with the onset of inflammation in the hippocampus in the absence of other disease conditions [40, 41].

The involvement of microglia in brain-related diseases is beginning to be uncovered, but the precise transcriptional and environmental mechanisms controlling these interactions remain to be described. Development of disease modifying therapies will be contingent upon our understanding of whether microglia cause, exacerbate, or prevent disease.

1D. Microglia Developmental Origins

As the largest TRM population of the CNS, microglia comprise 5-10% of the adult CNS cell population and are localized throughout the entire brain [42]. Recent studies have begun to elucidate the origins and dynamics of microglia development, a key step in further understanding the role of microglia in both homeostatic and disease states. During embryonic development, two major sources of hematopoiesis contribute to the

pool of early myeloid progenitors that seed primitive tissues. These hematopoietic sites include the embryonic yolk sac (YS), starting with primitive hematopoiesis at embryonic day (E)7.5 and the production of erythromyeloid precursors (EMPs) at ~E8, followed by the fetal liver, starting at E11 [43, 44]. Microglia progenitors arise from YS EMPs [45] and migrate to the brain upon establishment of the circulatory system at ~E9.5 [43]. Microglial progenitors become distinct from their CNS-resident myeloid counterparts, border associated macrophages, in the YS prior to migration into the brain [46].

Several proteins are critical for both the development and survival for early microglia. The transcription factors (TFs) PU.1 and IRF8 are necessary for the development of microglia; lack of these TFs leads to a loss of EMPs in the yolk sac and the brain [47]. External signals, such as tumor growth factor beta (TGFβ), interleukin-34 (IL-34) and CSF1 are critical for microglia development and maintenance [48-50]; the receptors for these signals, TGFBR2 and CSF1R are highly expressed on microglia and are necessary for microglia development and survival [46, 51].

After taking up residence in the embryonic brain, microglial precursors begin to express genes associated with mature microglia and proliferate to fill the brain niche [43, 45, 52]. A remaining question was whether embryonic and adult microglia arise from different sources. Various studies have shown that fetal EMPs contribute to TRM populations throughout the body, and that several of these populations, such as heart-, pancreatic-, gut,- and dermis-resident macrophages are replaced over time with hematopoietic stem cells (HSCs) under steady-state conditions [4]. Interestingly, lineage tracing studies revealed that YS-derived microglia persist in the adult brain, indicating

that a contribution from peripherally derived HSCs to the microglia population is unlikely at steady-state [53-56].

Additional work has shown that microglia are also capable of rapidly self-renewing to fill their surrounding niche. When 99% of microglia are depleted pharmacologically, subsequent repopulation of the CNS is achieved by the ~1% of remaining microglia and not via a contribution from the periphery [57]. This quorum sensing and subsequent self-renewal appears to be unique to microglia compared to other TRM populations; however, the mechanisms governing these aspects of microglial biology remain to be elucidated.

1E. Transcriptional Regulation of Microglia Identity

TRMs have highly plastic phenotypes depending on their tissue environment and embryonic origin; this diversity is reflected in the transcriptional profile of each TRM population captured by RNA-sequencing (RNA-seq) [58-60]. Studies examining the transcriptional profile of microglia have defined a set of key genes expressed highly in microglia compared to other TRMs, such as the zinc finger protein *Spalt Like Transcription Factor 1* (*Sall1), Purinergic Receptor P2Y12* (*P2ry12), Transmembrane Protein 119 (Tmem119), Crystallin Beta B1 (Crybb1), Selectin P Ligand (Selplg),* and *Solute Carrier Family 2 Member 5 (Slc2a5)* [58, 61]. The expression of cellular identity genes is orchestrated through the selection of cell-type specific enhancers by transcription factors and environment and ontogeny-derived signals.

While the precise combination of environment- and ontogeny-derived signals guiding microglia identity are not fully understood, analysis of DNA regulatory elements

and their sequences has allowed for the identification of regulatory proteins and signaling pathways influencing microglia phenotype and function. Promoters, sequences of DNA that are typically immediately adjacent to a gene, provide the necessary transcriptional start site (TSS) needed for the induction of messenger RNA (mRNA) synthesis. Gene expression levels are fine-tuned throughout cellular differentiation, development, and homeostasis by the activity of distal regulatory elements called enhancers, which loop over long genomic intervals to target genes; enhancers can be defined by distinct histone modification patterns such as Histone 3 Lysine 27 acetylation (H3K27ac) [62]. While the mammalian genome contains a multitude of DNA sequences that can potentially function as enhancers [63], each cell type utilizes only several thousand of these regions to ensure robust, accurate, cell-type specific gene expression [64]. Enhancer selection is achieved through a hierarchy of transcriptional regulators, beginning with lineage determining factors (LDTFs). TRMs rely on many of the same LDTFs, such as ETS family protein PU.1 [65] , the CCAAT enhancer binding protein (CEBP) [66] and Runt-related Transcription Factor 1 (RUNX1) [67], to establish key macrophage enhancer regions through their ability to bind to and remodel regions of inactive chromatin [64, 68]. Local activation signals in the microenvironment induce signal-dependent TFs (SDTFs) to bind these primed enhancers, resulting in changes in gene expression that are cell- and environment-specific. [64, 68]. Further, super-enhancers (SEs), which are dense regions of enhancers marked by an abundance of H3K27ac modifications, are particularly important in controlling genes associated with cell identity and development; these regions contain binding sites for TFs important for cell identity and response to environmental signals [69,

[70]. Comparison of chromatin immunoprecipitation followed by sequencing (ChIP-seq) data for histone modifications associated with regulatory elements showed that microglia share many enhancers with other TRMs; however, approximately 20% of the enhancers studied were unique to microglia and associated with microglia-specific gene expression [58, 59].

When microglia are removed from the brain and plated *in vitro,* the chromatin landscape at key gene regulatory elements is quickly remodeled and key microglial genes, such as *Sall1, Tmem119,* and *P2ry12,* are no longer expressed [59, 61]. Analysis of the environment-dependent enhancer landscape revealed an enrichment for sequence-specific TF binding sites including the interferon regulatory factor family, MEF2C [59, 61], and SMADs, the latter which are thought to be downstream of TGF-beta signaling in microglia [71]. TGF-beta expression in the CNS and expression of its receptor on microglia is critical for the development of microglia and the expression of key microglia genes, in addition the maintenance of a quiescent microglia phenotype [46, 50, 72, 73]. Lack of *Irf8* or *Mef2c* in microglia also leads to the disturbance of microglial gene expression and an activated microglial phenotype [74, 75].

While these factors are likely involved in shaping microglia identity, the full set of signals guiding microglia phenotypes is not fully known. For example, the altered gene expression and chromatin landscape observed in *in vitro* microglia is not rescued by treatment with recombinant cytokines such as TGFβ and IL-34 [46, 61]. Attempts to induce a fully microglia-like gene signature *in vitro* using human induced pluripotent stem cells (iPSCs) have failed thus far [76]; however, transplant of iPSCs into genetically modified mice has successfully induced the expression of key microglial genes such as SALL1 [77],

further cementing the importance of additional brain environment-derived signals in shaping microglia transcriptional identity.

In addition to requiring environment-derived signals, expression of the microglia gene expression signature is partially dependent on ontogeny. When peripheral hematopoietic progenitors are transplanted into mice with an empty CNS niche, whether due to irradiation or genetic depletion of microglia, the cells engraft long-term, assume microglia-like morphology, and express a subset of genes associated with microglia identity. However, these engrafted cells fail to become completely like yolk-sac derived microglia and do not upregulate one of the key microglial transcription factors, *Sall1* [78-80]. This indicates that while tissue environmental signals are key for induction of a microglia phenotype, other aspects such as ontogeny are critical for mediating microglia identity, likely through the formation of an initially permissive chromatin landscape; microglia gene expression is likely established by a combination of ontogeny-determined and environment-dependent transcriptional networks. A thorough understanding of these transcriptional networks and gene regulatory mechanisms we will allow us to better predict and modify the function of microglia in disease.

1F. Roles of SALL1 in Transcriptional Regulation

Spalt-Like Transcription Factor 1 (SALL1) has emerged as a candidate TF that promotes microglia identity and function at steady state [58, 61, 72, 81]. This protein is a conserved C2H2 zinc finger transcription factor (TF) and is one of four closely related Spalt-Like proteins expressed in mammals. *Spalt,* the *Drosophila* homolog of *SALL1*, was originally described as a Tumor Growth Factor Beta (TGFβ)-responsive homeotic

gene responsible for proper embryonic head, wing, and tail development [82, 83]. In humans, heterozygous mutations in *SALL1* resulting in a putative truncated protein were identified as causative for an autosomal dominant syndrome called Townes-Brocks Syndrome (TBS), a disorder with heterogeneous clinical presentation typically characterized by imperforate anus, pre-axial polydactyly, triphalangeal thumbs, external ear malformations, and sensorineural hearing loss, urogenital malformations, cardiac malformations, and neurodevelopmental abnormalities [84-94]. TBS is also known to be associated with urogenital malformations, cardiac malformations, and neurodevelopmental abnormalities. In line with the heterogeneity of clinical presentations for TBS, dozens of *SALL1* mutations have been identified in patients with TBS, ranging from large deletions encompassing the *SALL1* gene and surrounding regulatory regions to small indels resulting in a putatively truncated protein [88]. It has been proposed that truncated SALL1 results in gain of function and interference with the normal copy of SALL1 and other SALL family members, and that milder cases of TBS may be caused by a dosage effect of heterozygous loss of *SALL1* [87, 88].

Studies of embryonic development have shed light on the transcriptional roles of SALL1. Proper expression of SALL1 is critical for development of organ systems including the kidney. Mice lacking *Sall1* do not phenocopy TBS, rather, these *Sall1* null mice die shortly after birth due to renal agenesis [95]. Further work established that SALL1 is critical for formation of the metanephros [96, 97] and that it appears to be playing a role as both an activator of stemness-related genes and a repressor of genes related to terminal differentiation in nephron progenitors [98, 99]. Similar results were observed in embryonic stem cells (ESCs), where SALL1 was noted to collaborate with the stem cell

factor NANOG to promote expression of genes related to pluripotency and self-renewal [100, 101].

Several studies have focused on SALL1's role as a transcriptional repressor; a 'SALL1 repression motif' (SRM) located at the N-terminus of SALL1 was noted to associate with the NuRD histone remodeling complex, and SALL1 was found to repress gene expression in *in vitro* reporter assays [102-106],associate with heterochromatin, and directly bind AT-rich regions of DNA [99, 103, 107, 108]. It was proposed that SALL1 may be playing a role maintaining/forming heterochromatin, or as a nonclassical TF regulating higher order chromatin structure [103]. Prior work has also shown that phosphorylation of the SRM ablates SALL1's repressive activity, and SALL1 subnuclear localization is affected by sumoylation [102, 109, 110]. It is likely that context-dependent post-translational modifications of SALL1 mediate its role as a transcriptional repressor or activator.

Sall1 is more highly expressed in microglia than any other TRM [58]. While SALL1's function and regulation in microglia is not completely understood, various studies have pointed to its potential transcriptional roles and mechanisms of its regulation in microglia. Loss of *Sall1* in microglia resulted in the induction of an inflammatory gene expression program, downregulation of multiple key microglia genes, and changes in microglia morphology associated with cellular activation [72, 81], indicating that *Sall1* may be important for restraining an inflammatory phenotype in microglia. Studies of microglia development detected *Sall1* transcript shortly after microglial precursors enter the embryonic mouse brain, indicating that *Sall1* is induced by early signals in the brain [46, 52]. This concept was further reinforced by studies showing that early deletion of TGFβ in the CNS or its corresponding receptor, *Tgfbr2,* in microglia led

to ablation of *Sall1* expression, decreased expression of key microglial genes and increased expression of inflammation-related genes [46, 50]; the signaling cascade downstream of TGFβ is likely responsible for inducing and maintaining *Sall1* expression in microglia. When microglia are placed in culture, *Sall1* expression is completely lost and its surrounding chromatin landscape, including a putative super-enhancer, loses marks of active and open chromatin [59, 61]. However, whether this regulatory element has a functional role in controlling Sall1 expression is unknown. The change in epigenetic landscape corresponding with removal from the brain environment suggests that this regulatory region controls expression of Sall1 in response to external factors. A better understanding of *Sall1*'s regulation and its transcriptional role in microglia will be critical for gaining a more complete knowledge of microglial biology, both in health and disease.

Chapter 2: Regulation and Function of SALL1 in Mouse Microglia

2A. Abstract:

Spalt-Like Transcription Factor 1 (*Sall1*) is a critical regulator of organogenesis and microglia identity. Despite its known biological importance, mechanisms that specify the cell-specific expression of *Sall1* and its transcriptional functions remain poorly understood. Here, we demonstrate that targeted deletion of a conserved microglia-specific super enhancer interacting with the *Sall1* promoter results in complete and specific loss of *Sall1* expression in microglia. Microglia in *Sall1* enhancer knockout (EKO) mice exhibit more extensive downregulation of microglial identity genes and upregulation of genes associated with inflammation and aging than observed following conditional deletion of *Sall1* in microglia of adult mice. We defined genomic binding sites of SALL1 in microglia and leveraged EKO mice to probe how SALL1 shapes the regulatory landscape of microglia. From these studies, we identified thousands of putative enhancers whose activity was increased or abrogated by loss of SALL1; we further classified these enhancers as being 'directly' or 'indirectly' regulated by SALL1 based on overlap with SALL1 binding sites. Unexpectedly, motifs for SMAD proteins that mediate transcriptional effects of TGFβ signaling were enriched within the set of enhancers predicted to be directly activated by SALL1, suggesting that collaborative interactions between SALL1 and SMADs are required to establish microglia-specific gene expression. To test this hypothesis, we determined the transcriptional consequences of a conditional knockout of the common co-SMAD *Smad4* and defined the genome-wide locations of SMAD4 in wild type and EKO microglia. These studies revealed two layers of functional interdependence. First, we found that SMAD4 binds

directly to the *Sall1* super enhancer and is required for *Sall1* expression, suggesting an evolutionarily conserved relationship to the requirement of the TGFβ homologue *Dpp* for cell-specific expression of *Spalt* in the *Drosophila* wing. Second, we found that the ability of SMAD4 to bind to and activate a broad set of microglia-specific enhancers is dependent on co-binding with SALL1. Collectively, these results suggest molecular mechanisms by which SALL1 enforces microglia-specific functions of SMAD transcription factors that may be relevant to roles of SALL1 in other developmental contexts.

2B. Introduction:

Microglia, the major tissue resident macrophage (TRM) population of the central nervous system (CNS), are self-renewing, yolk-sac derived cells whose functions include regulation of brain development, maintenance of neural circuitry, and response to injury/infection [27]. Like other TRMs, microglia assume a spectrum of activation states and phenotypes in response to environmental signals and perturbations. In addition to their adaptive functions, numerous studies have implicated microglia as playing pathogenic roles in neurodevelopmental, psychiatric, and neurodegenerative diseases [111]. Unlike many populations of TRMs outside of the brain, microglia are not replaced by bone marrow derived macrophage precursors following birth under normal conditions.

Spalt-Like Transcription Factor 1(Sall1), a zinc-finger transcription factor, was recently identified through a loss of function study as a key transcriptional regulator of microglia identity and phenotype in the mouse [72, 81]. Members of the Spalt family of transcription factors are highly conserved in metazoan organisms and play diverse roles

in organ development. Heterozygous loss of function mutations of SALL1 in humans lead to Townes Brock syndrome, with features including dysplastic ears, preaxial polydactyly, imperforate anus and in some cases kidney and heart defects[93, 112] . *Sall1* deletion in mice results in perinatal lethality due to severe kidney defects [96]. At the molecular level, SALL1 has been proposed to function as a regulator of pericentric heterochromatin in embryonic stem cells through interactions with Nanog [100, 101]. *In vitro* studies have also provided evidence that SALL1 can function as both a transcriptional activator and a repressor [98, 103, 113], but the mechanisms that underly the diverse transcriptional and developmental phenotypes resulting from genetic loss of function of *Sall1* or *SALL1* in vivo are unknown.

In the mouse, *Sall1* expression is induced between embryonic days 11-12 in yolk sac derived hematopoietic progenitor cells (HPCs) that have entered the developing brain and are destined to become resident microglia [46, 52]. Expression of *Sall1* is dependent on TGFβ1 signaling, which is broadly required for microglia differentiation and survival [46, 114]. *Sall1* expression, in concert with many other microglia-specific genes, falls rapidly and dramatically when microglia are transferred from the brain to an *in vitro* environment, indicating a continuous requirement for brain environmental signals to maintain an *in vivo* microglia phenotype [59, 61]. The loss of *Sall1* expression *in vitro* can only be modestly rescued by TGFβ1 treatment, indicating essential roles of additional, unknown brain environmental factors[61]. Interestingly, human iPSC-derived HPCs that are engrafted into the brain turn on *Sall1* [77, 115, 116], whereas HSC-derived cells engrafting the mouse brain following injury or microglia depletion never gain expression of *Sall1* [78-80]. These findings indicate a qualitative, ontogeny-dependent

difference in how the *Sall1* locus responds to brain environmental signals, suggesting that *Sall1* is one of the critical determinants of the requirement for cells of yolk sac origin to subsequently acquire microglia identity.

Recent studies of mouse and human microglia identified clusters of putative microglia-specific enhancers located hundreds of kilobases upstream of the *Sall1/SALL1* promoters [32, 61]. In human microglia, Proximity Ligation Assisted ChIP-sequencing (PLAC-Seq) experiments demonstrated that these distant genomic regions form a close physical association with the *SALL1* promoter [32]. Furthermore, the activity states of these enhancers as inferred by H3K27ac, a histone modification associated with active enhancers and promoters [62], dramatically declined in concert with *Sall1/SALL1* mRNA levels when microglia were transferred from the brain to an in vitro environment[59, 61]. Collectively, these findings suggested that these genomic regions function to control *Sall1/SALL1* expression in response to brain environmental signals.

Here we show that *Sall1* expression in microglia is regulated by a microglia-specific enhancer, and that loss of this gene regulatory element results in a similar but more severe molecular phenotype than conditional knockout of *Sall1* in microglia in adult mice. We then define the genome-wide binding of SALL1 and leverage the enhancer knockout model to examine the transcriptional effects of SALL1, revealing that SALL1 is functioning as both an activator and a repressor in microglia. We provide evidence that signaling through SMAD4 maintains expression of *Sall1,* which in turn collaborates with SMAD4 at key gene regulatory elements associated with microglia identity and function.

2C. Results:

Sall1 expression in microglia is regulated by a cell type-specific super-enhancer

To identify regions of open and active chromatin that may be putative enhancers regulating *Sall1* transcription in microglia, we performed Assay for Transposase-Accessible Chromatin (ATAC-seq), chromatin immunoprecipitation (ChIP-seq) for Histone H3 Lysine 27 acetylation (H3K27ac), and ChIP-seq for p300, a transcriptional co-activator (Figure 2.1A). We located a region located approximately -300 kb from the *Sall1* promoter that was marked by a cluster of high levels of open chromatin, H3K27ac, and p300 that meets criteria described for super-enhancers (SEs), a class of regulatory elements known to control cell identity-defining genes (Figure 2.1A, yellow highlight; Supplement 2.1A) [69, 70, 117]. We performed Proximity Ligation Assisted ChIP-seq (PLAC-seq) using Histone H3 Lysine 4 trimethyl (H3K4me3) to detect interactions between active promoters and putative enhancers [32, 118], thereby allowing identification of target genes of enhancers and SEs. The SE proximal to *Sall1* loops solely to the *Sall1* gene (Figure 2.1A), similar to what is observed with the human microglia *SALL1* gene and its putative enhancer region [32]. Conservation of DNA sequences across species is often used to identify functional DNA-regulatory elements [119]; indeed, the open chromatin regions within the *Sall1* SE contain elements conserved across multiple vertebrate species (Figure 2.1A). Regions A and C of the *Sall1* SE contain sequences with ~75% homology to open chromatin regions in the human microglia *SALL1* SE (Supplement 2.1B). Region C from mouse microglia overlaps the most prominent region of open chromatin and the most robust binding site of the microglia lineage determining transcription factor (LDTF) PU.1 in the human *SALL1* SE (Supplement 2.1B). This site

also contains conserved TF binding motifs for SMADs, NR4A, PU.1, ETS, IRF, and RBPJ (Supplement 2.1B), suggesting that this region may be a point of convergence of multiple cellular signaling pathways that regulate *Sall1* expression. Since SALL1 is also known as a critical regulator of kidney development, we examined H3K27ac datasets from mouse embryonic day 15 and early postnatal kidney and found no overlap between the microglia SE and kidney H3K27ac signal (Supplement 2.1C).

To probe *in vivo* function of the *Sall1* SE in microglia, we utilized CRISPR/cas9-mediated deletion to generate mice with a homozygous knockout spanning 13 kB of the SE (EKO) (Figure 2.1A, blue highlight). The deletion was confirmed by Sanger sequencing (data not shown), sequencing of microglia input DNA, and polymerase chain reaction (PCR) (Supplement 2.1D). Unlike previously reported *Sall1* null mice [96], EKO mice survive after birth (Figure 2.1B) and through adulthood. Using RNA-sequencing (RNA-seq), we found that levels of *Sall1* transcript in microglia are affected in an enhancer-dosage dependent manner, with a 50% reduction of *Sall1* mRNA in heterozygous enhancer knockout mice (Het KO) and a complete loss of *Sall1* mRNA in EKO mice (Figure 2.1C). EKO led to complete loss of H3K27ac signal at the *Sall1* locus in microglia, while H3K27ac signal at *Sall1* in other brain cell types known to express *Sall1,* such as oligodendrocytes and neurons, was unaffected by the EKO (Figure 2.1D). Together, these results provide evidence that the effect of the enhancer deletion on the chromatin landscape is highly specific to microglia.

Immunofluorescence of SALL1 in whole mouse brain sections revealed that in WT brain, IBA1 positive microglia robustly express SALL1 in the nucleus; multiple bright puncta corresponding to SALL1 localize to regions of heterochromatin stained by DAPI

(Figure 2.1E), consistent with what has been described in other cell systems [103, 120]. In addition, a diffuse staining pattern is observed in the nucleus between regions that are intensely stained by DAPI. In contrast, brain sections of EKO mice do not exhibit either punctate or diffuse SALL1 staining in microglia nuclei (confirming antibody specificity) but do exhibit SALL1 staining in other brain cell types, consistent with marks of active promoter and enhancer regions in neurons and oligodendrocytes (Figure 2.1D). Microglia in EKO mice have notably decreased surface area, increased soma size, and decreased density in the cortex (Figure 2.1E, Supplementary Figure 2.1E). Similar changes in surface area and soma size were observed in prior studies of *Sall1* knockout microglia [72, 81], indicating that EKO microglia phenocopy morphological features of *Sall1* KO microglia. The loss of SALL1 was also confirmed by flow cytometry of brain nuclei stained with SALL1 and PU1 (Supplementary Figure 2.1F).

The complex staining pattern of SALL1 in microglia raised the question of whether it might play roles in genome organization, which has been proposed in past studies of SALL1 in other cell types [103, 107]. To better understand the consequences of the *Sall1* super enhancer deletion and loss of *Sall1* expression on three-dimensional chromatin architecture, we performed *in situ* high throughput chromatin conformation capture (Hi-C). In microglia isolated from wild type mice, the *Sall1* locus was highly inter-connected, forming a topological associated domain (TAD), consistent with the results of the PLAC-seq assay (Figure 2.1F). In contrast, these interactions were almost completely lost in EKO microglia, with the corresponding PC1 values at the *Sall1* locus shifting from positive values associated with euchromatin-containing “A” compartments (shaded black) to negative values associated with heterochromatin-containing “B”

compartments (shaded gray) (Figure 2.1F). These results indicate that the 13Kb region deleted from the *Sall1* super enhancer is essential for establishing the active regulatory features of this locus. However, despite the complete loss of *Sall1* expression, very few changes in chromatin connectivity or shifts in the PC1 component were observed at other loci. Of the nearly 104,000 PC1 values defined by these studies, only 406 are up (0.39%) and 219 down (0.21%) comparing EKO to WT microglia. In concert, these data provide evidence that expression of *Sall1* in microglia is regulated by a cell-specific super enhancer that is essential for the three-dimensional conformation of the *Sall1* locus and that SALL1 is not a global regulator of higher order chromatin structure in microglia.

Figure 2.1: *Sall1* expression is regulated by a microglia-specific super-enhancer
A. Genome browser tracks of ATAC-seq (sorted live cells), H3K27ac ChIP (sorted PU1+ nuclei) and p300 ChIP (sorted PU1+/SALL1+ nuclei), in addition to PLAC-seq signal at the *Sall1* locus. Green shading, *Sall1* gene. Yellow shading, *Sall1* super-enhancer. Labels A, B, and C denote the three main regions of open chromatin in the super-enhancer. Blue shading, region encompassing the *Sall1* super enhancer knockout.
B. Counts of WT, Het EKO, and EKO pups after weaning.
C. Barplots for expression of *Sall1* in WT, Het EKO, and EKO microglia. Data are from two or three experiments with n = 3 per group. The significance markers represent p-adj from DESeq2 comparing with WT. *p-adj < 0.05 and **p-adj <0.001. Error bars, SD.
D. Genome browser tracks of H3K27ac ChIP in EKO and WT brain nuclei at the *Sall1* locus. Microglia = PU1+ nuclei. Neurons = NeuN+ nuclei. Oligodendrocytes = Olig2+ nuclei. Green shading, *Sall1* gene. Yellow shading, *Sall1* SE.
E. Confocal image of WT and EKO brain showing DAPI, Iba1, and SALL1. White arrows denote location of SALL1 puncta in WT and lack of puncta in EKO.
F. Hi-C contact frequency map at the *Sall1* locus in WT and EKO microglia, normalized by coverage. PC1 values denote “A” euchromatin compartment (black) and “B” heterochromatin compartment (grey).

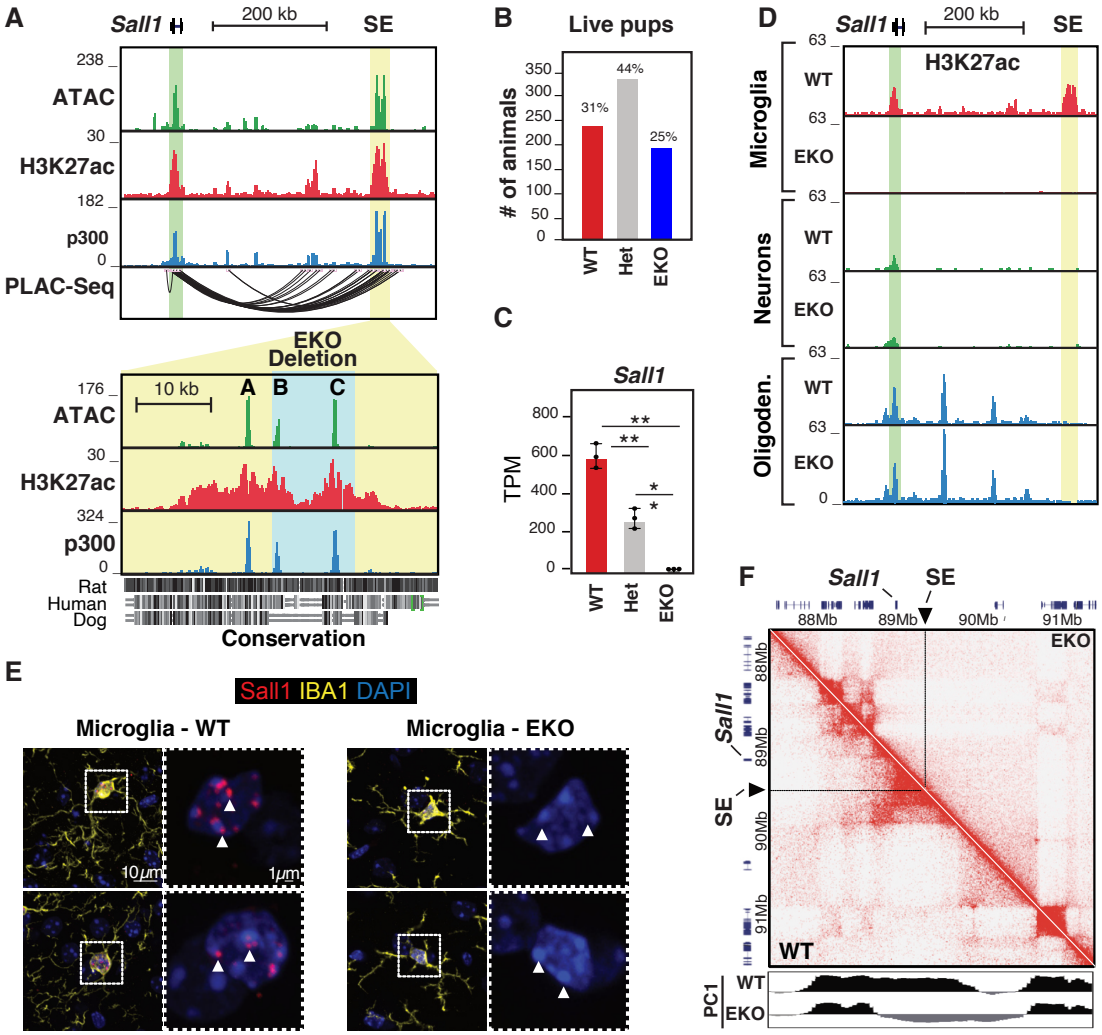
A
Sall1
200 kb
SE
ATAC
H3K27ac
p300
PLAC-Seq
EKO Deletion
10 kb
A
B
C
Rat
Human
Dog
Conservation
B
Live pups
# of animals
31%
44%
25%
WT
Het
EKO
C
Sall1
TPM
D
Sall1
200 kb
SE
H3K27ac
Microglia
Neurons
Oligoden.
WT
EKO
E
Sall1 IBA1 DAPI
Microglia - WT
Microglia - EKO
10μm
1μm
F
Sall1
SE
88Mb
89Mb
90Mb
91Mb
EKO
WT
PC1

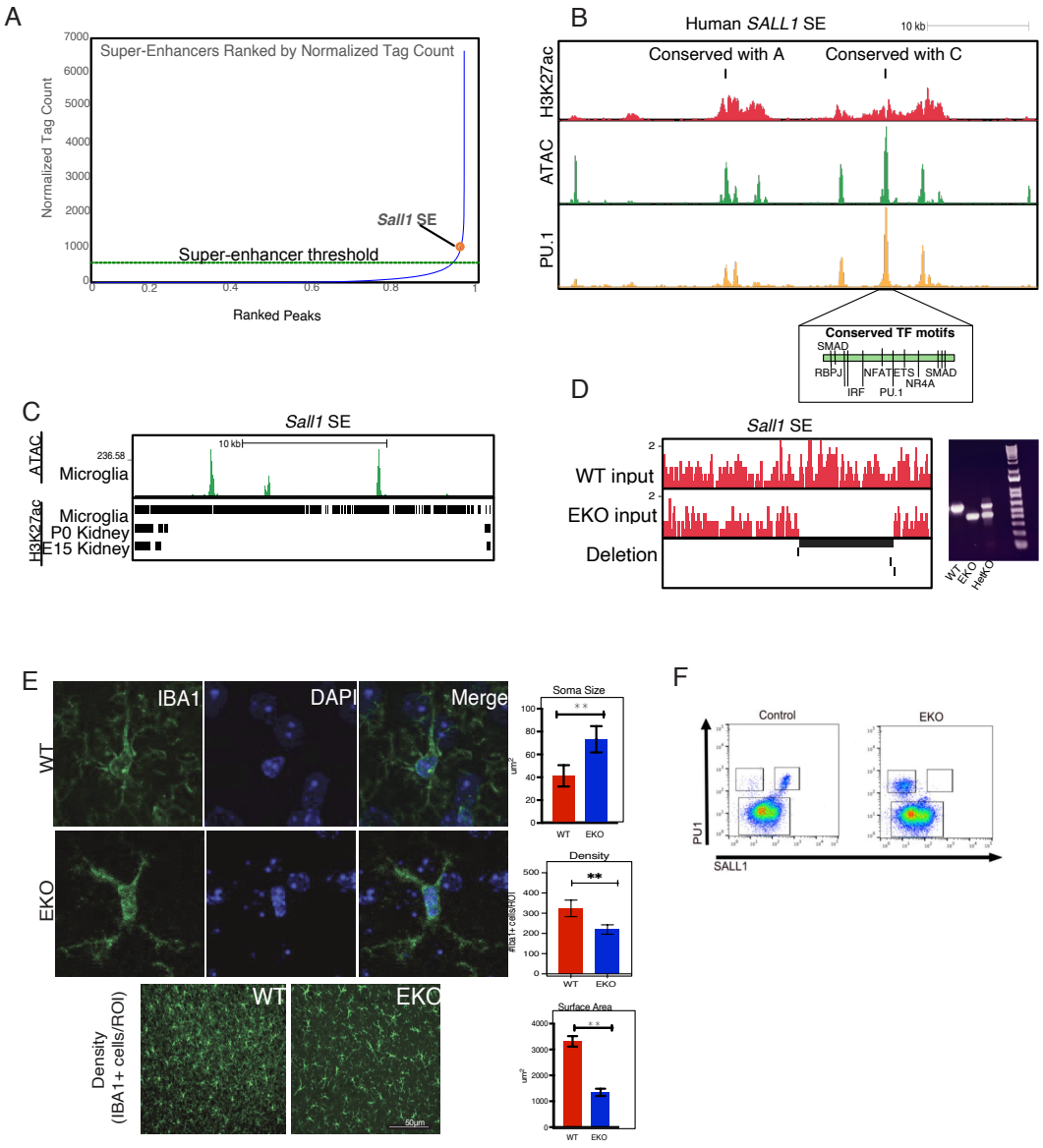

Supplemental Figure 2.1

A. Plot of WT microglia enhancers ranked by normalized H3K27ac tag count. Dotted line represents the cutoff for an enhancer to be considered a super-enhancer.

B. Genome browser of the human *SALL1* super-enhancer with H3K27ac ChIP, ATAC, and PU.1 ChIP. Regions conserved with the mouse *Sall1* super-enhancer Region A and Region C are marked above the H3K27ac. Conserved TF binding sites are annotated in the region homologous to mouse Region C.

C. Genome browser of the mouse *Sall1* super-enhancer and the overlap of mouse H3K27ac in microglia and embryonic/early postnatal kidney.

D. Genome browser showing input DNA from microglia and the *Sall1* SE deletion. Primers used for genotyping are marked below, and results from genotyping are shown on the right.

E. Imaging of WT and EKO brain sections stained for IBA1 and DAPI. Quantifications for n = 3 mice are shown on the right-hand side.

F. Flow cytometry of brain nuclei stained for PU1 and SALL1 in WT and EKO microglia.

Reduced expression of SALL1 leads to disruption of homeostatic genes in a dose-dependent manner

Analysis of transcriptomes of WT, Het KO and EKO microglia revealed progressive changes in microglia gene expression that correlated with the changing levels of *Sall1*. Het KO microglia, which express *Sall1* at around 50% of baseline levels (Figure 2.1C), exhibited upregulation of 111 genes and downregulation of 65 genes compared to WT microglia, while EKO microglia exhibited upregulation of 544 genes and downregulation 482 genes (fold-change >2 or <-2; adj. pvalue<0.05, Figure 2.2A, Supplementary Figure 2.2A). Nearly all genes observed to be differentially regulated in Het KO microglia are contained in the sets of differentially regulated genes in EKO microglia (Figure 2.2B). Differentially regulated genes in EKO microglia also overlapped the majority of genes observed to be differentially expressed following deletion of *Sall1* in mature mice using a conditional Cre recombinase expressed under the control of the *Sall1* locus itself [72] (Supplementary Figure 2.2B). The present studies identified a substantially larger set of differentially expressed genes, possibly due to the absence of *Sall1* throughout microglia differentiation.

Gene ontology analysis of differentially expressed genes in Het KO and EKO microglia reveals that genes with gained expression are significantly enriched for terms related to cytokine production, response to external stimuli, and regulation of immune system processes (Supplementary Figure 2.2C). Examples are provided by *Axl, Tnf, Apoe,* and *C3* genes (Figure 2.2C). In contrast, genes downregulated in Het KO and EKO microglia include many microglia signature genes that are tied to processes including cell adhesion, cell morphogenesis, and cell junction organization

(Supplementary Figure 2.2C). Examples are provided by *Selplg, Crybb1, Tmem119,* and *P2ry12* (Figure 2.2D).

We defined a set of 328 highly specific microglia signature genes based on a >10-fold higher level of expression in microglia compared to their average expression across 7 different macrophage subtypes using data derived from consistent methods for macrophage isolation and library preparation [59, 121, 122]. Notably, in this comparison, *Sall1* is the most differentially expressed mRNA. Of these microglia signature genes, 108 were among the 482 genes down-regulated >2-fold in the EKO, whereas only 6 overlapped with the 544 genes up-regulated >2-fold in the EKO (pvalue = 1.49e-63 and 0.99, respectively, Figure 2.2E). Although most of the highly *Sall1*-dependent genes are members of the microglia signature gene set (e.g., *Upk1b, Myo18b, Nav3, Adamts16, Mrc2, Slc2a5,* Figure 2.2A*),* very few have been systematically studied in microglia. Collectively, these findings confirm and extend the essential role of SALL1 in establishing microglia identity.

We considered the possibility that some of these changes in gene expression could be due to loss of yolk sac-derived microglia and replacement by hematopoietic stem cell (HSC)-derived cells. Several independent studies documented that HSC-derived cells that engraft the brain following depletion of embryonically derived microglia do not express *Sall1* even after long residence times in the brain [78-80]. These cells exhibit substantial differences in gene expression compared to yolk sac derived microglia, including some differences that are observed in Het KO and EKO microglia (Supplementary Figure 2.2D). However, HSC-derived cells cannot explain the altered pattern of gene expression in Het KO microglia, because ~95% of the microglia sorted

for gene expression express *Sall1,* albeit at ~50% of the level of WT microglia (Supplementary Figure 2.2E) and are thus of embryonic origin. As noted above, nearly all the genes differentially regulated in Het EKO are contained within the set of differentially regulated genes in EKO microglia but are more highly differentially expressed in EKO microglia (Supplementary Figure 2.2F), consistent with progressive loss of function of *Sall1* in embryonically derived cells. In addition, there are differences in the patterns of gene expression of Het KO and EKO microglia with HSC-derived cells that engraft the brain that are incompatible with significant replacement of yolk sac derived microglia. For example, *Sall3* is a member of the *Sall* transcription factor family that, like *Sall1*, is expressed in yolk sac-derived microglia but not at all in HSC-derived cells [78-80]. *Sall3* expression is unchanged in Het KO and EKO microglia (Figure 2.2F), which is inconsistent with significant replacement by HSC-derived cells. Conversely, HSC-derived cells express numerous genes that are not expressed by yolk sac-derived microglia, including *Ccr2* and *Lgals3*, the latter of which has recently been described as a long-lasting marker of HSC-derived cells that engraft the brain [123]. *Ccr2* and *Lgals3* are not expressed in WT, Het KO or EKO microglia as isolated for these studies (Figure 2.2F). Lastly, gene expression changes in EKO microglia are largely concordant with changes resulting from conditional deletion of *Sall1* in adult mice (Supplementary Figure 2.2B). In concert, these analyses are most consistent with Het KO and EKO microglia being of embryonic origin.

Recent studies have identified a spectrum of microglial phenotypes across multiple mouse models and disease states. We compared EKO gene expression (adj pvalue < 0.05) with previously published transcriptomic profiles from microglia in the

context of aging, microglia from the SOD1 model of ALS, microglia from mice after acute peripheral lipopolysaccharide (LPS) treatment [40], disease associated microglia (DAM) identified in the 5xFAD mouse model of Alzheimer's disease, and lipid droplet accumulating microglia (LDAM) identified in aging [37, 41]. Finally, we intersected mouse homologs of Alzheimer's disease risk loci with the EKO gene signature[116]. The genes downregulated in EKO overlapped significantly with genes known to be important for homeostatic microglia identity[50, 59, 61] and genes upregulated in LDAM (pvalue = 5.94e-58, 9.68e-16, respectively) (Figure 2.2G, Supplementary Figure 2.2G). Genes upregulated in EKO microglia were most strongly related to genes upregulated in aged microglia, including *Apoc2, Apoe, Axl, Cybb,* and *Mrc1* (pvalue = 3.18e-6) (Figure 2.2G, Supplementary Figure 2.2G). Genes upregulated in microglia from the SOD1 mouse model of ALS overlapping with EKO microglia included *Abca1, Cst7, Dab2,* and *Irf7,* and genes upregulated in microglia from LPS-stimulated mice shared upregulated expression of genes such as *Adam9, Bcl6* and *Ccl2* (pvalue = 3.58e-5, 0.95, respectively) *(*Figure 2.2G, Supplementary Figure 2.2H). Several genes associated with AD risk loci were increased in expression in EKO, such as *Aph1c, Ms4a6b, Ms4a6c,* and *Sorl1* (pvalue = 0.089) while another subset exhibit decreased expression in EKO, including *B4galt4, Bin1* and *Cass4 (*Figure 2.2G, Supplementary Figure 2.2G). Notably, in addition to *Ms4a6b* and *Ms4a6c*, four other tightly linked genes in the *Ms4a* locus are strongly upregulated in EKO microglia (Supplementary Figure 2.2H). EKO microglia also shared several upregulated genes with DAMs, such as *Sorbs3, Lyz2, Cd72,* and *Clec7a* (pvalue=0.58)*;* however, key genes that are upregulated in DAM, such as *Trem2* and *Cd9,* were not upregulated in EKO (Figure 2.2G, Supplementary Figure 2.2G). In

concert with the observation that haploinsufficiency of SALL1 is associated with altered gene expression, these data suggest that quantitative reductions in SALL1 expression during aging or disease could contribute to pathogenic microglia phenotypes.

Figure 2.2: Loss of *Sall1* leads to disruption of homeostatic gene expression in microglia
A. MA plot of RNA-seq data comparing WT and EKO microglia. n=3 per group. DE genes were defined as p.adj < 0.05, logFC > 2 or < -2, and log2(TPM+1) > 4 in at least one group.
B. Comparison of overlap between genes increased and decreased in EKO and Het KO microglia. p.values were calculated using Fisher exact test.
C. Barplots for expression of upregulated genes in WT, Het KO, and EKO microglia. Red = WT, Grey = Het KO, and Blue = EKO. The significance markers represent p-adj from DESeq2 comparing with WT. *p-adj < 0.05 and ***p-adj < 0.001. Error bars, SD.
D. Barplots for expression of downregulated genes across WT, Het KO, and EKO microglia. Red = WT, Grey = Het KO, and Blue = EKO. The significance markers represent p-adj from DESeq2 comparing with WT. *p-adj < 0.05 and ***p-adj < 0.001. Error bars, SD.
E. Overlap of significantly downregulated and upregulated genes in EKO versus genes expressed more highly in microglia than other tissue-resident macrophages (see supplementary table 1). Pvalue for overlaps was calculated using Fisher exact test.
F. Barplots for expression of genes differentially expressed in a model of peripherally engrafted microglia-like cells. The significance markers represent p-adj from DESeq2 comparing with circulating monocytes. *p-adj < 0.05 and ***p-adj < 0.001. Error bars, SD.
G. Heatmap of genes differentially expressed (p-adj from DEseq2 < 0.05) in EKO vs WT microglia that are associated with diverse microglia phenotypes. Each row is z-score normalized counts for each gene

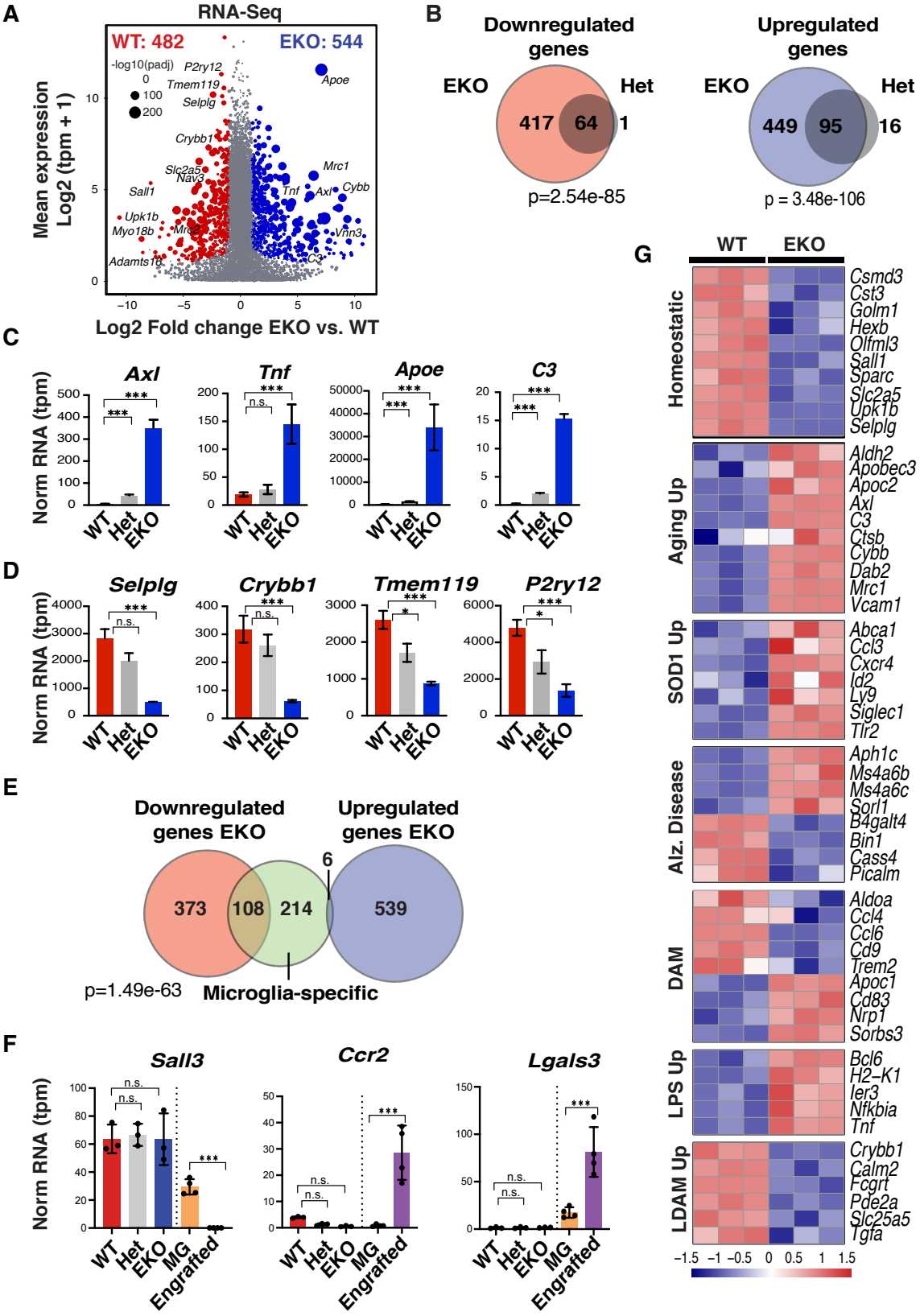
A
RNA-Seq
WT: 482
EKO: 544
-log10(padj)
0
100
200
P2ry12
Tmem119
Selplg
Apoe
Crybb1
Slc2a5
Nav3
Sall1
Upk1b
Myo18b
Mrc1
Adamts1
Tnf
Axl
Cybb
Vnn3
C3
Mean expression
Log2 (tpm + 1)
Log2 Fold change EKO vs. WT
B
Downregulated genes
EKO
Het
417
64
1
p=2.54e-85
Upregulated genes
EKO
Het
449
95
16
p = 3.48e-106
C
Axl
Tnf
Apoe
C3
Norm RNA (tpm)
WT
Het
EKO
n.s.
D
Selplg
Crybb1
Tmem119
P2ry12
E
Downregulated genes EKO
Upregulated genes EKO
373
108
214
6
539
p=1.49e-63
Microglia-specific
F
Sall3
Ccr2
Lgals3
MG
Engrafted
G
WT
EKO
Homeostatic
Csmd3
Cst3
Golm1
Hexb
Olfml3
Sall1
Sparc
Slc2a5
Upk1b
Selplg
Aging Up
Aldh2
Apobec3
Apoc2
Axl
C3
Ctsb
Cybb
Dab2
Mrc1
Vcam1
SOD1 Up
Abca1
Ccl3
Cxcr4
Id2
Ly9
Siglec1
Tlr2
Alz. Disease
Aph1c
Ms4a6b
Ms4a6c
Sorl1
B4galt4
Bin1
Cass4
Picalm
DAM
Aldoa
Ccl4
Ccl6
Cd9
Trem2
Apoc1
Cd83
Nrp1
Sorbs3
LPS Up
Bcl6
H2-K1
Ier3
Nfkbia
Tnf
LDAM Up
Crybb1
Calm2
Fcgrt
Pde2a
Slc25a5
Tgfa
−1.5 −1 −0.5 0 0.5 1 1.5

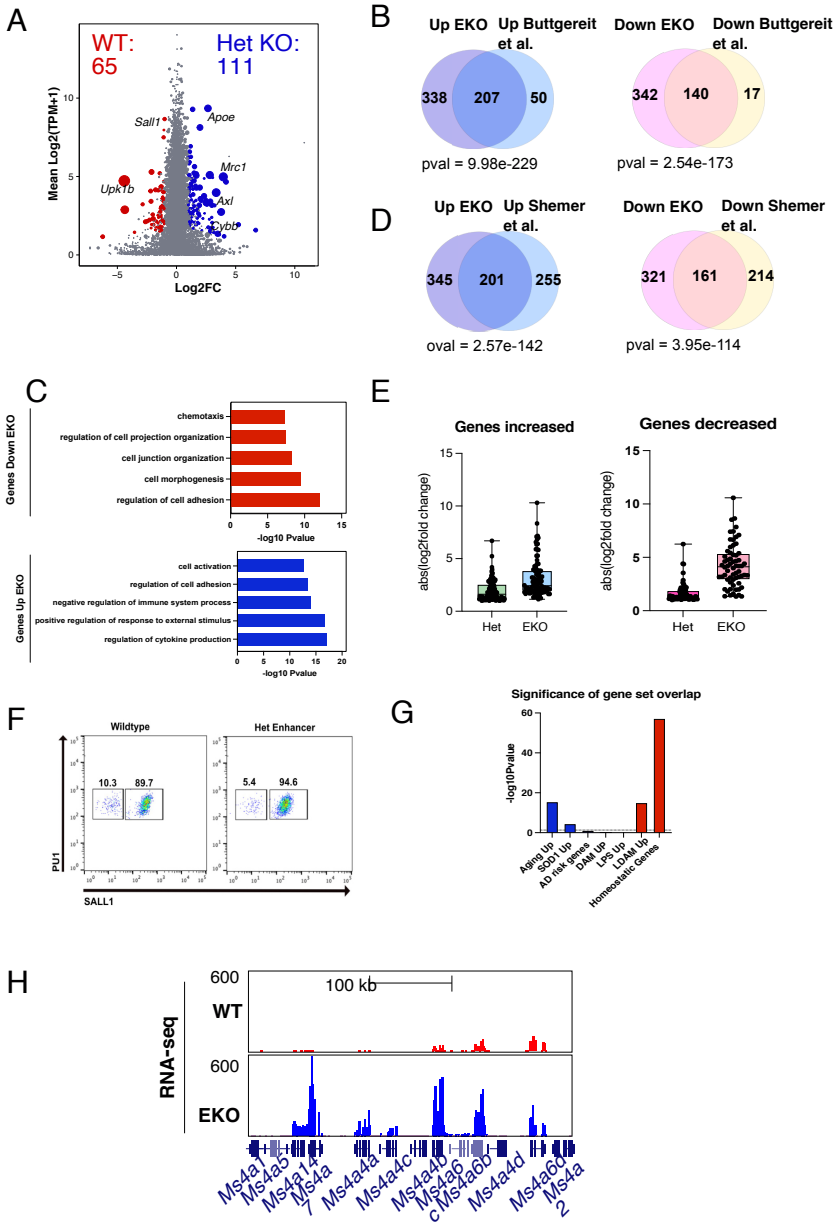

Supplemental Figure 2.2:

A. MA plot of RNA-seq data from WT versus Het EKO microglia. n=3

B. Overlap of differential genes identified in EKO vs WT and Sall1 conditional knockout versus control (Defined by DEseq2 adj. pvalue < 0.05 and logFC >2). Pvalues for overlaps were calculated using Fisher exact test.

C. Metascape GO analysis of genes significantly changed in EKO microglia

D. Overlap of differential genes identified in EKO vs WT microglia and engrafted vs. endogenous microglia. Pvalues for overlaps were calculated using Fisher exact test.

E. Flow cytometry of WT and Het brain nuclei stained for PU1 and SALL1.

F. Boxplot of log2fold change of differential genes shared between Het and EKO microglia.

G. Significance of gene set overlaps from Figure 2G. Dotted line represents pvalue = 0.05.

H. Expression of Ms4 family genes in EKO and WT microglia

SALL1 functions as both a repressor and an activator in microglia

Despite substantial evidence pointing to SALL1 as an essential regulator of microglia identity, little is known about the genes that SALL1 may directly regulate or the underlying mechanisms. To address these questions, we performed ChIP-seq for SALL1 in sorted SALL1+/PU1+ nuclei using a combination of formaldehyde and disuccinimidyl glutarate (DSG) to crosslink SALL1 to chromatin. 75% of the input DNA recovered for these experiments mapped to the A compartment of chromatin and 25% to the B component as defined by HiC data. Using this input DNA for ChIP-seq, we defined 20,139 reproducible SALL1 peaks, ~98% of which resided within the A compartment. ChIP-seq for SALL1 in EKO microglia recovered fewer than 100 reproducible peaks, demonstrating the specificity of the antibody for SALL1. The majority of SALL1 binding sites localized to intronic and intergenic regions, with a small portion of peaks falling within TSS-promoter regions (Figure 2.3A), including the *Sall1* promoter and enhancer itself (Supplementary Figure 2.3A). Interestingly, SALL1 was also observed to bind at key microglia genes, such as *Sparc* and *P2ry12 (*Supplementary Figure 2.3B.

In parallel, we performed ATAC-seq and H3K27ac ChIP-seq in EKO microglia. Regardless of their developmental origin, EKO microglia represent myeloid cells residing in the brain environment that completely lack *Sall1* expression. Comparison of the epigenetic landscapes of WT and EKO microglia thus provides a direct means of assessing the transcriptional functions of SALL1. Analysis of ATAC seq data from WT and EKO microglia indicated that loss of SALL1 resulted in a >2-fold decrease in ATAC signal at 5139 distal sites and a >2-fold increase at 6599 distal sites (adj pvalue < 0.05,

Supplementary Figure 2.3C). We then annotated every distal ATAC peak (> 3000 bp from TSS) with normalized H3K27ac tags (+/- 1000 bp from the peak center) in WT and EKO microglia to identify putative enhancers. Using a cutoff of >16 normalized H3K27ac tags, this analysis captured 38,864 ATAC peaks with features of active enhancers (Figure 2.3B). Among this set, 3213 distal regions exhibited a >2-fold increase in H3K27ac (blue points in Figure 2.3B) and 2493 distal regions exhibited a >2-fold decrease in H3K27ac (red points in Figure 2.3B) in EKO microglia (adj pvalue < 0.05) (Figure 2.3B). We then intersected the putative enhancers that gained or lost H3K27ac in EKO microglia with SALL1 peaks. This analysis revealed that 714 regions with increased H3K27ac overlapped with at least one SALL1 binding site (22% of total upregulated peaks), while 1058 regions with decreased H3K27ac overlapped with at least one SALL1 binding site (42% of downregulated peaks) (dark red and dark blue points in Figure 2.3B). These annotations were used to define four putative classes of enhancers (Figure 2.3C); those consistent with direct activation by SALL1 (presence of SALL1 and loss of H3K27ac in EKO n=1058), those consistent with direct repression by SALL1 (presence of SALL1 and gain of H3K27ac in EKO, n=714), those consistent with indirect activation by SALL1 (lack of SALL1 and loss of H3K27ac in EKO, n=1435) and those consistent with indirect repression by SALL1 (lack of SALL1 and increase in H3K27ac, n=2499).

Examples of putative enhancers exhibiting loss of H3K27ac in EKO microglia at sites of SALL1 binding are provided by a genomic region containing the microglia signature genes *Tmem119* and *Selplg* (Figure 2.3D). These genes, which are strongly dependent on *Sall1* for expression (Figure 2.2A), are located amidst multiple chromatin

loops defined by PLAC-seq that connect the *Tmem119* and *Selplg* promoters to SALL1 binding sites (shaded in lavender). In addition to reduced levels of H3K27ac, these SALL1 binding sites also exhibit reduced binding of p300 in the EKO microglia, suggesting that SALL1 contributes directly to p300 recruitment, H3K27 acetylation, and enhancer activation at these locations. A contrasting example is provided by a genomic region containing the *Apoe, Apoc1, Apoc2, Apoc4* and *Gm44805* genes. These genes reside within an active chromatin compartment as defined by Hi-C assays of both WT and EKO microglia but are upregulated from 10-fold to more than 100-fold in EKO microglia. These genes reside within PLAC-seq defined loops that are bounded at each end by SALL1 peaks (Figure 2.3D, blue stripes). ATAC-seq and H3K27ac signal do not change at these SALL1 binding sites in the EKO microglia but are markedly increased at multiple enhancer-like locations within the PLAC-seq loops that are not bound by SALL1 (yellow stripes, Figure 2.3D), consistent with an indirect mechanism of repression of the genes within this region in WT cells. Intriguingly, the genes immediately outside of the SALL1-bounded loops (*Clptm1* and *Tomm40*) are expressed at the same levels in WT and EKO microglia, raising the possibility that SALL1 functions to insulate genes within the loop from regulatory elements controlling these and potentially other genes. A similar pattern is observed within the *Ms4a* locus, where the tightly linked *Ms4a7*, *Ms4a4a*, *Ms4a4b* and *Ms4a4c* genes are upregulated more than 50-fold in EKO microglia (Supplementary Figure 2.3E).

To examine the relationships of changes in H3K27ac and SALL1 at distal regions with microglial gene expression at a genome-wide scale, we identified genes associated with each affected enhancer-like region and overlapped these genes with the EKO gene

signature (Figure 2.3E). Sites bound by SALL1 that lose H3K27ac in EKO are associated with 560 genes; 200 (36%) of these genes are significantly downregulated in EKO microglia, whereas only 16 (2.8%) are upregulated (adj pvalue <0.05). Conversely, sites bound by SALL1 that gain H3K27ac are associated with 439 genes, 153 (35%) of which are upregulated in EKO microglia in comparison to 30 (6.8%) that are downregulated. These findings are consistent with SALL1 acting to directly activate or repress gene expression via actions at nearby enhancers. At putative enhancers that gain or lose H3K27ac in EKO that do not contain a SALL1 peak and indirectly regulated, changes in nearby gene expression are consistent with the corresponding gain or loss of enhancer H3K27ac (Figure 2.3E).

We next performed *de novo* motif analysis of the four classes of differentially regulated enhancers. In all cases, the most highly enriched motif corresponded to the consensus binding site for PU.1, consistent with a major role in the selection of all four classes of microglia regulatory elements [47, 124] (Figure 2.3F, Supplementary Figure 2.3C). At the 1058 enhancer-like elements bound by SALL1 exhibiting loss of H3K27ac in EKO microglia, the next most significantly enriched sequences corresponded to motifs recognized by MEF transcription factors, a PU.1:IRF composite element, and motifs recognized by SMADs and MAF family members. *Mef2a*, *Mef2b* and *Mef2c* are expressed in microglia, consistent with the possibility that the encoded proteins colocalize with SALL1 at these locations. Mef2c has been reported to restrain microglia inflammatory responses in mice, and in humans is associated with risk alleles for Alzheimer's disease [75, 125]. The PU.1:IRF composite element is consistent with essential roles of PU.1:IRF8 ternary complexes in mediating a subset of PU.1 transcriptional

functions in microglia [47]. The presence of SMAD motifs was of particular interest because members of the SMAD transcription factor family mediate transcriptional responses to TGFβ signaling, which is required for microglia development [46, 50]. Deletion of *Mafb* in microglia has been demonstrated to disrupt developmental and immune functions [52]. These findings are consistent with SALL1 functioning as a transcriptional activator at these locations through collaborative interactions with PU.1, MEF, SMAD and MAF transcription factors.

PU.1, PU.1:IRF and MEF motifs were also observed at enhancer like elements bound by SALL1 exhibiting gain of H3K27ac in EKO microglia (Figure 2.3F, Supplementary Figure 2.3C). In addition, these regions exhibited preferential enrichment for motifs recognized by C/EBP and AP-1 family members, suggesting that SALL1 might function to directly repress their transcriptional activities at these locations. Peaks decreased in EKO not overlapping with SALL1 were enriched for ETV/ETS, AP1, the RFX family, and SMADs, indicating that these factors may be responsible for changes in chromatin independent of direct SALL1 binding (Supplementary Figure 2.3C). Regions with increased H3K27ac and no overlap with SALL1 binding sites were enriched with motifs for the CEBP family, the PU1:IRF8 heterodimer, the AP1 family, and the MITF/TFE family of TFs. The presence of AP1 in upregulated H3K27ac peaks indicates that activity of the AP1 family may play a role in these observed changes, independent of SALL1 binding sites. We also examined the expression of TFs and their family members identified in the *de novo* motif analysis and found that expression of *Irf7, Tfec,* and *Batf2* were significantly upregulated in EKO (fold change > 2,adj pvalue <0.05) and expression of *Ets1* was significantly decreased in EKO (fold change < -2,adj

pvalue <0.05)(Supplementary Figure 2.3F), indicating that the changes in *de novo* motifs in differentially acetylated peaks may be driven by changes in TF activity unrelated to their level of expression. Collectively, these results support a model in which SALL1 acts as a both a repressor and as an activator in microglia to select and regulate the microglia-specific enhancer landscape.

Figure 2.3: SALL1 is an activator and repressor in microglia
A. Pie Chart representing the distribution of the IDR-defined SALL1 binding sites in microglia. Data are from n=2 experiments.
C. Scatterplot of distal ATAC-associated H3K27ac overlapping with SALL1 binding sites. ATAC data n=5 per group. H3K27ac n = 2 per group. Color codes indicate significant changes (light red and light blue are p.adj < 0.05, FC >2) and significant changes overlapping with SALL1 binding sites (dark red and dark blue).
C. Histograms of normalized H3K27ac and SALL1 counts from EKO and WT microglia at peak subsets defined in C. Red = WT. Blue = EKO.
D. Genome browser tracks of WT SALL1, ATAC, H3K27ac, p300, and PLAC seq in addition to EKO ATAC, H3K27ac, and p300. Pink highlights indicate regions PLAC-connected to promoters where SALL1 binds in WT and loses H3K27ac/p300 signal in EKO. Blue highlights indicate regions where SALL1 binds in regions PLAC-connected to promoters and yellow highlights indicate regions with an absence of SALL1 binding and increased H3K27ac/p300 signal in EKO microglia.
E. Overlap of genes nearest to each H3K27ac subset and genes differentially expressed in EKO microglia (p-adj from DESeq2 < 0.05)
F. Enriched motifs in each subset of differential distal chromatin regions using GC-matched genomic background.

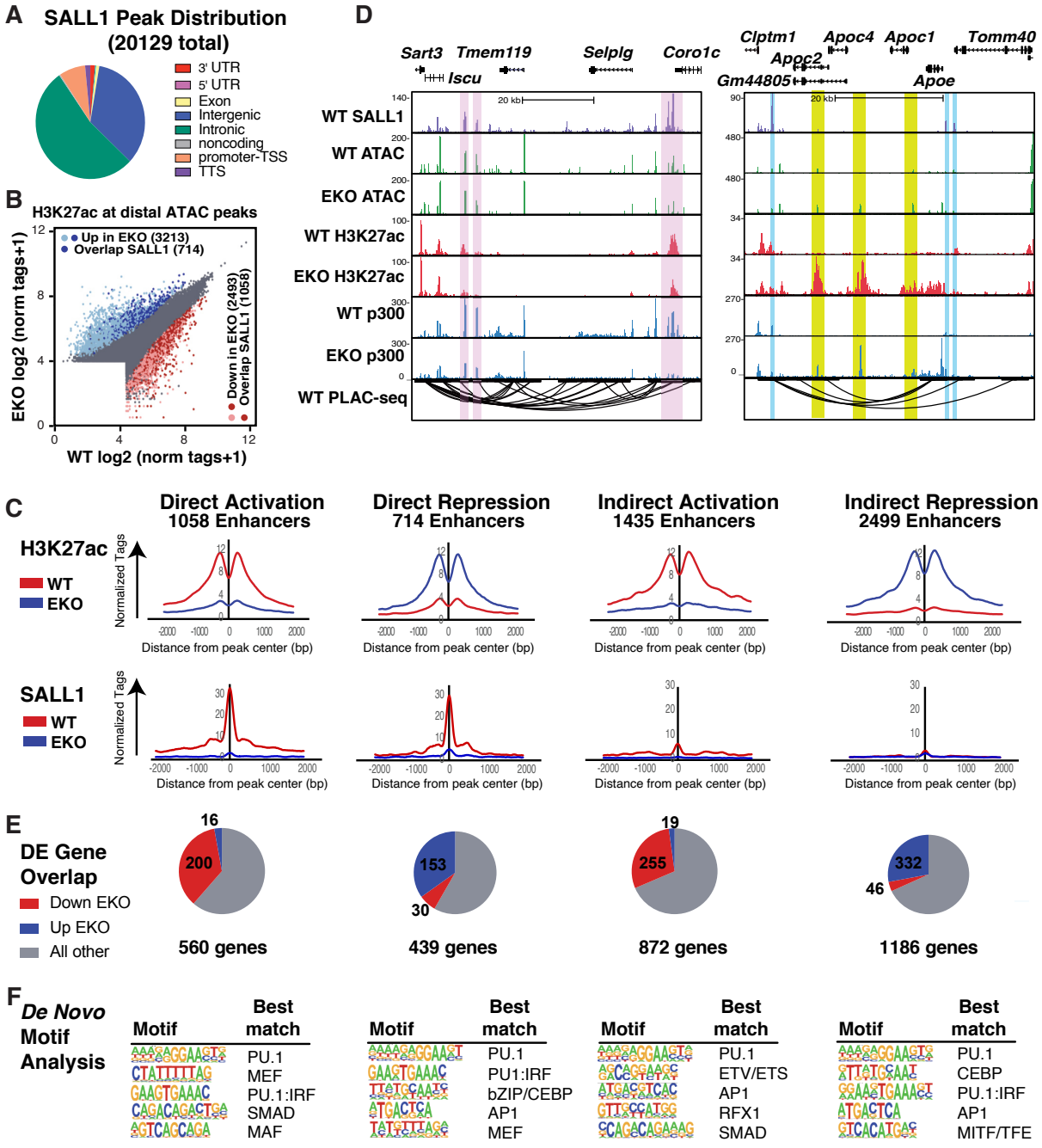
A
SALL1 Peak Distribution
(20129 total)
3' UTR
5' UTR
Exon
Intergenic
Intronic
noncoding
promoter-TSS
TTS
B
H3K27ac at distal ATAC peaks
Up in EKO (3213)
Overlap SALL1 (714)
Down in EKO (2499)
Overlap SALL1 (1058)
EKO log2 (norm tags+1)
WT log2 (norm tags+1)
D
Sart3
Tmem119
Iscu
Selplg
Coro1c
Clptm1
Apoc4
Apoc1
Tomm40
Apoc2
Gm44805
Apoe
20 kb
WT SALL1
WT ATAC
EKO ATAC
WT H3K27ac
EKO H3K27ac
WT p300
EKO p300
WT PLAC-seq
C
Direct Activation
1058 Enhancers
Direct Repression
714 Enhancers
Indirect Activation
1435 Enhancers
Indirect Repression
2499 Enhancers
H3K27ac
WT
EKO
SALL1
Normalized Tags
Distance from peak center (bp)
E
DE Gene
Overlap
Down EKO
Up EKO
All other
16
200
560 genes
153
30
439 genes
19
255
872 genes
332
46
1186 genes
F
De Novo
Motif
Analysis
Motif
Best match
PU.1
MEF
PU.1:IRF
SMAD
MAF
PU.1
PU1:IRF
bZIP/CEBP
AP1
MEF
PU.1
ETV/ETS
AP1
RFX1
SMAD
PU.1
CEBP
PU.1:IRF
AP1
MITF/TFE

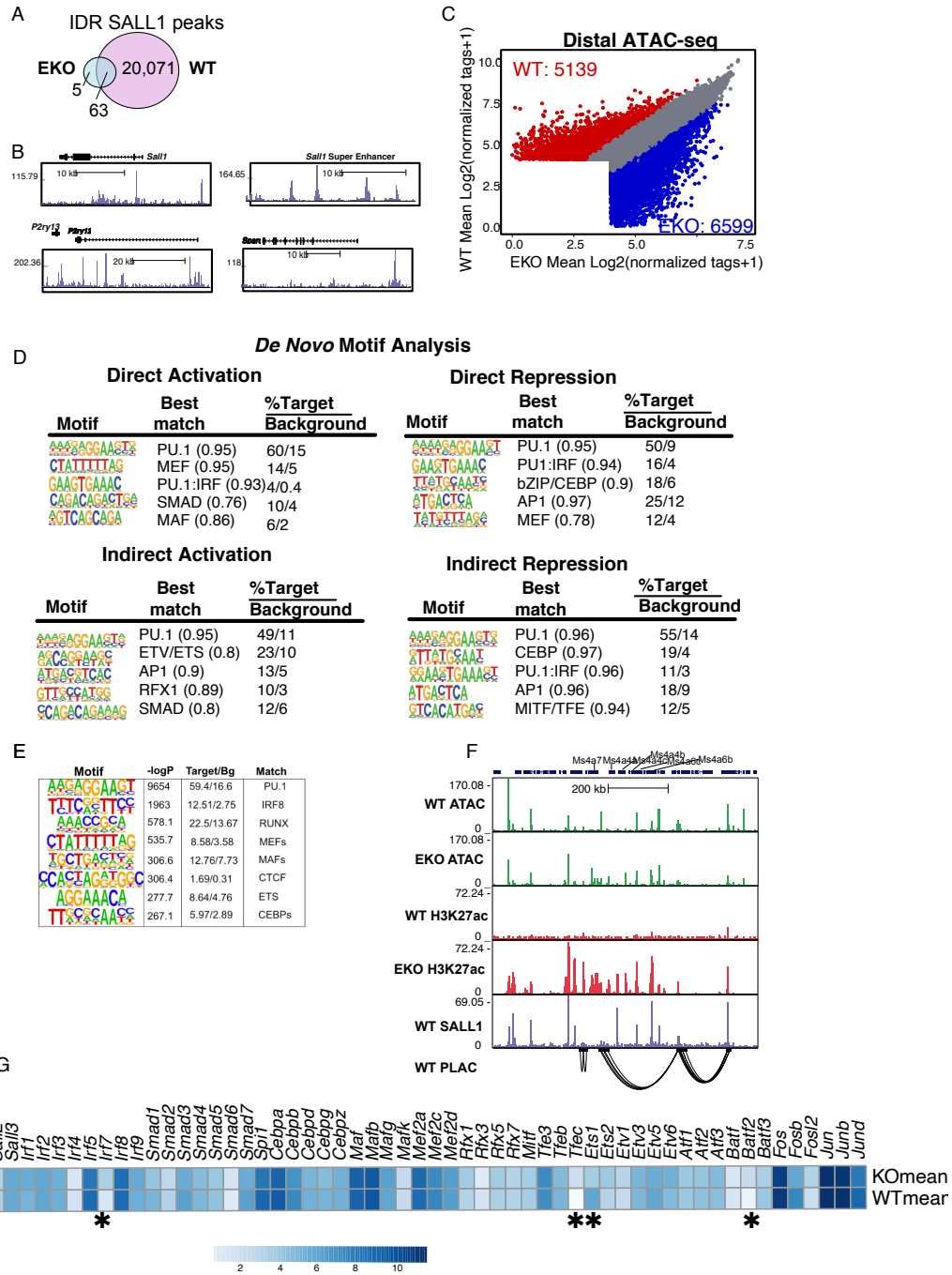

Supplemental Figure 2.3:

A. Overlap of WT and EKO SALL1 IDR ChIP peaks

B. Genome browser of WT SALL1 ChIP signal at loci associated with key microglia genes.

C. Scatterplot of ATAC peaks in WT vs EKO. N=5 per group. Color codes indicate significant changes (dark red and dark blue are p.adj < 0.05, FC >).

D. *De novo* motifs identified in Figure F.

d. *De novo* motifs identified from IDR-defined SALL1 peaks.

E. Genome browser of WT SALL1 ChIP and ATAC/H3K27ac ChIP in WT and EKO microglia at the Ms4 locus.

F. Heatmap of expression of TFs identified in the motif analysis in 3C in EKO and WT microglia.

Smad4 and Sall1 regulate a common set of microglia identity genes

TGF-Beta signaling, which plays a critical role in forming microglia identity and promoting microglial survival [46, 50], is known to control expression of *Sall1* and other key microglial genes [46, 50, 73, 126]. Signaling via TGFBR2 induces the activation of the receptor-associated SMADs (R-SMADs), SMAD2 and SMAD3. These R-SMADS complex with SMAD4 and translocate to the nucleus, where they localize to SMAD-binding elements at TGF-beta target genes [127]. The enrichment of SMAD family motifs in the *Sall1* SE and in enhancer-like regions losing H3K27ac in EKO suggested that SMADs may be both controlling *Sall1* expression and playing a role as important binding partners of SALL1 in microglia. Since SMAD4 is a unique co-factor utilized by all receptor-activated SMADs, we used an inducible, conditional deletion of *Smad4* (Cx3cr1^{ERT2}x Smad4$^{fl/fl}$, *Smad4* cKO, Supplement 2.4A) and measured the effects of *Smad4 c*KO on the microglial transcriptome. 832 genes were increased (logfold change >2, FDR < 0.05) in expression in *Smad4* cKO microglia, and 595 genes were decreased in expression (logfold change <-2, adj pvalue < 0.05) (Figure 2.4A). Genes upregulated in *Smad4* cKO microglia were related to cell cycle (*Birc5, Bub1b, Tuba1c, Cdc25b, Apbb1),* cytokine production (*C3ar1, Il1b, Ccl2, Cd83),* and response to external stimulus (*C5ar1, Il6, Nfkbia, Tnf) (*Supplementary Figure 2.4B). The presence of cell cycle genes is likely related to *Smad4's* role as a transducer of TGF-beta signaling in microglia development; indeed, numbers of microglia were somewhat reduced in *Smad4 c*KO microglia, congruent with what has been described in models disrupting TGF-beta signaling in early microglia [46, 50] (Supplementary Figure 4C). Downregulated genes were affiliated with categories such as regulation of cell adhesion (*Smad3,*

Smad7, Notch4, Apbb1ip, Inpp5d), cell junction organization (*Cx3cr1, Itgam, Pecam1),* and regulation of cell migration (*Adam10, Ccr6, Sparc).* (Supplementary Figure 2.4B). Loss of *Smad4* resulted in a 75% decrease in *Sall1* expression (Figure 2.4C), consistent with prior studies demonstrating that *Sall1* is positively regulated by TGFβ1 and further suggesting that the *Smad4* cKO should partially phenocopy the *Sall1* EKO.

To examine similarities between EKO and *Smad4 c*KO transcriptional signatures, we overlapped the differentially expressed genes from each condition (Figure 2.4B). 68% (370/545) of genes increased in EKO overlapped significantly with genes increased in *Smad4 c*KO microglia (pvalue = 9.69e-298). This subset of genes included *Apoe, Axl* and *Mrc1* (Figure 2.4D). 60% (290/482) of genes decreased in EKO overlapped with genes increased in *Smad4 c*KO (p value = 6.67e-257), and included genes such as *Crybb1, P2ry12,* and *Tmem119* (Figure 4C). We examined the genes differentially changed in *Smad4 c*KO alone and found that loss of *Smad4* caused a decrease in *Sall3* and members of the TGF-beta signaling pathway, such as *Smad3, Smad7,* and *Skil,* while EKO microglia did not have decreased levels of these genes (Figure 2.4E). Taken together, these results indicate that *Smad4* is upstream of *Sall1* and may potentially collaborate with SALL1 at multiple loci important for microglia identity and inflammation.

Figure 2.4: *Smad4* regulates the expression of microglial genes
A. MA plot of RNA-seq data comparing WT and *Smad4* cKO microglia.
n=2-4 per group. DE genes were defined as p.adj < 0.05, logFC > 2 or < -2, and log2(TPM+1) > 4 in at least one group.
B. Overlap of differential genes in EKO microglia versus *Smad4* cKO microglia. pvalue was calculated using Fisher exact test.
C. Barplots for expression of downregulated genes in WT and *Smad4* cKO microglia. Orange = WT. Green = *Smad4* cKO. The significance markers represent p-adj from DESeq2 comparing with WT. *p-adj < 0.05 and ***p-adj < 0.001. Error bars, SD.
D. Barplots for expression of upregulated genes in WT and *Smad4* cKO microglia. Orange = WT. Green = *Smad4* cKO. The significance markers represent p-adj from DESeq2 comparing with WT. *p-adj < 0.05 and ***p-adj < 0.001. Error bars, SD.
E. Barplots comparing expression of genes differentially expressed in WT versus EKO and WT versus *Smad4* cKO. The significance markers represent p-adj from DESeq2 comparing with WT. *p-adj < 0.05 and ***p-adj < 0.001. Error bars, SD.

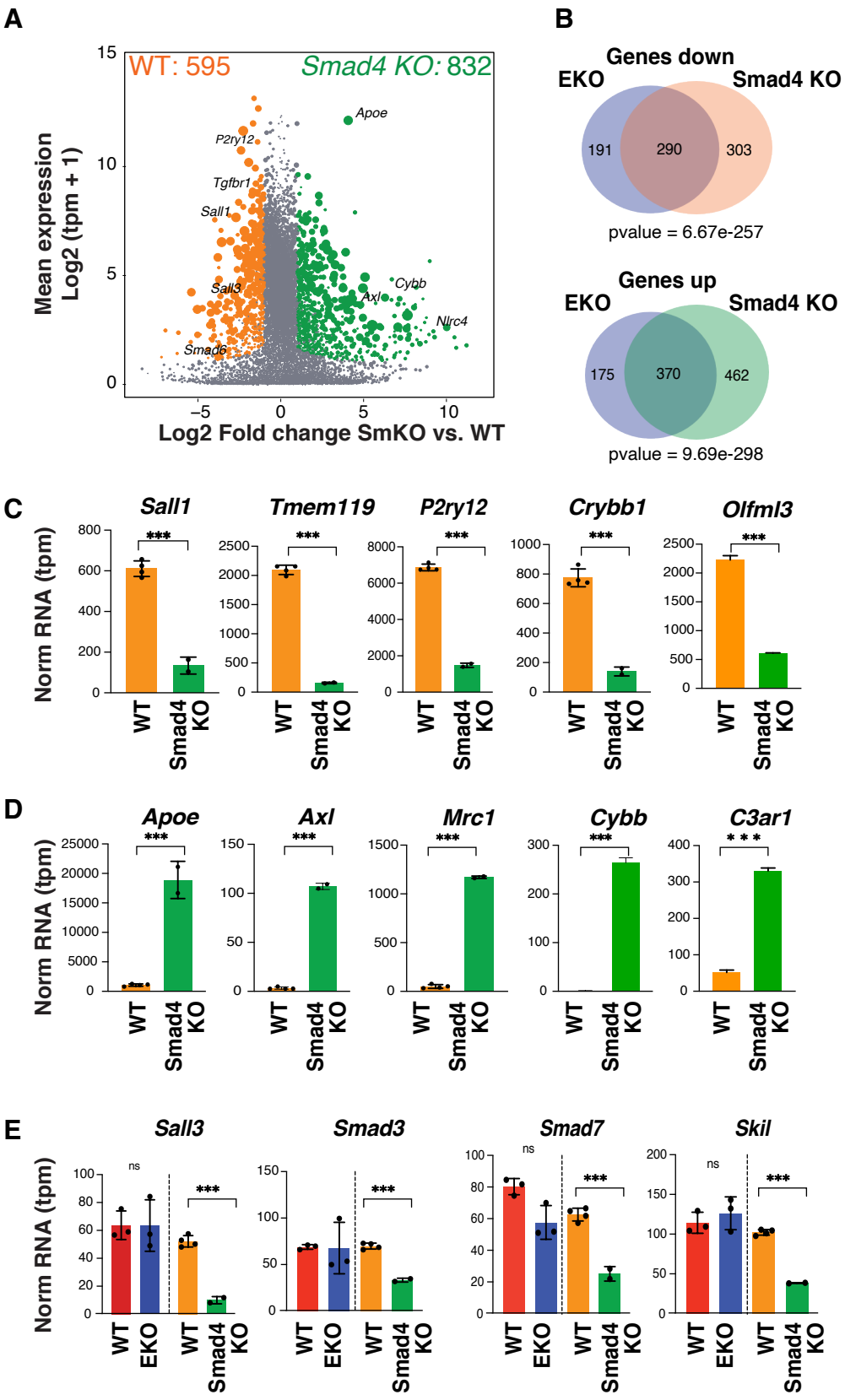
A
WT: 595
Smad4 KO: 832
Apoe
P2ry12
Tgfbr1
Sall1
Sall3
Smad6
Cybb
Axl
Nlrc4
Mean expression
Log2 (tpm + 1)
Log2 Fold change SmKO vs. WT
B
Genes down
EKO
Smad4 KO
191
290
303
pvalue = 6.67e-257
Genes up
EKO
Smad4 KO
175
370
462
pvalue = 9.69e-298
C
Sall1
Tmem119
P2ry12
Crybb1
Olfml3
Norm RNA (tpm)
WT
Smad4 KO
D
Apoe
Axl
Mrc1
Cybb
C3ar1
Norm RNA (tpm)
WT
Smad4 KO
E
Sall3
Smad3
Smad7
Skil
Norm RNA (tpm)
WT
EKO
Smad4 KO
ns

A

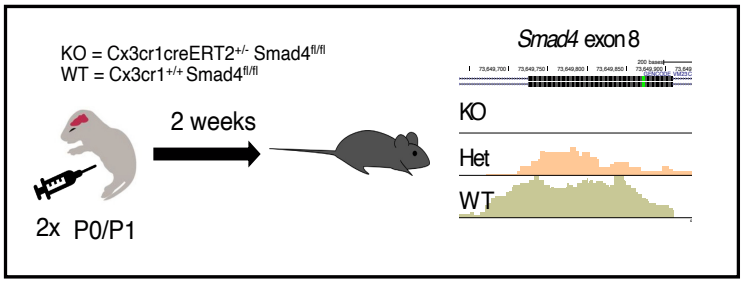

B

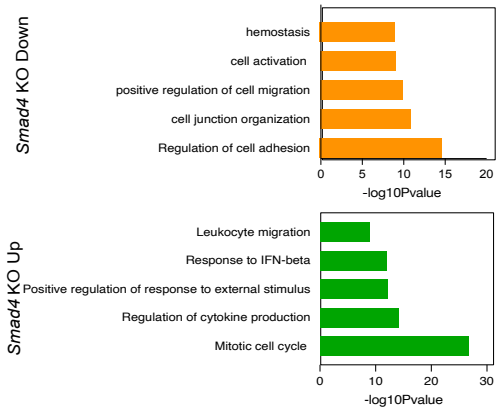

Supplemental Figure 2.4:
A. Schematic of experimental setup for conditional *Smad4* KO mice.
B. Metascape GO analysis of genes significantly changed in *Smad4* cKO microglia

SALL1 regulates DNA binding and function of SMAD4

To assess mechanisms underlying functional interactions between SMAD4 and SALL1 at the level of DNA binding, we performed ChIP-seq for SMAD4 in sorted microglia nuclei. We identified almost 8000 reproducible SMAD4 peaks, which localized primarily to distal intergenic and intronic regions (Figure 2.5A). *De novo* motif analysis revealed that SMAD4 peaks were enriched for PU.1, SMAD, IRF, and AT-rich MEF family motifs, indicating that SMAD4 binding is likely driven by collaborative interactions with microglia lineage determining factors (Supplementary Figure 2.5A). As expected, SMAD4 binds to promoters and putative enhancers of genes that are dependent on TGFβ signaling and are associated with microglia identity, such as *Olfml3,* as well as genes encoding known TGFβ pathway regulators, such as *Tgfbr2* and *Skil* (Supplementary Figure 2.5B). Notably, SMAD4 binds strongly to regions A, B and C of the *Sall1* super enhancer proximal to SALL1 and PU.1 (Figure 2.5A), consistent with the presence of conserved SMAD motifs (Supplementary Figure 2.1B).

Remarkably, we found that on a genome-wide scale 72% (5750/7985) of SMAD4 peaks overlapped with a SALL1 binding site (Figure 2.5C), suggesting that in addition to roles in the activation of *Sall1* expression, SMADs and SALL1 might also function as collaborative binding partners to regulate microglia-specific enhancers. To probe a potential relationship between SMAD4 and SALL1 binding, we leveraged the lack of SALL1 expression in EKO microglia to assess changes in SMAD4 binding at distal regulatory regions upon loss of SALL1. We performed SMAD4 ChIP in EKO microglia and observed that 645 distal SMAD4 peaks were decreased and 667 distal SMAD4 peaks were increased (>2-fold, FDR <0.05) in comparison to WT microglia (Figure

2.5D). Of the SMAD4 peaks that were reduced in EKO microglia, 75% (484/645) overlapped with a SALL1 peak (Figure 2.5D), consistent with SALL1 directly contributing to SMAD4 binding at these locations. An example is provided at the genomic locus containing *Tmem119* and *Selplg*, in which SMAD4 co-binds with SALL1 at putative enhancer elements in WT microglia (Figure 2.5E, yellow highlights). SMAD4 binding is significantly reduced at these locations in EKO microglia.

Of the SMAD4 peaks that were gained in EKO microglia, 46% (309/667) overlapped with a SALL1 peak in WT microglia (Figure 2.5D). This result suggests that at these sites, SALL1 functions to directly restrict SMAD4 binding. The 54% of SMAD4 peaks that are gained in EKO microglia and do not overlap with SALL1 peaks provide evidence that the absence of SALL1 also enables redistribution of SMAD4 to alternative locations. An example of SMAD4 redistribution in EKO microglia is provided by the genomic locus containing *Apoe, Apoc1, Apoc2, Apoc4* and *Gm44805.* SMAD4 binding is largely absent at this locus in WT microglia, while substantial binding is observed at multiple enhancer-like regions in EKO microglia (Figure 2.5F, green highlights).

A global analysis of H3K27ac signal at genomic locations exhibiting gain or loss of SMAD4 found that SMAD4 peaks that increased in EKO microglia, regardless of overlap with a SALL1 binding site, were characterized by an increase in EKO H3K27ac signal (Supplementary Figure 2.5C). Conversely, SMAD4 peaks that were downregulated in EKO microglia, regardless of overlap with a SALL1 binding site, were associated with reduced H3K27ac signal (Supplementary Figure 2.5C). These results indicate that SMAD4 is primarily acting as an activator of the chromatin landscape at sites that are directly or indirectly affected by SALL1. D*e novo* motif analysis revealed

that all subsets of differential SMAD4 peaks shared enrichment for PU1, ETS and SMAD motifs (Supplemental Figure 2.5D). SMAD4 peaks gained and lost in EKO that overlapped with a SALL1 binding site were further enriched for AT-rich MEF motifs. In contrast, SMAD4 peaks that were gained in EKO and non-overlapping with SALL1 binding sites were enriched for AP1 motifs (Supplemental Figure 2.5D). It is known that SMADs can partner with the AP-1 complex [128, 129] which may indicate that SMAD4 redistribution in EKO is in part driven by collaboration with AP-1.

Lastly, we evaluated SMAD4 binding at each of the four categories of enhancers defined by gain or loss of H3K27ac in EKO microglia and the presence or absence of a SALL1 peak in WT microglia illustrated in Figure 2.3C. High levels of SMAD4 binding were observed at enhancers occupied by SALL1 in WT microglia and in which H3K27ac levels fell in EKO microglia (directly activated enhancers). Notably, SMAD4 binding was markedly reduced at these enhancers in EKO microglia (Figure 2.5G, upper left panel). Conversely, low levels of SMAD4 binding were observed at enhancers occupied by SALL1 in WT microglia and in which H3K27ac levels increased in EKO microglia (directly repressed enhancers). At these locations, SMAD4 binding increased significantly in EKO microglia (Figure 2.5G, lower left panel). SMAD4 binding was also observed to decrease at indirectly activated enhancers and increase at indirectly repressed enhancers in EKO microglia, but to a lesser extent than at enhancers bound by SALL1 in WT microglia (Figure 2.5G upper and lower right panels). These findings provide evidence that SALL1 functions to specify the microglia-specific binding pattern of SMADs.

Figure 2.5: SALL1 and SMAD4 collaborate at key microglia genes

A. Pie chart representing distribution of IDR-defined SMAD4 peaks. n=2. B. Genome browser tracks of H3K27ac ChIP, ATAC, SALL1, PU.1 and SMAD4 ChIP at the *Sall1* super enhancer in WT microglia. Yellow highlights and A,B,C labels represent the three main regions of open chromatin in the super-enhancer.
C. Overlap of IDR-defined SALL1 and SMAD4 peaks in WT microglia.
D. Scatterplot of distal SMAD4 peaks overlapping with SALL1 binding sites. Color codes indicate significant changes (light red and light blue are p.adj < 0.05, FC >2) and significant changes overlapping with SALL1 binding sites (dark red and dark blue).
E. Genome browser tracks of WT ATAC, SALL1 and PLAC-seq, in addition to SMAD4 in EKO and WT at the *Selplg/Tmem119* locus. Yellow highlights indicate regions where SMAD4 binding is diminished in EKO upon loss of SALL1 binding.
F. Genome browser tracks of WT ATAC, SALL1 and PLAC-seq, in addition to SMAD4 in EKO and WT at the *Apoe* locus. Pink highlight shows region where loss of direct SALL1 binding leads to increased SMAD4 signal in EKO. Green highlights demonstrate regions where SMAD4 binding increases in EKO, independent of a SALL1 binding site.
G. Histograms of normalized H3K27ac and SMAD4 counts from EKO and WT microglia at peak subsets defined in 3C. Red = WT. Blue = EKO.
H. Schematic of the proposed collaboration between SALL1 and SMAD4 in determining microglia identity

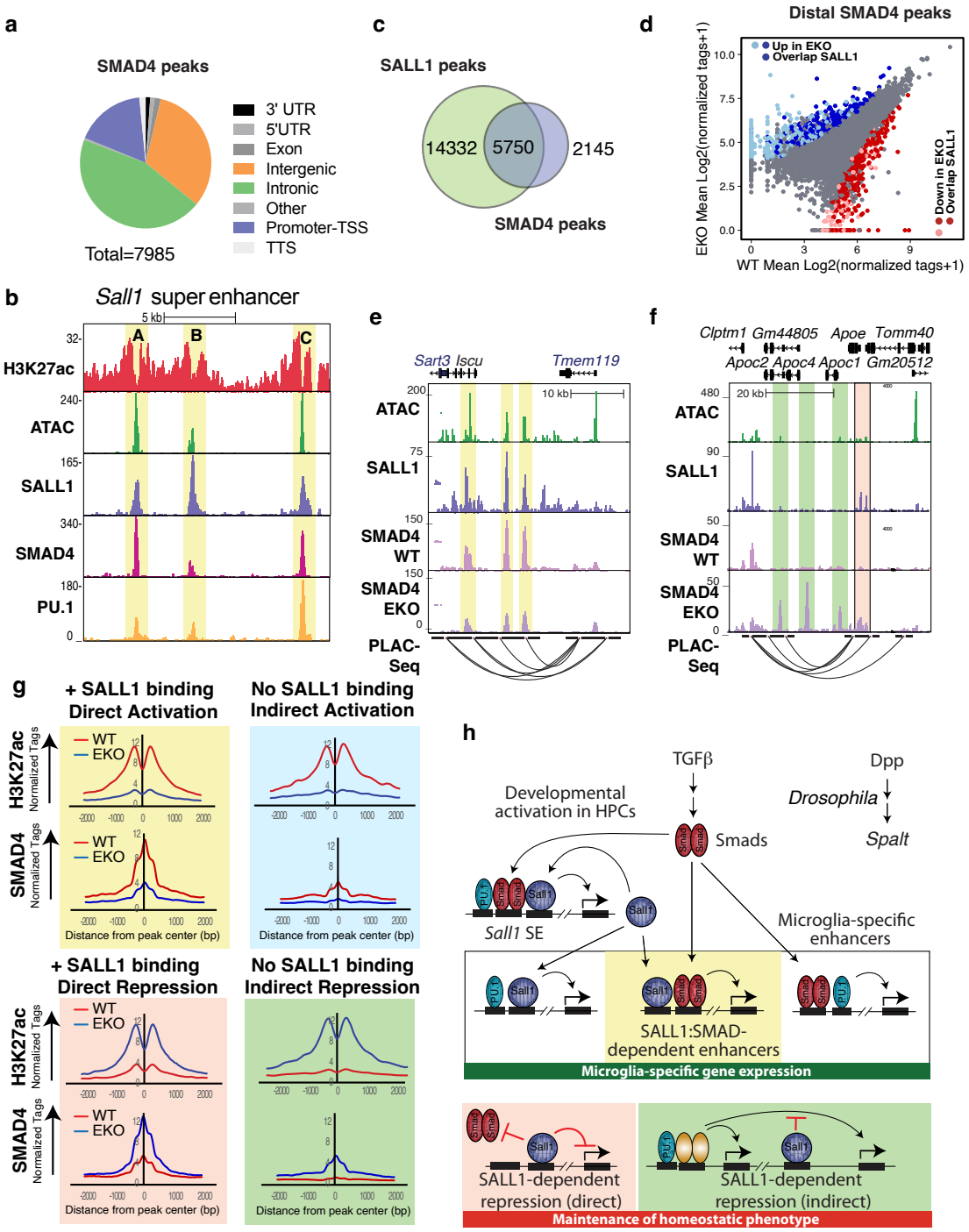
a
SMAD4 peaks
3' UTR
5'UTR
Exon
Intergenic
Intronic
Other
Promoter-TSS
TTS
Total=7985
c
SALL1 peaks
14332
5750
2145
SMAD4 peaks
d
Distal SMAD4 peaks
Up in EKO
Overlap SALL1
Down in EKO
Overlap SALL1
EKO Mean Log2(normalized tags+1)
WT Mean Log2(normalized tags+1)
b
Sall1 super enhancer
5 kb
A
B
C
H3K27ac
ATAC
SALL1
SMAD4
PU.1
e
Sart3 Iscu
Tmem119
10 kb
ATAC
SALL1
SMAD4 WT
SMAD4 EKO
PLAC-Seq
f
Clptm1 Gm44805 Apoe Tomm40
Apoc2 Apoc4 Apoc1 Gm20512
20 kb
ATAC
SALL1
SMAD4 WT
SMAD4 EKO
PLAC-Seq
g
+ SALL1 binding
Direct Activation
No SALL1 binding
Indirect Activation
H3K27ac
SMAD4
Normalized Tags
WT
EKO
Distance from peak center (bp)
+ SALL1 binding
Direct Repression
No SALL1 binding
Indirect Repression
h
TGFβ
Dpp
Developmental activation in HPCs
Drosophila
Spalt
Smads
Sall1 SE
Microglia-specific enhancers
SALL1:SMAD-dependent enhancers
Microglia-specific gene expression
SALL1-dependent repression (direct)
SALL1-dependent repression (indirect)
Maintenance of homeostatic phenotype

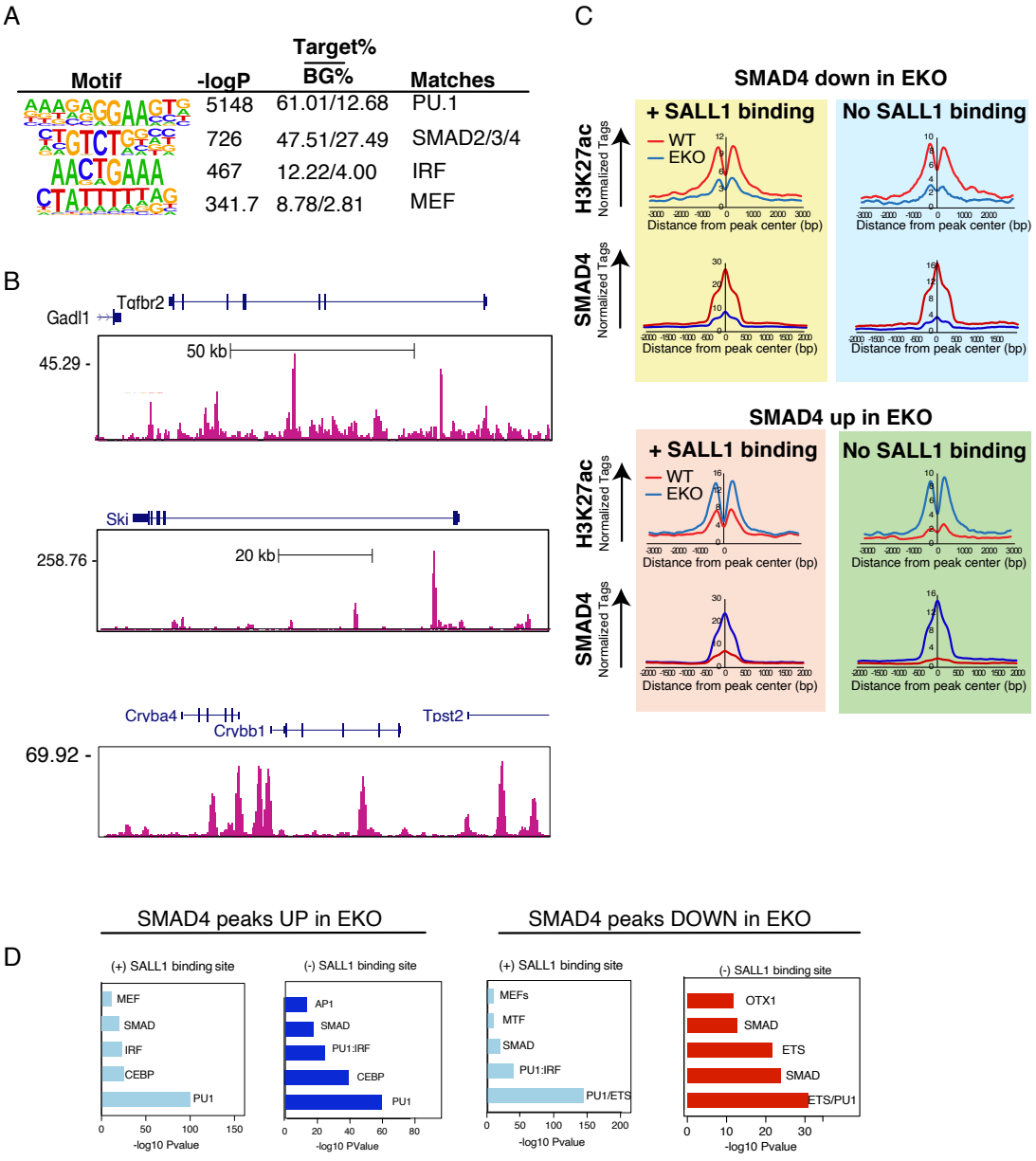

Supplemental Figure 2.5:
A. *De novo* motifs identified in IDR-defined SMAD4 peaks in WT microglia
B. Genome browser of WT SMAD4 binding at microglia genes and TGF-beta responsive genes
C. Histogram of H3K27ac and SMAD4 signal at differential, distal SMAD4 peaks in EKO vs WT.
D. *De novo* motif analysis of the SMAD4 peak subsets identified in Supplementary Figure 5C

2D. Discussion:

Here we demonstrate that a conserved genomic region 300kb upstream of the *Sall1* gene functions as a cell-specific super enhancer required for expression of *Sall1* in microglia. The finding that this regulatory region is occupied by SMAD4 and that *Sall1* expression requires TGFβ signaling [50] is consistent with a model in which TGFβ induces *Sall1* in yolk sac-derived hematopoietic progenitor cells that enter the embryonic brain by directly activating the *Sall1* super enhancer via SMADs (Figure 2.5H, top left). The observation that SALL1 itself binds to the super enhancer in concert with SMAD4 further suggests the possibility of a positive feedback loop that amplifies *Sall1* expression. Remarkably, studies of the homologous *Spalt* gene in *Drosophila* demonstrated that its expression in specific regions of the wing requires *Dpp*, a Drosophila homologue of TGFβ [83, 130]. The conservation of a hierarchical relationship in which TGFβ/Dpp regulate the expression of *Sall1/Spalt* in a cell-specific manner from *Drosophila* to mammalian cells suggests that the mechanisms by which *Sall1* shapes the transcriptional response to expanded upon here in microglia may operate in other organ systems in which loss of *Sall1* results in developmental defects. Although TGFβ signaling through SMADs is essential for developmental activation and homeostatic expression of *Sall1*, TGFβ is not sufficient to maintain *Sall1* expression when microglia are transferred to an *in vitro* environment, or to activate *Sall1* expression in microglia-like cells that are differentiated from iPSCs in vitro [61, 76]. The identities of the additional signaling factors required to induce Sall1 expression within the brain remain enigmatic, but we speculate that they are likely exerting their effects through the *Sall1* super enhancer.

The genome wide binding profiles of SALL1 and SMAD4, in concert with epigenetic analyses of WT and EKO microglia, provide strong evidence for an unexpected and additional layer of functional interactions between these two proteins that results in activation of hundreds of regulatory elements that are associated with the expression of microglia identity genes. We also find evidence that SALL1 can function as a transcriptional activator independently of SMAD4 and vice versa, which is likely occurring through collaborative interactions with other microglia lineage determining factors (microglia-specific enhancer box in model figure). Collectively, these findings support direct roles of SALL1 and SMADs acting together and independently in the selection and activation of a large fraction of the enhancers that regulate microglia-specific patterns of gene expression.

The downstream relationship of *Sall1* from the TGFβ -SMAD signaling axis is sufficient to partially explain similarities in altered gene expression resulting from loss of expression of *Sall1* in EKO microglia and conditional loss of expression of SMAD4. Past studies of SALL1's role in microglia have focused primarily on its ability to repress an inflammatory gene expression profile and amoeboid phenotype in microglia [72, 81]. However, studies of other cell systems, such as embryonic stem cells and kidney progenitors, revealed that SALL1 can potentially function as both an activator and as a repressor depending on posttranslational modifications of SALL1 and through its interactions with key cell lineage determining factors and the NuRD histone remodeling complex [100, 104, 105, 131, 132].

Prior studies of *Sall1* in other model systems have emphasized its roles as a transcriptional repressor [98, 103]. However, the genome wide binding profiles of SALL1

and SMAD4, in concert with epigenetic analyses of WT and EKO microglia, provide strong evidence for an unexpected layer of functional interactions between these two proteins that results in direct activation of hundreds of regulatory elements that are associated with the expression of microglia identity genes (Figure 2.5H, yellow box). We also find evidence that SALL1 can function as a transcriptional activator independently of SMAD4 and vice versa, likely through collaborative interactions with other microglia lineage determining factors (Figure 2.5H). Collectively, these findings support direct roles of SALL1 and SMADs acting together and independently in the selection and activation of a large fraction of the enhancers that regulate microglia-specific patterns of gene expression.

The observation that hundreds of genes are upregulated in EKO microglia also supports functions of SALL1 as a transcriptional repressor that is required to maintain a microglia-specific and homeostatic phenotype. We observe evidence for both direct and indirect mechanisms of repression. Examples of direct repression are provided by the ~309 SMAD4 peaks that are gained in EKO cells at genomic locations that are occupied by SALL1 in WT microglia. In these cases, SALL1 appears to exert a local repressive function by preventing access of SMADs that would otherwise contribute to enhancer activity (Figure 2.5H, pink box), thereby restricting the scope of TGFβ/SMAD-dependent gene expression to a microglia-specific pattern. The observation that H3K27ac levels increase at more than 700 SALL1 binding sites in EKO microglia suggests that SALL1 plays similar roles to restrict the binding and function of transcription factors beyond the family of SMADs. The mechanisms that determine

whether SALL1 acts to locally enhance or inhibit SMAD4 binding and functionality represent an important question for future investigation.

The most numerous examples of upregulated enhancers in EKO microglia are not associated with local binding of SALL1, as exemplified by enhancers in the vicinities of the *Apoe* and *Ms4a* genes. At these locations, clusters of closely positioned genes in EKO microglia are upregulated up to 100s of fold above levels observed in WT microglia. These regions reside within active chromatin domains as determined by Hi-C assays in WT microglia and exhibit basal levels of open chromatin and H3K27ac. Thus, the dramatic increases in H3K27ac and gene expression are not due to large scale shifts from heterochromatin to euchromatin. Although there is preferential enrichment for AP-1 motifs within these regions, there is otherwise no evidence for increased expression of these factors. These findings suggest that SALL1 exerts indirect control over distal regions of chromatin by binding to key regulatory elements within or at the borders of such regions. Such a mechanism would be consistent with the recent identification of coordinately regulated enhancers and genes within so called Cis Regulatory Domains [133], Variable Chromatin Domains [134] and Highly Inter-Connected Enhancers [135] in which the activities of many regulatory elements are proposed to be dependent on a master control element within the regulatory domain. In this context, SALL1 could serve to prevent the activation of such a master control element or serve as an insulator defining the boundary of its activity (Figure 5H, green box). In this model, loss of SALL1 would thus lead either to activation of an element controlling multiple genes and enhancers or allow such an element to act over a longer genomic distance. The positions of SALL1 peaks in the vicinity of the Apoe and Ms4a loci are

consistent with SALL1 functioning as an insulator to prevent activation of genes between these peaks from being activated by enhancers outside of the peaks.

We identified a significant overlap between genes increased in aged microglia and genes increased in EKO microglia. Our RNA-seq data also identified several loci associated with Alzheimer's disease whose expression is affected in EKO microglia. These data indicate that SALL1 may be playing a role in the transcriptional network associated with disease pathophysiology, and that changes in *Sall1* expression, whether due to genetic variation or changes in signals acting at the super-enhancer, may influence the behavior of microglia in disease.

Using ChIP-seq, we identified the putative binding sites of SALL1 in microglia; *de novo* motif analysis shows that SALL1 is likely binding at the same sites as several microglia LDTFs, such as PU.1, IRFs, and MEF family members. The enrichment of motifs for microglia lineage determining transcription factors at SALL1 binding sites is consistent with roles of these factors as collaborative binding partners that drive the selection and function of the microglia-specific regulatory landscape[61, 68]. Notably absent from the motif enrichment profiles of enhancer-like elements bound by SALL1 and either gaining or losing H3K27ac, or of the entire set of SALL1 peaks, was the presence of a motif that could be uniquely connected to SALL1 itself. It is unlikely that this is due to lack of specificity of the ChIP assay because ChIP-Seq for SALL1 in EKO microglia yielded a pattern similar to input DNA with 68 peaks, only 63 of which overlapped with WT peaks (0.3% of the total reproducible peaks, Supplementary Figure 3E). SALL1 is a member of the C2H2 zinc finger family of transcription factors; while this family is fairly well-studied, the precise manner in which these factors interact with

DNA, RNA, and other proteins is not fully understood[136]. Previous studies demonstrated that the fourth zinc finger of SALL1 and family members such as SALL4 binds to AT-rich sequences associated with pericentric heterochromatin, a form of constitutive heterochromatin located in chromocenters, which can organize into clusters in the nucleus and play a role in meiosis[100, 103, 107, 108, 137-139]. The present studies are limited with respect to interpretation of SALL1 binding and function at such heterochromatic regions in microglia due to the nearly exclusive representation of SALL1 peaks in regions of gene-rich open chromatin as defined by the PC1 component of HiC data. However, our findings are consistent with the major transcriptional effects of SALL1 in microglia being due to its binding to these gene-rich, euchromatin-associated regions. Interestingly, AT-rich sequences were among the most highly enriched motifs at SALL1 binding sites, but were assigned to MEF family members, which are also expressed in microglia. It is possible that SALL1 is using its multiple zinc finger clusters in different ways at positively and negatively regulated enhancers to either bind directly to DNA at MEF-like motifs or interact with DNA indirectly through collaborations with other transcriptional regulators. Future studies will be necessary to clarify these mechanisms. However, most studies describing SALL1's localization to AT-rich regions of DNA focused on the role of SALL1 at pericentromeric heterochromatin (PCH), a form of constitutive heterochromatin located in chromocenters, which can organize into clusters in the nucleus and play a role in meiosis[138, 139]. Given the technical challenges associated with sequencing the repetitive tandem satellite repeats inherent to PCH, our observations of SALL1 binding sites in microglia are most likely representative of its function in gene-rich regions rather than at regions of

heterochromatin. It is possible that the binding sites we identified represent loci where SALL1 is using its multiple zinc finger clusters to either bind directly to DNA or interact with DNA indirectly through collaborations with other transcriptional regulators; future studies will be necessary to further clarify the DNA binding motif and binding partners of SALL1 in microglia.

We show that staining for SALL1 in mouse brain sections reveals that SALL1 is localized to multiple bright puncta near DAPI-dense regions in the nucleus of microglia, and that these puncta disappear in EKO microglia, potentially reflecting its localization to chromocenters [103, 106]. SALL1's putative role in binding to PCH raises additional questions surrounding its function in basic microglial biology. Does SALL1 play a role in the formation and maintenance of PCH, and is this linked to SALL1's known role as a factor maintaining pools of progenitor cells during development? Microglia are one of the few TRM populations that rely on self-renewal to maintain appropriate cell numbers[140], and *Sall1* is uniquely expressed in microglia compared to other TRMs[58]; this raises the question as to whether SALL1 is involved in network of transcriptional regulators controlling the process of microglial self-renewal. Interestingly, we observe a lower density of Iba1+ cells in adult EKO versus WT brain sections, which indicates that loss of *Sall1* may 1) affect the number of microglia precursors entering the brain early in development, 2) impede the ability of microglia to initiate or complete self-renewal or 3) result in the premature death of microglia with no replacement. Future studies of the EKO mice will be needed to further characterize the effects of SALL1 on microglia self-renewal.

In the studies described here, we show that the *Sall1* super-enhancer is microglia-specific, and that deletion of this enhancer leads to loss of *Sall1* transcript, a complete ablation of active chromatin defined by H3K27ac-seq signal, open chromatin defined by ATAC-seq, and binding of several transcription factors across the entire *Sall1* locus in microglia. As expected, the chromatin at this locus switched from active chromatin in Compartment A to heterochromatin in Compartment B. These changes are reminiscent of what has been described for locus control regions (LCRs). LCRs are described as genomic regions that open chromosomal domains and enhance the tissue-specific, and copy-number dependent of expression of linked genes[141]. A closer look at the *Sall1* locus in microglia reveals that the *Sall1* gene is not the sole transcript in the region spanning from *Sall1* to its associated super-enhancer. A microRNA (miRNA), mir8110, lies +2367bp away from the *Sall1* gene. It is widely appreciated that miRNAs are expressed in microglia[50] and potentially play a role in microglial activation during disease conditions [142], yet the full profile and functions of miRNAs expressed in microglia at steady-state have not been comprehensively studied. It is possible that mir8110 is regulated in tandem with the *Sall1* gene by the SE in microglia; however, further work is needed to elucidate the function and regulation of this miRNA in microglia.

Interestingly, a long non-coding RNA (lncRNA) called Gm3134 (*Sall1os)* shares the *Sall1* promoter and runs in the opposite direction of *Sall1.* The human *SALL1* gene is similarly associated with a lncRNA, indicating that there may be conservation of the *Sall1* gene's association with a lncRNA. Promoter-associated noncoding RNAs (pancRNAs) are known to perform roles as cis-acting regulatory elements in the

transcription of neighboring genes through the recruitment of transcriptional regulators and the formation of active chromatin [143, 144]. lncRNAs can also play cell and tissue type-specific roles in cellular differentiation and development [145, 146]. Gm3134 is expressed in the adult and embryonic brain, kidney, and liver[147], but its expression in steady-state microglia is unknown. It is possible that this pancRNA is modulating the induction or maintenance of *Sall1* expression in a microglia-specific manner, but further studies will be required to validate its role in the regulation of *Sall1.*

Several predicted genes, including Gm35358, Gm6625, Gm5356, Gm35542, Gm26331, and Gm24212 are in the region spanning *Sall1* and its SE. Whether these transcripts are detectable or functional in microglia remains to be determined. Taken together, the effect of the EKO on the *Sall1* locus plus the presence of additional putative transcripts spanning this region suggests that the super-enhancer may be functioning as a LCR, however, more work, such as a more precise deletion of the *Sall1*-associated SE's individual elements and *in vitro* reporter assays, will be required to test this hypothesis.

We also found that dose of the *Sall1* SE and dose of *Sall1* regulated microglia gene expression. Het EKO microglia, which express *Sall1* at 50% of baseline levels, downregulate multiple key microglia genes and upregulate genes associated with inflammation, such as *Apoe* and *Axl.* This observation of full *Sall1* expression being necessary for proper gene expression is consistent with what is observed in patients presenting with mild Townes Brocks Syndrome whose mutations fall outside of the protein-coding region of *SALL1,* rendering them *SALL1* haploinsufficient [87]*.* Our finding that *Sall1* Het KO microglia exhibit altered transcriptional profiles has ramifications for

the neuroimmune field and the use of various transgenic mouse models. Multiple studies have utilized *Sall1*-GFP and *Sall1*^{creER} mouse models to observe microglia and to knockout genes in what is thought to be a microglia-specific manner[72, 81]. However, given that these mouse models were created using a knock-in approach, all microglia in these mice will be heterozygous for *Sall1.* Since we observe that *Sall1* dose is important for the expression of some microglia genes and the repression of inflammatory genes, it begs the question as to whether these mouse models are appropriate for studying microglial biology during both steady-state and disease conditions.

It is also known that mouse microglia express other SALL family members, *Sall2* and *Sall3,* and that SALL family members can homo- and heterodimerize[61, 148]. We found that *Sall1* does not regulate levels of *Sall3* or *Sall2* in microglia, which indicates that these factors might play a compensatory role in EKO microglia at regions where SALL1 binds. To better understand how SALL1 interacts with SALL2 and SALL3 in microglia to guide transcriptional responses to the brain environment, and therefore microglia identity, additional ChIP-seq assays will need to be performed in microglia throughout development and after perturbation.

Taken together, the completed studies are the first to examine the regulation of *Sall1* by a putative gene regulatory element and the binding sites, transcriptional function, and collaborating factors associated with SALL1 in microglia. The results of these studies will bolster the present understanding of basic microglial biology and provide a stronger framework for understanding how basal microglial conditions are altered in disease states.

In concert, the present studies identify a conserved microglia-specific super enhancer that is activated by SMADs and is required for expression of *Sall1*. Investigation of the genome wide binding of SALL1 and SMAD4 and the epigenetic consequences of the loss of each protein provide evidence for functional interactions between these proteins that enable TGFβ to induce a microglia-specific program of gene expression. The finding that haploinsufficiency for *Sall1* is associated with significant changes in the expression of genes associated with aging and neurodegenerative diseases raises the possibility that quantitative changes in its expression could contribute to disease phenotypes. Among the intriguing and unanswered questions that remain to be solved are why activation of the *Sall1* gene is restricted to hematopoietic progenitor cells and what are the identities of brain environmental factors required in addition to TGFβ to turn on and maintain *Sall1* expression in microglia. Further studies of the *Sall1* super enhancer are likely to provide insights into these questions.

2E. Materials and Methods:

Mice

All animal procedures were approved by the University of California San Diego Animal Care and Use Committee in accordance with the University of California San Diego research guidelines for the care and use of laboratory animals. The following mice were used in this study: C57BL/6J (The Jackson Laboratory, Stock No. 00064), *Sall1* EKO (generated by Glass lab and transgenic core facility, University of California, San Diego), Cx3cr1^{CreER} [54](The Jackson Laboratory, Stock No. 020940), and *Smad4*$^{fl/fl}$ [149](The Jackson Laboratory, Stock No. 017462). For experiments with C57BL/6J and *Sall1* EKO, mice were used between 8-12 weeks of age. Experiments for targeted, inducible deletion of *Smad4* were performed on mice at 2 weeks of age.

Generation of *Sall1* EKO Mouse

sgRNA Design and Testing

sgRNAs targeting the selected 5' and 3' regions of the *Sall1* enhancer were designed using the Broad Institute's Genetic Perturbation Platform sgRNA Designer with the mouse reference genome and 'NGG' specified for enzyme (https://portals.broadinstitute.org/gpp/public/analysis-tools/sgrna-design). The top 5 sgRNAs for each end of the deletion were further filtered using the Integrated DNA Technologies CRISPR-cas9 guide RNA design checker (https://www.idtdna.com /site/order/designtool /index/CRISPR_SEQUENCE), and the 3 guides per end of the enhancer with the highest scores were selected for additional testing in an *in vitro* cutting assay. To amplify DNA templates for the cutting assay, 50 ng of genomic DNA from C57Bl6J mice was amplified using 10 μM of primer pairs (primers:

TTGTACTCGAGTAGAGCCATGCTCGG, CAGGGCTCTGGGCTTTGATGCT , AGTGCTTCTGGGGCAACGTGGA , GGCTTCTGCAAAGTGAGGGCTCCA, CAGCAAGTGTTTGATGCTTATCTCCCGT, GCCCAAAGTTCAAAGACCTGCTGT, GGAGAGTGTTCTGGAAAGCAGGGAGA, CTGGCATCTGGAGTCCCAGACACT, CATCAGAGGTGGAAAGCCCAGCA, CCACTTTGGGAGGTGACACATGGT), 25 µL of 2x Xtreme buffer, 10 µL of 2mM dNTPs, 10 µL of nuclease free water, and 1 µL of KOD Xtreme Hot Start DNA polymerase. The DNA fragments were amplified according to the KOD manufacturer protocol, ran on a 1.5% agarose gel, and purified using Nucleospin gel extraction kits and eluted in 15 µL of nuclease free water. crRNAs and tracrRNAs were dissolved in IDTE (pH 7.5) at a concentration of 100 µM. To create 10 µM annealed guide RNA, 2 µL of crRNA, 2 µL of tracrRNA and 16 µL of IDTE (pH7.5) were mixed and incubated at 95℃ for 5 minutes with a ramp down of 5℃/min until 25℃. For *in vitro* digestion, 3 µL of Cas9 protein (300ng/ µL), 3 µL of 10 µM annealed guide RNA, 3 µL of 10X Cas9 reaction buffer 6 µL of 150 ng/ µL PCR product, and 15 µL of nuclease free water was incubated at 37℃ for 1 hour. Equal amounts of each reaction were run on a 1.5% agarose gel, and the cutting efficiency was measured using ImageJ [150]. The two best-cutting guide RNAs for each end of the enhancer were selected for use in the germline deletion of the enhancer.

Super Ovulation of mice

16 female mice were super-ovulated. Overnight matings were set up, and the following morning the oviducts of each female mouse were harvested. Injection of sgRNAs and Cas9 protein into pronuclei of one cell stage zygotes was performed by the UCSD Transgenic Animal Core.

Preparation of sgRNAs for injection into fertilized eggs

Preparation of sgRNAs was performed as previously described [151]. On the morning of the injection day the reagents were prepared as follows: Each crRNA (protospacers: GAATGACCCTGGCAATCATG, TCCATAAGATAGCTTAGGGA, CTTGACAGACATT ACACAGG, CTAGAATCGGCTTTGGTGCT) was annealed to tracRNA in IDTE (pH 7.5) at 95℃ for 5 minutes ramped down to 25℃ at 5℃ per minute. Cas9 protein (NEB#M0646T) was diluted in IDTE (pH 7.5) and incubated with annealed guide RNAs for 10 minutes at room temperature. ssODN and IDTE were then mixed and incubated at room temperature for another 5 minutes, and spun at 10,000 rpm for 1 minute. The supernatant was transferred to a new tube and transferred to the UCSD Transgenic Core for injection.

Confirmation of enhancer deletion and genotyping of enhancer deletion mice

Genetically targeted mice from the CRISPR-mediated deletion were screened by PCR with KOD Xtreme Hot Start DNA polymerase (EMD Millipore) using three primers: 5'F (GGAGAGTGTTCT GGAAAGCAGGGAGA), 5'R internal to the deletion (CTGGCATCTGGAGT CCCAGACACT) and 3'R (GCCCAAAGTTCAAAGACC TGCTGT). 5'F + 5'R internal amplified a 582-bp band from the WT allele and no band from the EKO allele. 5'F and 3'R amplified a 431 bp band from the EKO allele and no band from the WT allele. *Sall1* EKO mice were crossed to C57BL/6J WT mice for at least three generations.

Tamoxifen-mediated deletion of *Smad4*

Cx3cr1^{CreER} mice were crossed to *Smad4*$^{fl/fl}$ mice to generate Cx3cr1^{CreER} *Smad4*$^{fl/fl}$ mice. Mice were treated 2x with tamoxifen; 75µg at P0 and 50µg at P1 and microglia were harvested at P14.

Flow Cytometry to Sort Live Microglia

Mouse brains were homogenized as previously described [59, 61] by gentle mechanical dissociation in staining buffer (1x HBSS (GIBCO), 1mM EDTA, 0.5% BSA) on ice using a 2mL polytetrafluoroehthylene pestle in 5 mL FACs tubes, followed by a 2mL glass mortar. For PLAC-seq cell preparations, sodium butyrate was added to all buffers. Homogenates were filtered through 70 µM strainers and centrifuged for 10 minutes at 400xg at 4°C. The pelleted homogenate was then resuspended in 10mL of 33% isotonic Percoll in a 15 mL centrifuge tube. The tubes were centrifuged at 600xg for 30 minutes at 16-17°C, with no acceleration or deceleration. Supernatant was removed and the cell pellet was washed 3x with staining buffer. Cells were then incubated in staining buffer on ice with anti-CD16/32 blocking antibody (BioLegend 101319) for 15 minutes, and then with anti-mouse anti-CD11b-APC (BioLegend 101212), anti-CD45-Alexa488 (BioLegend 103122), and anti-CX3CR1-PE (BioLegend 149006) for 25 minutes. Cell preparations for H3K27ac ChIP-seq, PLAC-seq, and Hi-C were fixed with 1% formaldehyde for 10 minutes and quenched with 0.125M glycine for 5 minutes after staining, and subsequently washed three times. Cells were washed once and filtered through a 40 µM cell strainer. Sorting was performed on a Sony MA900 or MoFlo Astrios EQ cell sorter. Microglia were defined as events that were DAPI negative,

singlets, and $CD11b^{+}CD45^{low}CX3CR1^{+}$. Isolated microglia were then processed according to protocols for RNA-seq, ATAC-seq and ChIP-seq, Hi-C, and PLAC-seq.

Immunostaining for SALL1 and IBA1

8 weeks old female WT and *Sall1* EKO mice were perfused with 2% PFA, and then the brains were harvested and fixed in 4% PFA in PBS overnight at 4°C. After fixation, the brains were washed three times in PBS and cryoprotected in 30% sucrose and embedded in Neg-50 (epredia) for subsequent cryosection. 20 μm sections were cut on cryostat, mounted on Superfrost plus slides (Thermo Scientific, Menzel-Glaser), dried at 37ºC and subjected to immunofluorescence staining. For immunofluorescence, sections were rehydrated, rinsed in PBS for three times, 5 min each. Sections were permeabilized in 0.3% Triton X-100 in PBS and blocked in Blocking Solution (5% normal donkey serum in PBST) in a humidified chamber for 1 hour at room temperature (RT). Slides were then incubated with the appropriate primary antibodies diluted in blocking solution at 4°C overnight. The primary antibodies were Rat anti-Sall1 (Proprietary antibody, Thermo Fisher), and Rabbit anti-IBA1 (FijiFilm, 019-19741).The next day, sections were washed three times (10 min each) in PBST, incubated with appropriate fluorophore-conjugated secondary antibodies (Donkey anti-Rat 555, Invitrogen SA5-10027; Donkey anti-Rabbit 488, Invitrogen R37118) diluted in blocking solution at RT for 2 hrs, washed three times (10 min each) in PBST, counter-stained with DAPI for 10 min, rinsed once in PBS and mounted with Prolong Gold antifade reagent (Invitrogen, P36931).

Quantification of cell morphology and density

Deeply anesthetized mice were transcardially perfused at room temperature with 0.9% saline followed by freshly prepared 4% paraformaldehyde (PFA) in phosphate-buffered saline (PBS) and then post-fixed in 4% PFA at 4 °C for 24 h followed by cryoprotection for 24 h at 4 °C in 20% sucrose. Brains were frozen in a plastic mold containing Tissue Freezing Medium (General Data Inc.), and quickly frozen in isopentane on dry ice. Briefly, 30μM coronal slices were collected and kept in 0.01M PBS at 4°C until use. Sectioned brains were scored according to their distance from Bregma (Franklin & Paxinos, 2007). Brain slices containing the prefrontal cortex (PFC) (AP: +2.8 to +1.8) were permeabilized in optimized detergent (e.g. 0.1% Triton-X-100) and blocked in normal horse serum (Thermo Fisher) for 1 hour at room temperature. Sections were then incubated with primary antibodies overnight at 4 °C. Sections were then incubated with the corresponding secondary antibody for 2 h at room temperature. Finally, sections were mounted, dehydrated, and cover slipped with Immunoblot mounting medium (Thermo Fisher). Sections were imaged on a TCS SPE confocal microscope (Leica) (1024 × 1024 pixel, 16-bit depth, pixel size 0.63-micron, zoom 0.7). Images were acquired within brain regions using 40x-63x objectives. Z-stack images containing 6-10 microglia per ROI (40 μm depth, 1 μm steps, 40x magnification, n=15/brain region) were obtained. Raw files were used for further analysis using ImageJ [150]. Microglia were then segmented, and morphology was assessed in two-dimensional (2D) and three-dimensional (3D) space. For 2D analysis, maximum intensity projections of the XY planes were used. ImageJ's analysis for perimeter were measured in 2D for soma size and surface area was measured in 3D using the custom '3DShape' plugin as

previously described[152]. Density was measured using maximum intensity projections of the XY plane and the ImageJ automated cell-counting plugin ITCN [153].

Sorting crosslinked brain nuclei

Brain nuclei were isolated as previously described[32, 154]. Frozen brain tissue was homogenized in 1 mL of fixative (either 1% formaldehyde in Dulbecco's phosphate buffered saline or 2mM DSG (Proteochem) in Dulbecco's phosphate buffered saline) and incubated (10 minutes for formaldehyde or 30 minutes for DSG followed by 10 minutes of 1% formaldehyde fixation) at room temperature. The fixation was quenched by adding 0.125 M glycine for 5 minutes at room temperature. The fixed homogenate was pelleted at 1600xg for 5 minutes at 4°C. The following steps were performed at 4°C or on ice. The homogenate was washed two times with NF1 buffer (10mM Tris-HCl pH 8.0, 1mM EDTA, 5 mM MgCl2, 0.1M sucrose, 0.5% TritonX-100). The homogenate was then incubated on ice in 5mL NF1 buffer for 30 minutes and was subsequently dounced using a 7mL Wheaton Dounce Tissue grinder 20 times with the loose pestle and 5 times with the tight pestle. Homogenates were underlaid with a 1.2M sucrose cushion and centrifuged at 3900xg for 30 minutes at 4°C with no brake and no acceleration. Pelleted nuclei were washed one time with NF1 buffer and one time with FACs buffer (PBS, 1% BSA, 1mM EDTA). Nuclei were resuspended in 300 µL FACs buffer and stained overnight with PU.1-PE (Cell Signaling 81886S), OLIG2-AF488 (Abcam 225099) or SALL1 AF647 (Thermo, clone NRNSTNX 51-9279-82) or NEUN-AF488 (Millipore MAB 377X). Nuclei were washed the following day with 4 mL FACs buffer, passed through a 40 uM strainer, and stained with 0.5 µg/mL DAPI. Nuclei for each cell type were sorted

with a Beckman Coulter MoFlo Astrio EQ cell sorter and pelleted at 1600xg for 5 minutes at 4°C in FACs buffer. Nuclei pellets were snap frozen and stored at -80°C prior to library preparation.

ATAC-seq library preparation

ATAC-seq libraries were prepared as previously described [155, 156]. Approximately 50,000 sorted live microglia were washed once with cold lysis buffer (10mM Tris-HCl, pH 7.4, 10mM NaCl, 3mM MgCl2, 0.1% IGEPAL CA-630). Cells were then suspended in 50 μL 1X reaction buffer (25 μL Tagment Buffer, 2.5 μL Tagment DNA enzyme I, and 22.5 μL water)(Nextera DNA Library Preparation Kit, Illumina) as previously described [155]. DNA was purified using ChIP DNA Clean & Concentrator kits (Zymo Research). DNA was amplified using the Nextera primer Ad1 and a unique Ad2.n barcoding primer using NEBNext High-Fidelity 2XPCR Master Mix (NEB) for 12 cycles. Resulting libraries were size selected by gel excision to 155-250 bp, purified, and single end sequenced using a HiSeq 4000 (Illumina) for 51 cycles according to the manufacturer's instructions.

RNA-seq library preparation

Approximately 100,000 sorted live microglia were pelleted at 450xg at 4°C for 10 minutes. 100 μL of supernatant was left on the cell pellet and 500 μL of Trizol-LS (Thermo Fisher) was mixed with the sample prior to freezing at -80°C. Total RNA was isolated and purified using a Direct-zol RNA Microprep kit (Zymo Research) according to the manufacturer's instructions. mRNAs were enriched by incubation with Oligo d(T) Magnetic beads (NEB, S1419S) in 2X DTBB buffer (20 mM Tris-HCl pH 7.5, 1 M LiCl,

2mM EDTA, 1% lithium dodecyl sulfate, 0.1% Triton X-100) at 65°C for 2 minutes and were incubated at room temperature while rotating for 15 minutes. The beads were then washed 1x with RNA Wash Buffer 1 (10mM TrisHCl pH 7.5, 0.15M LiCl, 1mM EDTA, 0,1% lithium dodecyl sulfate 0.1% Triton X-100) and 1x with RNA Wash Buffer 3 (10mM Tris-HCl pH 7.5, 0.15 M NaCl, 1mM EDTA) before elution in RNA Elution Buffer (10mM Tris-HCl pH 7.5, 1mM EDTA) at 80°C for 2 minutes. PolyA selection was performed a second time, and samples were washed 1x with Wash Buffer 1, 1x with Wash Buffer 3, and 1x with 1x SuperScript III first-strand buffer. Beads were then resuspended in 10 µL 2x SuperScript III buffer plus 10 mM DTT, and RNA was fragmented at 94°C for 9 minutes and immediately chilled on ice before the next step. For first-strand synthesis, 10 µL of fragmented mRNA, 0.5 µL Random primers (50 µM)(Thermo Fisher), 0.5 µL SUPERase-In (Ambion), 1µL dNTPs (10mM), and 1µL of DTT (10mM) were heated for 50°C for one minute. At the end of incubation, 5.8 µL of water, 1 µL of DTT (100mM), 0.1 µL Actinomycin D (2µg/uL), 0.2uL of 1% Tween-20 (Sigma) and 0.5µL of SuperScript III (Thermo Fisher Scientific) were added and incubated in a PCR machine using the following conditions: 25°C for 10 minutes, 50°C for 50 minutes, and a 4°C hold. The product was then purified with RNAClean XP beads (Beckman Coulter) according to manufacturer's instruction and eluted with 10 µL nuclease-free wate. The RNA/cDNA double-stranded hybrid was then added to 1.5 µL Blue Buffer (Enzymatics), 1.1 µL of dUTP mix (10mM dATP, dCTP, dGTP and 20 mM dUTP), 0.2 µL RNase H (5U/uL), 1.05 µL of water, 1µL of DNA Polymerase I (Enzymatics) and 0.15 µL of 1% Tween-20. The mixture was incubated at 16°C overnight. The following day, the dUTP marked dsDNA was purified using 28 µL of SpeedBeads (GE Healthcare), diluted with

20% PEG8000, 2.5M NaCl to a final concentration of 13% PEG, eluted with 40 µL elution buffer (DNA elution buffer from Zymo ChIP Clean and Concentrator Kit). The purified dsDNA underwent end repair by blunting, A-tailing, and adaptor ligation as previously described [157] using barcoded adapters (NextFlex, Bioo Scientific). Libraries were PCR amplified for 16 cycles, size for 200-500bp size range, quantified using a Qubit dsDNA HS Assay Kit (Thermo Fisher Scientific) and sequenced on a HiSeq 4000 for 51 cycles according to the manufacturer's instructions.

ChIP-seq Library Preparation

Chromatin immunoprecipitation was performed as previously described [158, 159]. For H3K27ac ChIP, 500,000-1,000,000 fixed cells or nuclei were thawed on ice and resuspended in ice-cold LB3 (10mM Tris-HCl pH 7.5, 100mM NaCl, 1 mM EDTA, 0.5mM EGTA, 0.1% Na-Deoxycholate, 0.5% N-lauroylsarcosine), 1x protease inhibitor cocktail (Sigma). Chromatin was sheared by sonication. Samples were sonicated in a 96 Place microtube Rack (Covaris cat#500282) using a Covaris E220 for 12 cycles with the following setting: time 60 seconds, duty cycle 5.0, PIP 175, cycles, 200, amplitude 0.0, velocity 0.0, dwell 0.0. Samples were recovered and spun down at max speed, 4°C for 10 minutes. The supernatant was then diluted 1.1-fold with ice-cold 10% Triton X-100. One percent of the lysate was kept as ChIP input. 25 µL of Dynabeads Protein A were added per sample, in addition to 1µg of a specific antibody for H3K27ac (Active Motif 39685). The samples were rotated overnight at 4°C and were washed as follows the next day: 3x with Wash Buffer I (20mM Tris-HCl pH 7.5, 150 mM NaCl, 2mM EDTA, 0.1% SDS, 1% Triton X-100) + protease inhibitor cocktail, 3x with Wash Buffer III

(10mM Tris-HCl pH 7.5, 250 mM LiCl, 1% Triton X-100, 1mM EDTA, 0.7% Sodium Deoxycholate)+ protease inhibitor cocktail, 2x with TET (0.2% Tween-20/TE) + 1/3 protease inhibitor cocktail, 1x with TE-NaCl (50mM NaCl + TE), and 1x with IDTET (0.2% Tween-20, 10mM Tris pH8, 0,1mM EDTA). Samples were finally resuspended in TT buffer (10mM Tris pH 8 + 0.05% Tween 20) prior to on-bead library preparation. For SALL1, SMAD4, and P300 ChIPs, 500,0000-2million nuclei were thawed on ice and resuspended in ice-cold RLNR1 buffer (20mM Tris HCl pH 7.5, 150 mM NaCl, 1 mM EDTA, 0.5 mM EGTA, 0.4% sodium deoxycholate, 1% NP-40, 0,1% SDS, 0.5mM DTT) + 1x protease inhibitor cocktail/PMSF. Samples were sonicated in a 96 Place microtube Rack (Covaris cat#500282) using a Covaris E220 for 20 cycles with the following setting: time 60 seconds, duty cycle 5.0, PIP 175, cycles, 200, amplitude 0.0, velocity 0.0, dwell 0.0. Samples were recovered and spun down at max speed, 4°C for 10 minutes. One percent of the lysate was kept as ChIP input. 10 µL of Dynabead Protein A and 10 µL of Dynabead Protein G beads per sample were coupled to either 4 µg of SALL1 antibody (Abcam, ab41974), SMAD4 antibody (1µg each of *Cell Signaling* technology 46535 and 38454), or P300 antibody (1 µg each of EMD Millipore RW128 and Diagenode C15200211). Beads/antibody was added to each sample, which were then rotated overnight at 4°C. The samples were washed with the following buffers: 3x RLNR1 + PIC/PMSF/DTT, 6x LWB-RCNR1 (10mM Tris HCl pH 7.5, 1mM EDTA, 0.7% sodium deoxycholate, 1% NP-40, 250mM LiCl)+ PIC/PMSF, 3x TET, 2x IDTET, and then resuspended in TT for on-bead library preparation. Libraries for ChIP and input samples were prepared with NEBNext Ultra II DNA library prep kit (NEB) reagents according to the manufacturer's protocol on the beads suspended in 25 µL TT

(10mM Tris/HCl pH7.5, 0.05% Tween-20), with reagent volumes reduced by half. DNA was eluted and crosslinks reversed by adding 4 µL10% SDS, 4.5 µL 5 M NaCl, 3 µL EDTA, 4 µL EGTA, 1 µL proteinase K (20 mg/ml), 16 µL water, incubating for 1 h at 55°C, then 30 minutes to overnight at 65°C. DNA was purified using 2 µL of SpeedBeads (GE Healthcare), diluted with 20% PEG8000, 1.5M NaCl to final of 12% PEG, eluted with 25 µL TT. DNA contained in the eluate was then amplified for 12-14 cycles in 25 µL PCR reactions using NEBNext High-Fidelity 2X PCR Master Mix (NEB) and 0.5 mM each of primers *Solexa* 1GA and Solexa 1GB. Resulting libraries were size selected by gel excision to 200-500 bp, purified, and single-end sequenced using a HiSeq 4000.

PLAC-seq library preparation

PLAC-seq libraries were prepared for *ex vivo* microglia as previously described with minor modifications[32, 61, 118]. To isolate nuclei, cross-linked cells were resuspended in 200 µL lysis buffer (10 mM Tris-HCl (pH 8.0), 10 mM NaCl, 0.2% IPEGAL CA-630) and incubated on ice for 15 minutes. The suspension was then centrifuged at 2,500xg for 5 mins and the pellet was washed by resuspending in 300 µL lysis buffer and centrifuging at 2,500 xg for 5 mins. The pellet was resuspended in 50 µL 0.5% SDS and incubated for 10 mins at 62°C. 160 µL 1.56% Triton X-100 was added to the suspension and incubated for 15 mins at 37°C. 25 µl of 10X NEBuffer 2 and 100 U MboI were added to digest chromatin for 2 hours at 37°C with rotation (1,000 rpm). Enzymes were inactivated by heating for 20 mins at 62°C. Fragmented ends were biotin labeled by adding 50 µL of a mix containing 0.3 mM biotin-14-dATP, 0.3 mM dCTP, 0.3 mM dTTP,

0.3 mM dGTP, and 0.8 U μl^{-1} Klenow and incubated for 60 mins at 37°C with rotation (900 rpm). Ends were subsequently ligated by adding a 900 µL master mix containing 120 µL 10X T4 DNA ligase buffer (NEB), 100 µL 10% TritionX-100, 6 µL 20 mg ml^{-1} BSA, 10 µL 400 U μl^{-1} T4 DNA Ligase (NEB, high concentration formula) and 664 µL H_2O and incubated for 120 mins at 23°C with 300 rpm slow rotation. Nuclei were pelleted for 5 mins at 4°C with centrifugation at 2,500 xg. For the ChIP, nuclei were resuspended in RIPA Buffer (10 mM Tris (pH 8.0), 140 mM NaCl, 1 mM EDTA, 1% Triton X-100, 0.1% SDS, 0.1% sodium deoxycholate) with proteinase inhibitors and incubated on ice for 10 mins. Sonication was performed using a Covaris M220 instrument (Power 75W, duty factor 10%, cycle per bust 200, time 10 mins, temperature 7°C) and nuclei were spun for 15 mins at 14,000 rpm at 4°C. 5% of supernatant was taken as input DNA. To the remaining cell lysate was added anti-H3K4me3 antibody-coated Dynabeads M-280 Sheep anti-Rabbit IgG (5 µg antibody per sample, Millipore, 04-745), followed by rotation at 4°C overnight for immunoprecipitation. The sample was placed on a magnetic stand for 1 min and the beads were washed three times with RIPA buffer, two times with high-salt RIPA buffer (10 mM Tris pH 8.0, 300 mM NaCl, 1 mM EDTA, 1% Triton X-100, 0.1% SDS, 0.1% deoxycholate), one time with LiCl buffer (10 mM Tris (pH 8.0), 250 mM LiCl, 1 mM EDTA, 0.5% IGEPAL CA-630, 0.1% sodium deoxycholate) and two times with TE buffer (10 mM Tris (pH 8.0), 0.1 mM EDTA). Washed beads were treated with 10 µg RNase A in extraction buffer (10 mM Tris (pH 8.0), 350 mM NaCl, 0.1 mM EDTA, 1% SDS) for 1 hour at 37°C, and subsequently 20 µg proteinase K was added at 65°C for 2 hours. ChIP DNA was purified with Zymo DNA clean and concentrator. For Biotin pull down, 25 µL of 10 mg ml^{-1} Dynabeads My One

T1 Streptavidin beads was washed with 400 µl of 1X Tween Wash Buffer (5 mM Tris-HCl (pH 7.5), 0.5 mM EDTA, 1 M NaCl, 0.05% Tween) and supernatant removed after separation on a magnet. Beads were resuspended with 2X Binding Buffer (10 mM Tris-HCl (pH 7.5), 1 mM EDTA, 2 M NaCl), added to the sample and incubated for 15 mins at room temperature. Beads were subsequently washed twice with 1X Tween Wash Buffer and in between heated on a thermomixer for 2 mins at 55°C with mixing and washed once with 1X NEB T4 DNA ligase buffer. Library prep was prepared using QIAseq Ultralow Input Library Kit (Qiagen, 180492). KAPA qPCR assay was performed to estimate concentration and cycle number for final PCR. Final PCR was directly amplified off the T1 beads according to the qPCR results, and DNA was size selected with 0.5X and 1X SPRI Cleanup and eluted in 1X Tris Buffer and paired-end sequenced.

In Situ Hi-C Library Preparation

In situ Hi-C was performed as described previously with minor modifications [158]. Nuclei were isolated by resuspending the cell pellet in 200 µL Wash Buffer (50 mM Tris/HCl pH 7.5, 10 mM NaCl, 1 mM EDTA, 0.5% SDS, 1x protease inhibitor cocktail (Sigma). Nuclei were incubated at 37°C for 60 minutes in PCR tubes in a PCR cycler. Nuclei were spun down at 1000xg for 5 minutes at room temperature. Most of the supernatant was discarded, leaving 10µL of liquid with the nuclei. Samples were resuspended in DpnII buffer (25 μL 10% TrixonX-100, 25 μL 10x DpnII buffer (NEB), 188μL water) and rotated for 15 minutes at 37°C. Chromatin was then digested overnight with 2 μL (100U) DpnII (NEB) at 37°C, rotating end over end at 8 RPM. The next day, nuclei were spun down for 5 minutes, 1000xg. 225 μL of the supernatant was

discarded, leaving ~25 μL of liquid remaining with the nuclei pellet. Overhangs were filled in with Biotin-14-dATP (Thermo) by adding 75 μL of Klenow master mix (54.45 μL water, 7.5 μL NEBuffer 2 (NEB), 0.35 μL dCTP, 0.35 μL dTTP, 0.35 μL dGTP, 7.5 μL 0.4 mM Biotin-14-dATP, 2μL 10% TritonX-100, 2.4 μL (12.5 U) Klenow Fragment (Enzymatics) and rotating end over end at room temperature for 40 minutes. Proximity ligation was performed by transferring the reaction into an Eppendorff tube and adding ligation master mix (322.75 μL water, 40 μL 10x T4 ligase buffer (Enzymatics), 36 μL 10% TritonX-100, 20% 1000x BSA, and HC T4 DNA ligase (Enzymatics). Samples were incubated at 16°C overnight rotating end over end. The following day, reactions were stopped by adding 20uL 0.5M EDTA plus 1 μL 10 μg/μL RNAse A at 42°C for 15 minutes. To reverse crosslinks and digest proteins, 31 μL 5M NaCl, 29 μL 10% SDS, and 5 μL 20mg/mL proteinase K were added to each sample. Samples were incubated at 55°C for 1 hour, then at 65°C overnight. The following day, DNA was extracted using 600 μL pH 8-buffered phenol/chloroform/isoamyl alcohol (Invitrogen), followed by 550 μL chloroform. DNA was then precipitated with 1.5 μL (15mg/mL) Glycoblue (Thermo) and 1400 μL 100% ethanol overnight at -20°C, pelleted for 20 minutes at 160000xg, 4°C and washed 2x with 1 mL 80% EtOH. The pellet was air-dried and dissolved in 131 μL TT buffer (0.05% Tween20/10 mM Tris pH 8). DNA was then sheared to ~300 bp average size in 130 μL TT on a Covaris E220 for 120 seconds, duty cycle 5 , PIP 175, and cycles per burst 200. Biotinylated DNA was incubated with 20uL DynaBeads MyOne Streptavidin T1 beads that had been washed 1x with B&W buffer (2x B&W: 10mM Tris HCl pH 7.5, 1mM EDTA, 2M NaCl) and resuspended in 130 μL 2x B&W buffer with 0.2% Tween 20. The binding reaction was incubated for 45 minutes at room

temperature, rotating end over end. The beads were washed 2x with 150 μL 1x B&W plus 0.1% TritonX-100, 1x with 180 μL TET (TE + 0.05% Tween-20) and resuspended in 30 μL ice cold NebNext Ultra II end prep mix (1.5 μL NebNext Ultra II EndPrep Enzyme, 3.5 μL EndPrep Buffer, 25 μL TT buffer) and incubated 20°C for 30 minutes followed by 65°C for 30 minutes. Beads were resuspended in ligation master mix (15 μL NebNext Ultra II ligation master mix, 0.5 μL ligation enhancer) and 1 μL of BIOO Nextflex DNA sequencing adapters were added. The mixture was incubated at 20°C for 20 minutes and the reaction was stopped using 5 μL 0.5M EDTA. Following this, the beads were washed twice in 1x B&W with 0.1% TritonX-100, twice with TET, and resuspended in 20 μL TT buffer. Libraries were amplified by PCR for 10 cycles (98°C, 30 sec; [98°C, 10 sec; 63°C, 25 sec; 72°C, 30sec]; 72°C 5 minutes, 4°C hold) using 10 uL of the bead resuspension in a 50 μL reaction with NEBNext Ultra II Q5 mastermix (NEB), 0.5 μM each Solexa 1GA/1GB primers (Solexa 1GA: AATGATACGGCGACCACC GA, Solexa 1GB: CAAGCAGAAGA CGGCATACGA). Libraries were precipitated onto magnetic beads by adding 2 μL of Speedbeads, 40 μL 20% PEG/2.5M NaCl and incubating for 15 minutes at room temperature. The beads were washed 2x with 180 uL 80% EtOH and air dried. Samples were eluted by adding 20 μL TT buffer per sample. Libraries were sequenced to a depth of approximately 500 million paired end reads per experiment on Illumina NovaSeq.

Conservation of enhancer sequences and TF binding sites between mouse and human

The *Sall1* enhancer sequences were extracted from the mm10 genome using HOMER v4.11.1 "homerTools extract" [157] and then aligned to the NCBI nt database v5 using BLASTn [160] by specifying homo sapiens taxon ID 9606 and gap opening penalty at 5 and gap extension penalty at 2. We reported the top alignment of each sequence with E-value < 0.01. For successfully aligned enhancers, we scanned through both mouse enhancers and human homologs with position weight matrices (PWMs) from the JASPAR database[161] to compute PWM scores [162]. An array of PWM scores were computed for every sequence using MAGGIE v1.1 "find_motif" function[163] and were used to identify motif matches based on a PWM score larger than four, meaning 16-fold more likely than random backgrounds to be bound by the corresponding TF. The motif matches at homologous positions were considered conserved between mouse and human.

Data mapping

FASTQ files from sequencing experiments were mapped to mm10. RNA-seq files were mapped using STAR[164] with default parameters. ATAC-seq and Hi-C FASTQ files were trimmed prior to mapping with Bowtie 2; ATAC-seq files were trimmed to 30 bp and Hi-C fastq files were trimmed at DpnII recognition sites (GATC). Following trimming, ATAC-seq and Hi-C FASTQ files were mapped using Bowtie 2[165]. After mapping, tag directories were created using the HOMER command makeTagDirectory (*9*).

RNA-seq Analysis

The gene expression raw counts were quantified by HOMER's[157] analyzeRepeats command with the option "-condenseGenes -count exons -noadj". TPM (transcript per kilobase million) were quantified for all genes matching accession number to raw counts. Differentially expressed genes were assessed with DESeq2[166] at p-adj (adjusted pvalue) < 0.05 and FC (fold change) > 2 where indicated. Genes with TPM < 4 in all conditions were removed from analysis. Gene ontology enrichment analyses were performed using Metascape [167].

Hi-C data Analysis and Visualization

Hi-C interaction matrices were generated using juicertools [168] and were visualized using juicebox [169]. PC1 values for each sample were calculated using HOMER's runHiCpca.pl with -res 50000 [170]and were visualized using the UCSC genome browser [171]. TADs and loops were called using HOMER's findTADsAndLoops.pl find with parameters -res 3000 and -window 15000. To compare TADs and loops between groups, TADs and loops were merged using merge2Dbed.pl -tad and -loop, respectively. Differential enrichment of these features was then calculated using Homer's getDiffExpression.pl.

IDR analysis of ChIP and ATAC peaks

ChIP-seq experiments were performed in replicates with corresponding input experiments. Peaks were called with HOMER for each tag directory with relaxed peak finding parameters "-L 0 -C 0 -fdr 0.9". ATAC peaks were called with additional

parameters “-minDist 200 -size 200”. IDR was used to test for reproducibility between replicates [172], only peaks with an IDR < 0.05 were used for downstream analyses. For sample groups with > 2 libraries, peak sets from all pairwise IDR comparisons were merged into a final set of peaks for further analysis.

ATAC-seq and ChIP-seq analysis

To quantify the TF binding and chromatin accessibility between conditions, raw tag counts at merged IDR peaks identified by HOMER’s mergePeaks were identified using HOMER’s annotatePeaks with “-noadj,” “-size 500” for TF ChIP-seq peaks and “-size 1000” for ATAC peaks annotated with H3K27ac reads. DESeq2 was used to identify differentially bound TF binding distal sites or differential distal chromatin accessibility (p-adj. < 0.05 and FC >2). Super-enhancers were defined using the HOMER ‘findPeaks -style super’ command.

PLAC-seq Analysis

H3K4me3 ChIP-seqs from purified *ex-vivo* microglia were performed in duplicate with input controls. Alignment, QC and peak calling were performed with the official ENCODE-ChIP-seq pipeline (https://github.com/ENCODE-DCC/chip-seq-pipeline2) as previously described[32].PLAC-seq fastq-files were processed with MAPS [173] at 5000-bp resolution as previously described[32]; the H3K4me3-ChIP-seq peak files from the ENCODE pipeline were used as a template.

Motif Analysis

To identify motifs enriched in peak regions over the background, HOMER's motif analysis (findMotifsGenome.pl) including known default motifs and de novo motifs was used[157]. The background peaks used random genome sequences generated automatically by HOMER.

Data Visualization

Heatmap of RNA expression or tags of ATAC-Seq peaks were generated by pheatmap, an R package. Significance indicated by "*" in bar-plot represents the p-adj defined by DESeq2. MA-plots were used to demonstrate the differentially expressed genes for RNA-Seq data with log2fold change against expression value TPM, additionally with the sizes of dots representing the significant p values. Scatterplots were used for direct comparison of two conditions, normalized tag counts were used for ChIP-/ATAC-Seq. Data were further visualized using the HOMER command makeMultiWigHub.pl and the UCSC genome browser. GraphPad Prism was used to create barplots of TPMs in individual gene comparisons.

Acknowledgements:

This work was funded in part by NIH NS R01 NS096170. BRF was supported by F30AG062159-01. This thesis includes data generated at the UC San Diego IGM Genomics Center utilizing an Illumina NovaSeq 6000 that was purchased with funding from a National Institutes of Health SIG grant (#S10 OD026929).

Chapter 2, in full, is a reprint of material submitted for publication as: Fixsen, Bethany R.; Sakai, Mashito; Zhou, Yi; Han, Claudia Z.; Cobo, Isidoro; Holtman, Inge R.; Warden, Anna S.; Ramirez, Gabriela; Collier, Jana G.; Pasillas, Martina P.; Shen, Zeyang; Yu, Miao; Hu, Rong; Li, Bin; Belhocine, Sarah; Gosselin, David; Coufal, Nicole G.; Ren, Bing; Glass, Christopher K. “SALL1 enforces microglia-specific DNA binding and function of SMADs to establish microglia identity”. The dissertation author was one of the primary investigators and authors of this paper.

References

1. Nau GJ, Richmond JF, Schlesinger A, Jennings EG, Lander ES, Young RA. Human macrophage activation programs induced by bacterial pathogens. Proc Natl Acad Sci U S A. 2002;99(3):1503-8. Epub 20020122. doi: 10.1073/pnas.022649799. PubMed PMID: 11805289; PMCID: PMC122220.

2. Murray PJ, Wynn TA. Protective and pathogenic functions of macrophage subsets. Nat Rev Immunol. 2011;11(11):723-37. Epub 20111014. doi: 10.1038/nri3073. PubMed PMID: 21997792; PMCID: PMC3422549.

3. Davies LC, Jenkins SJ, Allen JE, Taylor PR. Tissue-resident macrophages. Nat Immunol. 2013;14(10):986-95. Epub 20130918. doi: 10.1038/ni.2705. PubMed PMID: 24048120; PMCID: PMC4045180.

4. Ginhoux F, Guilliams M. Tissue-Resident Macrophage Ontogeny and Homeostasis. Immunity. 2016;44(3):439-49. doi: 10.1016/j.immuni.2016.02.024. PubMed PMID: 26982352.

5. Ginhoux F, Jung S. Monocytes and macrophages: developmental pathways and tissue homeostasis. Nature Reviews Immunology. 2014;14(6):392-404. doi: 10.1038/nri3671. PubMed PMID: WOS:000337849700013.

6. Cox N, Pokrovskii M, Vicario R, Geissmann F. Origins, Biology, and Diseases of Tissue Macrophages. Annu Rev Immunol. 2021;39:313-44. doi: 10.1146/annurev-immunol-093019-111748. PubMed PMID: WOS:000647687900012.

7. Metschnikoff E. Lecture on Phagocytosis and Immunity. Br Med J. 1891;1(1570):213-7. doi: 10.1136/bmj.1.1570.213. PubMed PMID: 20753232; PMCID: PMC2197023.

8. Kaufmann SH. Immunology's foundation: the 100-year anniversary of the Nobel Prize to Paul Ehrlich and Elie Metchnikoff. Nat Immunol. 2008;9(7):705-12. doi: 10.1038/ni0708-705. PubMed PMID: 18563076.

9. Sotelo C. Viewing the brain through the master hand of Ramon y Cajal. Nat Rev Neurosci. 2003;4(1):71-7. doi: 10.1038/nrn1010. PubMed PMID: WOS:000180225700018.

10. Garcia-Marin V, Garcia-Lopez P, Freire M. Cajal's contributions to glia research. Trends Neurosci. 2007;30(9):479-87. Epub 20070831. doi: 10.1016/j.tins.2007.06.008. PubMed PMID: 17765327.

11. Perez-Cerda F, Sanchez-Gomez MV, Matute C. Pio del Rio Hortega and the discovery of the oligodendrocytes. Front Neuroanat. 2015;9:92. Epub 20150707. doi: 10.3389/fnana.2015.00092. PubMed PMID: 26217196; PMCID: PMC4493393.

12. Nimmerjahn A, Kirchhoff F, Helmchen F. Resting microglial cells are highly dynamic surveillants of brain parenchyma in vivo. Science. 2005;308(5726):1314-8. Epub 20050414. doi: 10.1126/science.1110647. PubMed PMID: 15831717.

13. Davalos D, Grutzendler J, Yang G, Kim JV, Zuo Y, Jung S, Littman DR, Dustin ML, Gan WB. ATP mediates rapid microglial response to local brain injury in vivo. Nat Neurosci. 2005;8(6):752-8. Epub 20050515. doi: 10.1038/nn1472. PubMed PMID: 15895084.

14. Hanisch UK, Kettenmann H. Microglia: active sensor and versatile effector cells in the normal and pathologic brain. Nature Neuroscience. 2007;10(11):1387-94. doi: 10.1038/nn1997. PubMed PMID: WOS:000250508400013.

15. Paolicelli RC, Bolasco G, Pagani F, Maggi L, Scianni M, Panzanelli P, Giustetto M, Ferreira TA, Guiducci E, Dumas L, Ragozzino D, Gross CT. Synaptic Pruning by Microglia Is Necessary for Normal Brain Development. Science. 2011;333(6048):1456-8. doi: 10.1126/science.1202529. PubMed PMID: WOS:000294672200045.

16. Schafer DP, Lehrman EK, Kautzman AG, Koyama R, Mardinly AR, Yamasaki R, Ransohoff RM, Greenberg ME, Barres BA, Stevens B. Microglia Sculpt Postnatal Neural Circuits in an Activity and Complement-Dependent Manner. Neuron. 2012;74(4):691-705. doi: 10.1016/j.neuron.2012.03.026. PubMed PMID: WOS:000304747200013.

17. Stevens B, Allen NJ, Vazquez LE, Howell GR, Christopherson KS, Nouri N, Micheva KD, Mehalow AK, Huberman AD, Stafford B, Sher A, Litke AM, Lambris JD, Smith SJ, John SWM, Barres BA. The classical complement cascade mediates CNS synapse elimination. Cell. 2007;131(6):1164-78. doi: 10.1016/j.cell.2007.10.036. PubMed PMID: WOS:000252217100023.

18. Cunningham CL, Martinez-Cerdeno V, Noctor SC. Microglia Regulate the Number of Neural Precursor Cells in the Developing Cerebral Cortex. J Neurosci.

2013;33(10):4216-33. doi: 10.1523/Jneurosci.3441-12.2013. PubMed PMID: WOS:000315926300002.

19. Parkhurst CN, Yang G, Ninan I, Savas JN, Yates JR, Lafaille JJ, Hempstead BL, Littman DR, Gan WB. Microglia Promote Learning-Dependent Synapse Formation through Brain-Derived Neurotrophic Factor. Cell. 2013;155(7):1596-609. doi: 10.1016/j.cell.2013.11.030. PubMed PMID: WOS:000328693300015.

20. Hagemeyer N, Hanft KM, Akriditou MA, Unger N, Park ES, Stanley ER, Staszewski O, Dimou L, Prinz M. Microglia contribute to normal myelinogenesis and to oligodendrocyte progenitor maintenance during adulthood. Acta Neuropathol. 2017;134(3):441-58. doi: 10.1007/s00401-017-1747-1. PubMed PMID: WOS:000407931900007.

21. Pollard JW. Trophic macrophages in development and disease. Nat Rev Immunol. 2009;9(4):259-70. doi: 10.1038/nri2528. PubMed PMID: 19282852; PMCID: PMC3648866.

22. Priller J, Prinz M. Targeting microglia in brain disorders. Science. 2019;365(6448):32-3. doi: 10.1126/science.aau9100. PubMed PMID: 31273114.

23. Gordon S, Taylor PR. Monocyte and macrophage heterogeneity. Nat Rev Immunol. 2005;5(12):953-64. doi: 10.1038/nri1733. PubMed PMID: 16322748.

24. Hume DA. The Many Alternative Faces of Macrophage Activation. Front Immunol. 2015;6:370. Epub 20150722. doi: 10.3389/fimmu.2015.00370. PubMed PMID: 26257737; PMCID: PMC4510422.

25. Ransohoff RM. A polarizing question: do M1 and M2 microglia exist? Nature Neuroscience. 2016;19(8):987-91. doi: 10.1038/nn.4338. PubMed PMID: WOS:000380773200004.

26. Zhang CY, Yang M, Ericsson AC. Function of Macrophages in Disease: Current Understanding on Molecular Mechanisms. Frontiers in Immunology. 2021;12. doi: ARTN 620510
10.3389/fimmu.2021.620510. PubMed PMID: WOS:000631058500001.

27. Gomez-Nicola D, Perry VH. Microglial dynamics and role in the healthy and diseased brain: a paradigm of functional plasticity. Neuroscientist. 2015;21(2):169-84.

Epub 20140410. doi: 10.1177/1073858414530512. PubMed PMID: 24722525; PMCID: PMC4412879.

28. Shemer A, Erny D, Jung S, Prinz M. Microglia Plasticity During Health one Disease: An Immunological Perspective. Trends Immunol. 2015;36(10):614-24. doi: 10.1016/j.it.2015.08.003. PubMed PMID: WOS:000363070300006.

29. Liddelow SA, Guttenplan KA, Clarke LE, Bennett FC, Bohlen CJ, Schirmer L, Bennett ML, Munch AE, Chung WS, Peterson TC, Wilton DK, Frouin A, Napier BA, Panicker N, Kumar M, Buckwalter MS, Rowitch DH, Dawson VL, Dawson TM, Stevens B, Barres BA. Neurotoxic reactive astrocytes are induced by activated microglia. Nature. 2017;541(7638):481-7. Epub 20170118. doi: 10.1038/nature21029. PubMed PMID: 28099414; PMCID: PMC5404890.

30. Sarlus H, Heneka MT. Microglia in Alzheimer's disease. J Clin Invest. 2017;127(9):3240-9. Epub 20170901. doi: 10.1172/JCI90606. PubMed PMID: 28862638; PMCID: PMC5669553.

31. Maurano MT, Humbert R, Rynes E, Thurman RE, Haugen E, Wang H, Reynolds AP, Sandstrom R, Qu H, Brody J, Shafer A, Neri F, Lee K, Kutyavin T, Stehling-Sun S, Johnson AK, Canfield TK, Giste E, Diegel M, Bates D, Hansen RS, Neph S, Sabo PJ, Heimfeld S, Raubitschek A, Ziegler S, Cotsapas C, Sotoodehnia N, Glass I, Sunyaev SR, Kaul R, Stamatoyannopoulos JA. Systematic localization of common disease-associated variation in regulatory DNA. Science. 2012;337(6099):1190-5. Epub 20120905. doi: 10.1126/science.1222794. PubMed PMID: 22955828; PMCID: PMC3771521.

32. Nott A, Holtman IR, Coufal NG, Schlachetzki JCM, Yu M, Hu R, Han CZ, Pena M, Xiao J, Wu Y, Keulen Z, Pasillas MP, O'Connor C, Nickl CK, Schafer ST, Shen Z, Rissman RA, Brewer JB, Gosselin D, Gonda DD, Levy ML, Rosenfeld MG, McVicker G, Gage FH, Ren B, Glass CK. Brain cell type-specific enhancer-promoter interactome maps and disease-risk association. Science. 2019;366(6469):1134-9. Epub 20191114. doi: 10.1126/science.aay0793. PubMed PMID: 31727856; PMCID: PMC7028213.

33. Villegas-Llerena C, Phillips A, Garcia-Reitboeck P, Hardy J, Pocock JM. Microglial genes regulating neuroinflammation in the progression of Alzheimer's disease. Curr Opin Neurobiol. 2016;36:74-81. doi: 10.1016/j.conb.2015.10.004. PubMed PMID: WOS:000370303900012.

34. Lambert JC, Ibrahim-Verbaas CA, Harold D, Naj AC, Sims R, Bellenguez C, DeStafano AL, Bis JC, Beecham GW, Grenier-Boley B, Russo G, Thorton-Wells TA,

Jones N, Smith AV, Chouraki V, Thomas C, Ikram MA, Zelenika D, Vardarajan BN, Kamatani Y, Lin CF, Gerrish A, Schmidt H, Kunkle B, Dunstan ML, Ruiz A, Bihoreau MT, Choi SH, Reitz C, Pasquier F, Cruchaga C, Craig D, Amin N, Berr C, Lopez OL, De Jager PL, Deramecourt V, Johnston JA, Evans D, Lovestone S, Letenneur L, Moron FJ, Rubinsztein DC, Eiriksdottir G, Sleegers K, Goate AM, Fievet N, Huentelman MW, Gill M, Brown K, Kamboh MI, Keller L, Barberger-Gateau P, McGuiness B, Larson EB, Green R, Myers AJ, Dufouil C, Todd S, Wallon D, Love S, Rogaeva E, Gallacher J, St George-Hyslop P, Clarimon J, Lleo A, Bayer A, Tsuang DW, Yu L, Tsolaki M, Bossu P, Spalletta G, Proitsi P, Collinge J, Sorbi S, Sanchez-Garcia F, Fox NC, Hardy J, Deniz Naranjo MC, Bosco P, Clarke R, Brayne C, Galimberti D, Mancuso M, Matthews F, European Alzheimer's Disease I, Genetic, Environmental Risk in Alzheimer's D, Alzheimer's Disease Genetic C, Cohorts for H, Aging Research in Genomic E, Moebus S, Mecocci P, Del Zompo M, Maier W, Hampel H, Pilotto A, Bullido M, Panza F, Caffarra P, Nacmias B, Gilbert JR, Mayhaus M, Lannefelt L, Hakonarson H, Pichler S, Carrasquillo MM, Ingelsson M, Beekly D, Alvarez V, Zou F, Valladares O, Younkin SG, Coto E, Hamilton-Nelson KL, Gu W, Razquin C, Pastor P, Mateo I, Owen MJ, Faber KM, Jonsson PV, Combarros O, O'Donovan MC, Cantwell LB, Soininen H, Blacker D, Mead S, Mosley TH, Jr., Bennett DA, Harris TB, Fratiglioni L, Holmes C, de Bruijn RF, Passmore P, Montine TJ, Bettens K, Rotter JI, Brice A, Morgan K, Foroud TM, Kukull WA, Hannequin D, Powell JF, Nalls MA, Ritchie K, Lunetta KL, Kauwe JS, Boerwinkle E, Riemenschneider M, Boada M, Hiltuenen M, Martin ER, Schmidt R, Rujescu D, Wang LS, Dartigues JF, Mayeux R, Tzourio C, Hofman A, Nothen MM, Graff C, Psaty BM, Jones L, Haines JL, Holmans PA, Lathrop M, Pericak-Vance MA, Launer LJ, Farrer LA, van Duijn CM, Van Broeckhoven C, Moskvina V, Seshadri S, Williams J, Schellenberg GD, Amouyel P. Meta-analysis of 74,046 individuals identifies 11 new susceptibility loci for Alzheimer's disease. Nat Genet. 2013;45(12):1452-8. Epub 20131027. doi: 10.1038/ng.2802. PubMed PMID: 24162737; PMCID: PMC3896259.

35. Rustenhoven J, Smith AM, Smyth LC, Jansson D, Scotter EL, Swanson MEV, Aalderink M, Coppieters N, Narayan P, Handley R, Overall C, Park TIH, Schweder P, Heppner P, Curtis MA, Faull RLM, Dragunow M. PU.1 regulates Alzheimer's disease-associated genes in primary human microglia. Mol Neurodegener. 2018;13(1):44. Epub 20180820. doi: 10.1186/s13024-018-0277-1. PubMed PMID: 30124174; PMCID: PMC6102813.

36. Tansey KE, Cameron D, Hill MJ. Genetic risk for Alzheimer's disease is concentrated in specific macrophage and microglial transcriptional networks. Genome Med. 2018;10(1):14. Epub 20180226. doi: 10.1186/s13073-018-0523-8. PubMed PMID: 29482603; PMCID: PMC5828245.

37. Keren-Shaul H, Spinrad A, Weiner A, Matcovitch-Natan O, Dvir-Szternfeld R, Ulland TK, David E, Baruch K, Lara-Astaiso D, Toth B, Itzkovitz S, Colonna M, Schwartz M, Amit I. A Unique Microglia Type Associated with Restricting Development of

Alzheimer's Disease. Cell. 2017;169(7):1276-90 e17. Epub 2017/06/13. doi: 10.1016/j.cell.2017.05.018. PubMed PMID: 28602351.

38. Krasemann S, Madore C, Cialic R, Baufeld C, Calcagno N, El Fatimy R, Beckers L, O'Loughlin E, Xu Y, Fanek Z, Greco DJ, Smith ST, Tweet G, Humulock Z, Zrzavy T, Conde-Sanroman P, Gacias M, Weng Z, Chen H, Tjon E, Mazaheri F, Hartmann K, Madi A, Ulrich JD, Glatzel M, Worthmann A, Heeren J, Budnik B, Lemere C, Ikezu T, Heppner FL, Litvak V, Holtzman DM, Lassmann H, Weiner HL, Ochando J, Haass C, Butovsky O. The TREM2-APOE Pathway Drives the Transcriptional Phenotype of Dysfunctional Microglia in Neurodegenerative Diseases. Immunity. 2017;47(3):566-81 e9. doi: 10.1016/j.immuni.2017.08.008. PubMed PMID: 28930663; PMCID: PMC5719893.

39. Masuda T, Sankowski R, Staszewski O, Bottcher C, Amann L, Sagar, Scheiwe C, Nessler S, Kunz P, van Loo G, Coenen VA, Reinacher PC, Michel A, Sure U, Gold R, Grun D, Priller J, Stadelmann C, Prinz M. Spatial and temporal heterogeneity of mouse and human microglia at single-cell resolution (vol 566, pg 388, 2019). Nature. 2019;568(7751):E4-E. doi: 10.1038/s41586-019-1045-2. PubMed PMID: WOS:000464412700015.

40. Holtman IR, Raj DD, Miller JA, Schaafsma W, Yin Z, Brouwer N, Wes PD, Moller T, Orre M, Kamphuis W, Hol EM, Boddeke EW, Eggen BJ. Induction of a common microglia gene expression signature by aging and neurodegenerative conditions: a co-expression meta-analysis. Acta Neuropathol Commun. 2015;3:31. Epub 20150523. doi: 10.1186/s40478-015-0203-5. PubMed PMID: 26001565; PMCID: PMC4489356.

41. Marschallinger J, Iram T, Zardeneta M, Lee SE, Lehallier B, Haney MS, Pluvinage JV, Mathur V, Hahn O, Morgens DW, Kim J, Tevini J, Felder TK, Wolinski H, Bertozzi CR, Bassik MC, Aigner L, Wyss-Coray T. Lipid-droplet-accumulating microglia represent a dysfunctional and proinflammatory state in the aging brain. Nat Neurosci. 2020;23(2):194-208. Epub 20200120. doi: 10.1038/s41593-019-0566-1. PubMed PMID: 31959936; PMCID: PMC7595134.

42. Lawson LJ, Perry VH, Dri P, Gordon S. Heterogeneity in the Distribution and Morphology of Microglia in the Normal Adult-Mouse Brain. Neuroscience. 1990;39(1):151-70. doi: Doi 10.1016/0306-4522(90)90229-W. PubMed PMID: WOS:A1990EK59000013.

43. Mass E, Ballesteros I, Farlik M, Halbritter F, Gunther P, Crozet L, Jacome-Galarza CE, Handler K, Klughammer J, Kobayashi Y, Gomez-Perdiguero E, Schultze JL, Beyer M, Bock C, Geissmann F. Specification of tissue-resident macrophages during organogenesis. Science. 2016;353(6304). doi: ARTN aaf4238

10.1126/science.aaf4238. PubMed PMID: WOS:000382626800042.

44. Perdiguero EG, Klapproth K, Schulz C, Busch K, Azzoni E, Crozet L, Garner H, Trouillet C, De Bruijn M, Geissmann F, Rodewald HR. Tissue-Resident Macrophages Originate from Yolk Sac-Derived Erythro-Myeloid Progenitors. Exp Hematol. 2015;43(9):S64-S. doi: DOI 10.1016/j.exphem.2015.06.130. PubMed PMID: WOS:000361417400112.

45. Alliot F, Godin I, Pessac B. Microglia derive from progenitors, originating from the yolk sac, and which proliferate in the brain. Dev Brain Res. 1999;117(2):145-52. doi: Doi 10.1016/S0165-3806(99)00113-3. PubMed PMID: WOS:000083881400003.

46. Utz SG, See P, Mildenberger W, Thion MS, Silvin A, Lutz M, Ingelfinger F, Rayan NA, Lelios I, Buttgereit A, Asano K, Prabhakar S, Garel S, Becher B, Ginhoux F, Greter M. Early Fate Defines Microglia and Non-parenchymal Brain Macrophage Development. Cell. 2020;181(3):557-73 e18. Epub 20200406. doi: 10.1016/j.cell.2020.03.021. PubMed PMID: 32259484.

47. Kierdorf K, Erny D, Goldmann T, Sander V, Schulz C, Perdiguero EG, Wieghofer P, Heinrich A, Riemke P, Holscher C, Muller DN, Luckow B, Brocker T, Debowski K, Fritz G, Opdenakker G, Diefenbach A, Biber K, Heikenwalder M, Geissmann F, Rosenbauer F, Prinz M. Microglia emerge from erythromyeloid precursors via Pu.1- and Irf8-dependent pathways. Nature Neuroscience. 2013;16(3):273-80. doi: 10.1038/nn.3318. PubMed PMID: WOS:000315474800009.

48. Greter M, Lelios I, Pelczar P, Hoeffel G, Price J, Leboeuf M, Kundig TM, Frei K, Ginhoux F, Merad M, Becher B. Stroma-derived interleukin-34 controls the development and maintenance of langerhans cells and the maintenance of microglia. Immunity. 2012;37(6):1050-60. Epub 20121121. doi: 10.1016/j.immuni.2012.11.001. PubMed PMID: 23177320; PMCID: PMC4291117.

49. Wang YM, Szretter KJ, Vermi W, Gilfillan S, Rossini C, Cella M, Barrow AD, Diamond MS, Colonna M. IL-34 is a tissue-restricted ligand of CSF1R required for the development of Langerhans cells and microglia. Nat Immunol. 2012;13(8):753-+. doi: 10.1038/ni.2360. PubMed PMID: WOS:000306569600011.

50. Butovsky O, Jedrychowski MP, Moore CS, Cialic R, Lanser AJ, Gabriely G, Koeglsperger T, Dake B, Wu PM, Doykan CE, Fanek Z, Liu L, Chen Z, Rothstein JD, Ransohoff RM, Gygi SP, Antel JP, Weiner HL. Identification of a unique TGF-beta-dependent molecular and functional signature in microglia. Nat Neurosci.

2014;17(1):131-43. Epub 20131208. doi: 10.1038/nn.3599. PubMed PMID: 24316888; PMCID: PMC4066672.

51. Rojo R, Raper A, Ozdemir DD, Lefevre L, Grabert K, Wollscheid-Lengeling E, Bradford B, Caruso M, Gazova I, Sanchez A, Lisowski ZM, Alves J, Molina-Gonzalez I, Davtyan H, Lodge RJ, Glover JD, Wallace R, Munro DAD, David E, Amit I, Miron VE, Priller J, Jenkins SJ, Hardingham GE, Blurton-Jones M, Mabbott NA, Summers KM, Hohenstein P, Hume DA, Pridans C. Deletion of a Csf1r enhancer selectively impacts CSF1R expression and development of tissue macrophage populations. Nat Commun. 2019;10. doi: ARTN 3215
10.1038/s41467-019-11053-8. PubMed PMID: WOS:000476471300024.

52. Matcovitch-Natan O, Winter DR, Giladi A, Vargas Aguilar S, Spinrad A, Sarrazin S, Ben-Yehuda H, David E, Zelada Gonzalez F, Perrin P, Keren-Shaul H, Gury M, Lara-Astaiso D, Thaiss CA, Cohen M, Bahar Halpern K, Baruch K, Deczkowska A, Lorenzo-Vivas E, Itzkovitz S, Elinav E, Sieweke MH, Schwartz M, Amit I. Microglia development follows a stepwise program to regulate brain homeostasis. Science. 2016;353(6301):aad8670. Epub 20160623. doi: 10.1126/science.aad8670. PubMed PMID: 27338705.

53. Ginhoux F, Greter M, Leboeuf M, Nandi S, See P, Gokhan S, Mehler MF, Conway SJ, Ng LG, Stanley ER, Samokhvalov IM, Merad M. Fate Mapping Analysis Reveals That Adult Microglia Derive from Primitive Macrophages. Science. 2010;330(6005):841-5. doi: 10.1126/science.1194637. PubMed PMID: WOS:000283855700049.

54. Yona S, Kim KW, Wolf Y, Mildner A, Varol D, Breker M, Strauss-Ayali D, Viukov S, Guilliams M, Misharin A, Hume DA, Perlman H, Malissen B, Zelzer E, Jung S. Fate mapping reveals origins and dynamics of monocytes and tissue macrophages under homeostasis. Immunity. 2013;38(1):79-91. Epub 20121227. doi: 10.1016/j.immuni.2012.12.001. PubMed PMID: 23273845; PMCID: PMC3908543.

55. Reu P, Khosravi A, Bernard S, Mold JE, Salehpour M, Alkass K, Perl S, Tisdale J, Possnert G, Druid H, Frisen J. The Lifespan and Turnover of Microglia in the Human Brain. Cell Rep. 2017;20(4):779-84. doi: 10.1016/j.celrep.2017.07.004. PubMed PMID: 28746864; PMCID: PMC5540680.

56. Sheng JP, Ruedl C, Karjalainen K. Most Tissue-Resident Macrophages Except Microglia Are Derived from Fetal Hematopoietic Stem Cells. Immunity. 2015;43(2):382-93. doi: 10.1016/j.immuni.2015.07.016. PubMed PMID: WOS:000360101200019.

57. Huang YB, Xu Z, Xiong SS, Sun FF, Qin GR, Hu GL, Wang JJ, Zhao L, Liang YX, Wu TZ, Lu ZH, Humayun MS, So KF, Pan YH, Li NN, Yuan TF, Rao YX, Peng B. Repopulated microglia are solely derived from the proliferation of residual microglia after acute depletion. Nature Neuroscience. 2018;21(4):530-+. doi: 10.1038/s41593-018-0090-8. PubMed PMID: WOS:000428796000012.

58. Lavin Y, Winter D, Blecher-Gonen R, David E, Keren-Shaul H, Merad M, Jung S, Amit I. Tissue-resident macrophage enhancer landscapes are shaped by the local microenvironment. Cell. 2014;159(6):1312-26. doi: 10.1016/j.cell.2014.11.018. PubMed PMID: 25480296; PMCID: PMC4437213.

59. Gosselin D, Link VM, Romanoski CE, Fonseca GJ, Eichenfield DZ, Spann NJ, Stender JD, Chun HB, Garner H, Geissmann F, Glass CK. Environment drives selection and function of enhancers controlling tissue-specific macrophage identities. Cell. 2014;159(6):1327-40. doi: 10.1016/j.cell.2014.11.023. PubMed PMID: 25480297; PMCID: PMC4364385.

60. Gautier EL, Shay T, Miller J, Greter M, Jakubzick C, Ivanov S, Helft J, Chow A, Elpek KG, Gordonov S, Mazloom AR, Ma'ayan A, Chua WJ, Hansen TH, Turley SJ, Merad M, Randolph GJ, Consortium IG. Gene-expression profiles and transcriptional regulatory pathways that underlie the identity and diversity of mouse tissue macrophages. Nat Immunol. 2012;13(11):1118-28. doi: 10.1038/ni.2419. PubMed PMID: WOS:000310091700015.

61. Gosselin D, Skola D, Coufal NG, Holtman IR, Schlachetzki JCM, Sajti E, Jaeger BN, O'Connor C, Fitzpatrick C, Pasillas MP, Pena M, Adair A, Gonda DD, Levy ML, Ransohoff RM, Gage FH, Glass CK. An environment-dependent transcriptional network specifies human microglia identity. Science. 2017;356(6344). Epub 20170525. doi: 10.1126/science.aal3222. PubMed PMID: 28546318; PMCID: PMC5858585.

62. Creyghton MP, Cheng AW, Welstead GG, Kooistra T, Carey BW, Steine EJ, Hanna J, Lodato MA, Frampton GM, Sharp PA, Boyer LA, Young RA, Jaenisch R. Histone H3K27ac separates active from poised enhancers and predicts developmental state. Proc Natl Acad Sci U S A. 2010;107(50):21931-6. Epub 20101124. doi: 10.1073/pnas.1016071107. PubMed PMID: 21106759; PMCID: PMC3003124.

63. Meuleman W, Muratov A, Rynes E, Halow J, Lee KS, Bates D, Diegel M, Dunn D, Neri F, Teodosiadis A, Reynolds A, Haugen E, Nelson J, Johnson A, Frerker M, Buckley M, Sandstrom R, Vierstra J, Kaul R, Stamatoyannopoulos J. Index and biological spectrum of human DNase I hypersensitive sites. Nature. 2020;584(7820):244-+. doi: 10.1038/s41586-020-2559-3. PubMed PMID: WOS:000553758900002.

64. Heinz S, Romanoski CE, Benner C, Glass CK. The selection and function of cell type-specific enhancers. Nat Rev Mol Cell Bio. 2015;16(3):144-54. doi: DOI 10.1038/nrm3949. PubMed PMID: WOS:000350259500006.

65. Nerlov C, Graf T. PU.1 induces myeloid lineage commitment in multipotent hematopoietic progenitors. Genes Dev. 1998;12(15):2403-12. doi: 10.1101/gad.12.15.2403. PubMed PMID: 9694804; PMCID: PMC317050.

66. Nakajima H, Cleveland JL, Nagata S, Ihle JN. Granulocyte colony-stimulating factor regulates myeloid differentiation through ccaat enhancer binding protein epsilon. Blood. 1998;92(10):712a-a. PubMed PMID: WOS:000077121302912.

67. Himes SR, Cronau S, Mulford C, Hume DA. The Runx1 transcription factor controls CSF-1-dependent and -independent growth and survival of macrophages. Oncogene. 2005;24(34):5278-86. doi: 10.1038/sj.onc.1208657. PubMed PMID: 16007221.

68. Heinz S, Benner C, Spann N, Bertolino E, Lin YC, Laslo P, Cheng JX, Murre C, Singh H, Glass CK. Simple combinations of lineage-determining transcription factors prime cis-regulatory elements required for macrophage and B cell identities. Mol Cell. 2010;38(4):576-89. doi: 10.1016/j.molcel.2010.05.004. PubMed PMID: 20513432; PMCID: PMC2898526.

69. Whyte WA, Orlando DA, Hnisz D, Abraham BJ, Lin CY, Kagey MH, Rahl PB, Lee TI, Young RA. Master transcription factors and mediator establish super-enhancers at key cell identity genes. Cell. 2013;153(2):307-19. doi: 10.1016/j.cell.2013.03.035. PubMed PMID: 23582322; PMCID: PMC3653129.

70. Hnisz D, Schuijers J, Lin CY, Weintraub AS, Abraham BJ, Lee TI, Bradner JE, Young RA. Convergence of Developmental and Oncogenic Signaling Pathways at Transcriptional Super-Enhancers. Mol Cell. 2015;58(2):362-70. doi: 10.1016/j.molcel.2015.02.014. PubMed PMID: WOS:000353222900016.

71. Abutbul S, Shapiro J, Szaingurten-Solodkin I, Levy N, Carmy Y, Baron R, Jung S, Monsonego A. TGF-beta signaling through SMAD2/3 induces the quiescent microglial phenotype within the CNS environment. Glia. 2012;60(7):1160-71. Epub 20120417. doi: 10.1002/glia.22343. PubMed PMID: 22511296.

72. Buttgereit A, Lelios I, Yu XY, Vrohlings M, Krakoski NR, Gautier EL, Nishinakamura R, Becher B, Greter M. Sall1 is a transcriptional regulator defining

microglia identity and function. Nat Immunol. 2016;17(12):1397-406. doi: 10.1038/ni.3585. PubMed PMID: WOS:000388056400010.

73. Zoller T, Schneider A, Kleimeyer C, Masuda T, Potru PS, Pfeifer D, Blank T, Prinz M, Spittau B. Silencing of TGFbeta signalling in microglia results in impaired homeostasis. Nat Commun. 2018;9(1):4011. Epub 20181001. doi: 10.1038/s41467-018-06224-y. PubMed PMID: 30275444; PMCID: PMC6167353.

74. Van Hove H, Martens L, Scheyltjens I, De Vlaminck K, Pombo Antunes AR, De Prijck S, Vandamme N, De Schepper S, Van Isterdael G, Scott CL, Aerts J, Berx G, Boeckxstaens GE, Vandenbroucke RE, Vereecke L, Moechars D, Guilliams M, Van Ginderachter JA, Saeys Y, Movahedi K. A single-cell atlas of mouse brain macrophages reveals unique transcriptional identities shaped by ontogeny and tissue environment. Nat Neurosci. 2019;22(6):1021-35. Epub 20190506. doi: 10.1038/s41593-019-0393-4. PubMed PMID: 31061494.

75. Deczkowska A, Matcovitch-Natan O, Tsitsou-Kampeli A, Ben-Hamo S, Dvir-Szternfeld R, Spinrad A, Singer O, David E, Winter DR, Smith LK, Kertser A, Baruch K, Rosenzweig N, Terem A, Prinz M, Villeda S, Citri A, Amit I, Schwartz M. Mef2C restrains microglial inflammatory response and is lost in brain ageing in an IFN-I-dependent manner. Nat Commun. 2017;8. doi: ARTN 717 10.1038/s41467-017-00769-0. PubMed PMID: WOS:000411989800001.

76. Abud EM, Ramirez RN, Martinez ES, Healy LM, Nguyen CHH, Newman SA, Yeromin AV, Scarfone VM, Marsh SE, Fimbres C, Caraway CA, Fote GM, Madany AM, Agrawal A, Kayed R, Gylys KH, Cahalan MD, Cummings BJ, Antel JP, Mortazavi A, Carson MJ, Poon WW, Blurton-Jones M. iPSC-Derived Human Microglia-like Cells to Study Neurological Diseases. Neuron. 2017;94(2):278-93 e9. doi: 10.1016/j.neuron.2017.03.042. PubMed PMID: 28426964; PMCID: PMC5482419.

77. Hasselmann J, Coburn MA, England W, Velez DXF, Shabestari SK, Tu CH, McQuade A, Kolahdouzan M, Echeverria K, Claes C, Nakayama T, Azevedo R, Coufal NG, Han CZ, Cummings BJ, Davtyan H, Glass CK, Healy LM, Gandhi SP, Spitale RC, Blurton-Jones M. Development of a Chimeric Model to Study and Manipulate Human Microglia In Vivo. Neuron. 2019;103(6):1016-+. doi: 10.1016/j.neuron.2019.07.002. PubMed PMID: WOS:000487763400011.

78. Shemer A, Grozovski J, Tay TL, Tao J, Volaski A, Suss P, Ardura-Fabregat A, Gross-Vered M, Kim JS, David E, Chappell-Maor L, Thielecke L, Glass CK, Cornils K, Prinz M, Jung S. Engrafted parenchymal brain macrophages differ from microglia in transcriptome, chromatin landscape and response to challenge. Nat Commun.

2018;9(1):5206. Epub 20181206. doi: 10.1038/s41467-018-07548-5. PubMed PMID: 30523248; PMCID: PMC6284018.

79. Bennett FC, Bennett ML, Yaqoob F, Mulinyawe SB, Grant GA, Hayden Gephart M, Plowey ED, Barres BA. A Combination of Ontogeny and CNS Environment Establishes Microglial Identity. Neuron. 2018;98(6):1170-83 e8. Epub 20180531. doi: 10.1016/j.neuron.2018.05.014. PubMed PMID: 29861285; PMCID: PMC6023731.

80. Cronk JC, Filiano AJ, Louveau A, Marin I, Marsh R, Ji E, Goldman DH, Smirnov I, Geraci N, Acton S, Overall CC, Kipnis J. Peripherally derived macrophages can engraft the brain independent of irradiation and maintain an identity distinct from microglia. J Exp Med. 2018;215(6):1627-47. Epub 20180411. doi: 10.1084/jem.20180247. PubMed PMID: 29643186; PMCID: PMC5987928.

81. Koso H, Tsuhako A, Lai CY, Baba Y, Otsu M, Ueno K, Nagasaki M, Suzuki Y, Watanabe S. Conditional rod photoreceptor ablation reveals Sall1 as a microglial marker and regulator of microglial morphology in the retina. Glia. 2016;64(11):2005-24. Epub 20160726. doi: 10.1002/glia.23038. PubMed PMID: 27459098.

82. Jurgens G. Head and tail development of the Drosophila embryo involves spalt, a novel homeotic gene. EMBO J. 1988;7(1):189-96. PubMed PMID: 16453820; PMCID: PMC454247.

83. de Celis JF, Barrio R, Kafatos FC. A gene complex acting downstream of dpp in Drosophila wing morphogenesis. Nature. 1996;381(6581):421-4. doi: 10.1038/381421a0. PubMed PMID: 8632798.

84. Kohlhase J, Wischermann A, Reichenbach H, Froster U, Engel W. Mutations in the SALL1 putative transcription factor gene cause Townes-Brocks syndrome. Nature Genetics. 1998;18(1):81-3. doi: DOI 10.1038/ng0198-81. PubMed PMID: WOS:000071259600028.

85. Blanck C, Kohlhase J, Engels S, Burfeind P, Engel W, Bottani A, Patel MS, Kroes HY, Cobben JM. Three novel SALL1 mutations extend the mutational spectrum in Townes-Brocks syndrome. J Med Genet. 2000;37(4):303-7. doi: 10.1136/jmg.37.4.303. PubMed PMID: 10819639; PMCID: PMC1734570.

86. Bohm J, Munk-Schulenburg S, Felscher S, Kohlhase J. SALL1 mutations in sporadic Townes-Brocks syndrome are of predominantly paternal origin without obvious paternal age effect. Am J Med Genet A. 2006;140(18):1904-8. doi: 10.1002/ajmg.a.31383. PubMed PMID: 16892410.

87. Borozdin W, Steinmann K, Albrecht B, Bottani A, Devriendt K, Leipoldt M, Kohlhase J. Detection of Heterozygous SALL1 Deletions by Quantitative Real Time PCR Proves the Contribution of a SALL1 Dosage Effect in the Pathogenesis of Townes-Brocks Syndrome. Hum Mutat. 2006;27(2). doi: 10.1002/humu.9396. PubMed PMID: WOS:000209426100002.

88. Botzenhart EM, Bartalini G, Blair E, Brady AF, Elmslie F, Chong KL, Christy K, Torres-Martinez W, Danesino C, Deardorff MA, Fryns JP, Marlin S, Garcia-Minaur S, Hellenbroich Y, Hay BN, Penttinen M, Shashi V, Terhal P, Van Maldergem L, Whiteford ML, Zackai E, Kohlhase J. Townes-Brocks syndrome: twenty novel SALL1 mutations in sporadic and familial cases and refinement of the SALL1 hot spot region. Hum Mutat. 2007;28(2):204-5. doi: 10.1002/humu.9476. PubMed PMID: 17221874.

89. Devriendt K, Fryns JP, Lemmens F, Kohlhase J, Liebers M. Somatic mosaicism and variable expression of Townes-Brocks syndrome. Am J Med Genet. 2002;111(2):230-1. doi: 10.1002/ajmg.10485. PubMed PMID: 12210359.

90. Faguer S, Pillet A, Chassaing N, Merhenberger M, Bernadet-Monrozies P, Guitard J, Chauveau D. Nephropathy in Townes-Brocks syndrome (SALL1 mutation): imaging and pathological findings in adulthood. Nephrol Dial Transplant. 2009;24(4):1341-5. Epub 20090209. doi: 10.1093/ndt/gfp014. PubMed PMID: 19204018.

91. Furniss D, Critchley P, Giele H, Wilkie AO. Nonsense-mediated decay and the molecular pathogenesis of mutations in SALL1 and GLI3. Am J Med Genet A. 2007;143A(24):3150-60. doi: 10.1002/ajmg.a.32097. PubMed PMID: 18000979.

92. Kiefer SM, Ohlemiller KK, Yang J, McDill BW, Kohlhase J, Rauchman M. Expression of a truncated Sall1 transcriptional repressor is responsible for Townes-Brocks syndrome birth defects. Hum Mol Genet. 2003;12(17):2221-7. Epub 20030715. doi: 10.1093/hmg/ddg233. PubMed PMID: 12915476.

93. Kohlhase J. SALL1 mutations in Townes-Brocks syndrome and related disorders. Hum Mutat. 2000;16(6):460-6. doi: 10.1002/1098-1004(200012)16:6<460::AID-HUMU2>3.0.CO;2-4. PubMed PMID: 11102974.

94. Kohlhase J, Taschner PE, Burfeind P, Pasche B, Newman B, Blanck C, Breuning MH, ten Kate LP, Maaswinkel-Mooy P, Mitulla B, Seidel J, Kirkpatrick SJ, Pauli RM, Wargowski DS, Devriendt K, Proesmans W, Gabrielli O, Coppa GV, Wesby-van Swaay E, Trembath RC, Schinzel AA, Reardon W, Seemanova E, Engel W. Molecular analysis

of SALL1 mutations in Townes-Brocks syndrome. Am J Hum Genet. 1999;64(2):435-45. doi: 10.1086/302238. PubMed PMID: 9973281; PMCID: PMC1377753.

95. Nishinakamura R, Takasato M. Essential roles of Sall1 in kidney development. Kidney Int. 2005;68(5):1948-50. doi: 10.1111/j.1523-1755.2005.00626.x. PubMed PMID: 16221172.

96. Nishinakamura R, Matsumoto Y, Nakao K, Nakamura K, Sato A, Copeland NG, Gilbert DJ, Jenkins NA, Scully S, Lacey DL, Katsuki M, Asashima M, Yokota T. Murine homolog of SALL1 is essential for ureteric bud invasion in kidney development. Development. 2001;128(16):3105-15. PubMed PMID: 11688560.

97. Nishinakamura R. Kidney development conserved over species: essential roles of Sall1. Semin Cell Dev Biol. 2003;14(4):241-7. doi: 10.1016/s1084-9521(03)00027-2. PubMed PMID: 14627123.

98. Kanda S, Tanigawa S, Ohmori T, Taguchi A, Kudo K, Suzuki Y, Sato Y, Hino S, Sander M, Perantoni AO, Sugano S, Nakao M, Nishinakamura R. Sall1 maintains nephron progenitors and nascent nephrons by acting as both an activator and a repressor. J Am Soc Nephrol. 2014;25(11):2584-95. Epub 20140417. doi: 10.1681/ASN.2013080896. PubMed PMID: 24744442; PMCID: PMC4214521.

99. Ohmori T, Tanigawa S, Kaku Y, Fujimura S, Nishinakamura R. Sall1 in renal stromal progenitors non-cell autonomously restricts the excessive expansion of nephron progenitors. Sci Rep. 2015;5:15676. Epub 20151029. doi: 10.1038/srep15676. PubMed PMID: 26511275; PMCID: PMC4625151.

100. Karantzali E, Lekakis V, Ioannou M, Hadjimichael C, Papamatheakis J, Kretsovali A. Sall1 regulates embryonic stem cell differentiation in association with nanog. J Biol Chem. 2011;286(2):1037-45. Epub 20101109. doi: 10.1074/jbc.M110.170050. PubMed PMID: 21062744; PMCID: PMC3020710.

101. Novo CL, Tang C, Ahmed K, Djuric U, Fussner E, Mullin NP, Morgan NP, Hayre J, Sienerth AR, Elderkin S, Nishinakamura R, Chambers I, Ellis J, Bazett-Jones DP, Rugg-Gunn PJ. The pluripotency factor Nanog regulates pericentromeric heterochromatin organization in mouse embryonic stem cells. Genes Dev. 2016;30(9):1101-15. Epub 20160428. doi: 10.1101/gad.275685.115. PubMed PMID: 27125671; PMCID: PMC4863740.

102. Sanchez J, Talamillo A, Gonzalez M, Sanchez-Pulido L, Jimenez S, Pirone L, Sutherland JD, Barrio R. Drosophila Sal and Salr are transcriptional repressors.

Biochem J. 2011;438:437-45. doi: 10.1042/Bj20110229. PubMed PMID: WOS:000295182100005.

103. Netzer C, Rieger L, Brero A, Zhang CD, Hinzke M, Kohlhase J, Bohlander SK. SALL1, the gene mutated in Townes-Brocks syndrome, encodes a transcriptional repressor which interacts with TRF1/PIN2 and localizes to pericentromeric heterochromatin. Hum Mol Genet. 2001;10(26):3017-24. doi: 10.1093/hmg/10.26.3017. PubMed PMID: 11751684.

104. Lauberth SM, Bilyeu AC, Firulli BA, Kroll KL, Rauchman M. A phosphomimetic mutation in the Sall1 repression motif disrupts recruitment of the nucleosome remodeling and deacetylase complex and repression of Gbx2. J Biol Chem. 2007;282(48):34858-68. Epub 20070925. doi: 10.1074/jbc.M703702200. PubMed PMID: 17895244.

105. Lauberth SM, Rauchman M. A conserved 12-amino acid motif in Sall1 recruits the nucleosome remodeling and deacetylase corepressor complex. J Biol Chem. 2006;281(33):23922-31. Epub 20060517. doi: 10.1074/jbc.M513461200. PubMed PMID: 16707490.

106. Netzer C, Bohlander SK, Hinzke M, Chen Y, Kohlhase J. Defining the heterochromatin localization and repression domains of SALL1. Biochim Biophys Acta. 2006;1762(3):386-91. Epub 20060106. doi: 10.1016/j.bbadis.2005.12.005. PubMed PMID: 16443351.

107. Yamashita K, Sato A, Asashima M, Wang PC, Nishinakamura R. Mouse homolog of SALL1, a causative gene for Townes-Brocks syndrome, binds to A/T-rich sequences in pericentric heterochromatin via its C-terminal zinc finger domains. Genes Cells. 2007;12(2):171-82. doi: 10.1111/j.1365-2443.2007.01042.x. PubMed PMID: 17295837.

108. Kong NR, Bassal MA, Tan HK, Kurland JV, Yong KJ, Young JJ, Yang Y, Li F, Lee JD, Liu Y, Wu CS, Stein A, Luo HR, Silberstein LE, Bulyk ML, Tenen DG, Chai L. Zinc Finger Protein SALL4 Functions through an AT-Rich Motif to Regulate Gene Expression. Cell Rep. 2021;34(1):108574. doi: 10.1016/j.celrep.2020.108574. PubMed PMID: 33406418; PMCID: PMC8197658.

109. Barroso-Gomila O, Trulsson F, Muratore V, Canosa I, Merino-Cacho L, Cortazar AR, Perez C, Azkargorta M, Iloro I, Carracedo A, Aransay AM, Elortza F, Mayor U, Vertegaal ACO, Barrio R, Sutherland JD. Identification of proximal SUMO-dependent interactors using SUMO-ID. Nat Commun. 2021;12(1). doi: ARTN 6671

10.1038/s41467-021-26807-6. PubMed PMID: WOS:000720682300005.

110. Netzer C, Bohlander SK, Rieger L, Muller S, Kohlhase J. Interaction of the developmental regulator SALL1 with UBE2I and SUMO-1. Biochem Bioph Res Co. 2002;296(4):870-6. doi: Pii S0006-291x(02)02003-X
Doi 10.1016/S0006-291x(02)02003-X. PubMed PMID: WOS:000180887000014.

111. Li Q, Barres BA. Microglia and macrophages in brain homeostasis and disease. Nat Rev Immunol. 2018;18(4):225-42. Epub 20171120. doi: 10.1038/nri.2017.125. PubMed PMID: 29151590.

112. Powell CM, Michaelis RC. Townes-Brocks syndrome. J Med Genet. 1999;36(2):89-93. PubMed PMID: 10051003; PMCID: PMC1734298.

113. Yamashita K, Sato A, Asashima M, Wang PC, Nishinakamura R. Mouse homolog of SALL1, a causative gene for Townes-Brocks syndrome, binds to A/T-rich sequences in pericentric heterochromatin via its C-terminal zinc finger domains. Genes to Cells. 2007;12(2):171-82. doi: 10.1111/j.1365-2443.2007.01042.x. PubMed PMID: WOS:000243679900004.

114. Butovsky O, Jedrychowski MP, Moore CS, Cialic R, Lanser AJ, Gabriely G, Koeglsperger T, Dake B, Wu PM, Doykan CE, Fanek Z, Liu LP, Chen ZX, Rothstein JD, Ransohoff RM, Gygi SP, Antel JP, Weiner HL. Identification of a unique TGF-beta-dependent molecular and functional signature in microglia (vol 17, pg 131, 2014). Nature Neuroscience. 2014;17(9):1286-. doi: DOI 10.1038/nn0914-1286d. PubMed PMID: WOS:000341125400027.

115. Svoboda DS, Barrasa MI, Shu J, Rietjens R, Zhang S, Mitalipova M, Berube P, Fu D, Shultz LD, Bell GW, Jaenisch R. Human iPSC-derived microglia assume a primary microglia-like state after transplantation into the neonatal mouse brain. Proc Natl Acad Sci U S A. 2019;116(50):25293-303. Epub 20191126. doi: 10.1073/pnas.1913541116. PubMed PMID: 31772018; PMCID: PMC6911218.

116. Mancuso R, Van Den Daele J, Fattorelli N, Wolfs L, Balusu S, Burton O, Liston A, Sierksma A, Fourne Y, Poovathingal S, Arranz-Mendiguren A, Sala Frigerio C, Claes C, Serneels L, Theys T, Perry VH, Verfaillie C, Fiers M, De Strooper B. Stem-cell-derived human microglia transplanted in mouse brain to study human disease. Nat Neurosci. 2019;22(12):2111-6. Epub 20191028. doi: 10.1038/s41593-019-0525-x. PubMed PMID: 31659342.

117. Parker SC, Stitzel ML, Taylor DL, Orozco JM, Erdos MR, Akiyama JA, van Bueren KL, Chines PS, Narisu N, Program NCS, Black BL, Visel A, Pennacchio LA, Collins FS, National Institutes of Health Intramural Sequencing Center Comparative Sequencing Program A, Authors NCSP. Chromatin stretch enhancer states drive cell-specific gene regulation and harbor human disease risk variants. Proc Natl Acad Sci U S A. 2013;110(44):17921-6. Epub 20131014. doi: 10.1073/pnas.1317023110. PubMed PMID: 24127591; PMCID: PMC3816444.

118. Fang R, Yu M, Li G, Chee S, Liu T, Schmitt AD, Ren B. Mapping of long-range chromatin interactions by proximity ligation-assisted ChIP-seq. Cell Res. 2016;26(12):1345-8. Epub 20161125. doi: 10.1038/cr.2016.137. PubMed PMID: 27886167; PMCID: PMC5143423.

119. Snetkova V, Ypsilanti AR, Akiyama JA, Mannion BJ, Plajzer-Frick I, Novak CS, Harrington AN, Pham QT, Kato M, Zhu Y, Godoy J, Meky E, Hunter RD, Shi M, Kvon EZ, Afzal V, Tran S, Rubenstein JLR, Visel A, Pennacchio LA, Dickel DE. Ultraconserved enhancer function does not require perfect sequence conservation. Nat Genet. 2021;53(4):521-8. Epub 20210329. doi: 10.1038/s41588-021-00812-3. PubMed PMID: 33782603; PMCID: PMC8038972.

120. Sato A, Kishida S, Tanaka T, Kikuchi A, Kodama T, Asashima M, Nishinakamura R. Sall1, a causative gene for Townes-Brocks syndrome, enhances the canonical Wnt signaling by localizing to heterochromatin. Biochem Biophys Res Commun. 2004;319(1):103-13. doi: 10.1016/j.bbrc.2004.04.156. PubMed PMID: 15158448.

121. Sakai M, Troutman TD, Seidman JS, Ouyang Z, Spann NJ, Abe Y, Ego KM, Bruni CM, Deng Z, Schlachetzki JCM, Nott A, Bennett H, Chang J, Vu BT, Pasillas MP, Link VM, Texari L, Heinz S, Thompson BM, McDonald JG, Geissmann F, Glass CK. Liver-Derived Signals Sequentially Reprogram Myeloid Enhancers to Initiate and Maintain Kupffer Cell Identity. Immunity. 2019;51(4):655-70 e8. Epub 20191003. doi: 10.1016/j.immuni.2019.09.002. PubMed PMID: 31587991; PMCID: PMC6800814.

122. Sajti E, Link VM, Ouyang Z, Spann NJ, Westin E, Romanoski CE, Fonseca GJ, Prince LS, Glass CK. Transcriptomic and epigenetic mechanisms underlying myeloid diversity in the lung. Nat Immunol. 2020;21(2):221-31. Epub 20200120. doi: 10.1038/s41590-019-0582-z. PubMed PMID: 31959980; PMCID: PMC7667722.

123. Hohsfield LA, Tsourmas KI, Ghorbanian Y, Syage AR, Kim SJ, Cheng YT, Furman S, Inlay MA, Lane TE, Green KN. MAC2 is a long-lasting marker of peripheral cell infiltrates into the mouse CNS after bone marrow transplantation and coronavirus infection. Glia. 2022. doi: 10.1002/glia.24144. PubMed PMID: WOS:000742110300001.

124. Holtman IR, Skola D, Glass CK. Transcriptional control of microglia phenotypes in health and disease. J Clin Invest. 2017;127(9):3220-9. Epub 20170731. doi: 10.1172/JCI90604. PubMed PMID: 28758903; PMCID: PMC5669536.

125. Novikova G, Kapoor M, Tcw J, Abud EM, Efthymiou AG, Chen SX, Cheng H, Fullard JF, Bendl J, Liu Y, Roussos P, Bjorkegren JL, Liu Y, Poon WW, Hao K, Marcora E, Goate AM. Integration of Alzheimer's disease genetics and myeloid genomics identifies disease risk regulatory elements and genes. Nat Commun. 2021;12(1):1610. Epub 20210312. doi: 10.1038/s41467-021-21823-y. PubMed PMID: 33712570; PMCID: PMC7955030.

126. Spittau B, Dokalis N, Prinz M. The Role of TGFbeta Signaling in Microglia Maturation and Activation. Trends Immunol. 2020;41(9):836-48. Epub 20200730. doi: 10.1016/j.it.2020.07.003. PubMed PMID: 32741652.

127. Schmierer B, Hill CS. TGFbeta-SMAD signal transduction: molecular specificity and functional flexibility. Nat Rev Mol Cell Biol. 2007;8(12):970-82. doi: 10.1038/nrm2297. PubMed PMID: 18000526.

128. Liberati NT, Datto MB, Frederick JP, Shen X, Wong C, Rougier-Chapman EM, Wang XF. Smads bind directly to the Jun family of AP-1 transcription factors. Proc Natl Acad Sci U S A. 1999;96(9):4844-9. doi: 10.1073/pnas.96.9.4844. PubMed PMID: 10220381; PMCID: PMC21779.

129. Wong C, Rougier-Chapman EM, Frederick JP, Datto MB, Liberati NT, Li JM, Wang XF. Smad3-Smad4 and AP-1 complexes synergize in transcriptional activation of the c-Jun promoter by transforming growth factor beta. Mol Cell Biol. 1999;19(3):1821-30. doi: 10.1128/MCB.19.3.1821. PubMed PMID: 10022869; PMCID: PMC83975.

130. Lecuit T, Brook WJ, Ng M, Calleja M, Sun H, Cohen SM. Two distinct mechanisms for long-range patterning by Decapentaplegic in the Drosophila wing. Nature. 1996;381(6581):387-93. doi: 10.1038/381387a0. PubMed PMID: 8632795.

131. Basta JM, Robbins L, Denner DR, Kolar GR, Rauchman M. A Sall1-NuRD interaction regulates multipotent nephron progenitors and is required for loop of Henle formation. Development. 2017;144(17):3080-94. Epub 20170731. doi: 10.1242/dev.148692. PubMed PMID: 28760814; PMCID: PMC5611954.

132. Basta JM, Robbins L, Kiefer SM, Dorsett D, Rauchman M. Sall1 balances self-renewal and differentiation of renal progenitor cells. Development. 2014;141(5):1047-58. doi: 10.1242/dev.095851. PubMed PMID: 24550112; PMCID: PMC3929412.

133. Link VM, Duttke SH, Chun HB, Holtman IR, Westin E, Hoeksema MA, Abe Y, Skola D, Romanoski CE, Tao J, Fonseca GJ, Troutman TD, Spann NJ, Strid T, Sakai M, Yu M, Hu R, Fang R, Metzler D, Ren B, Glass CK. Analysis of Genetically Diverse Macrophages Reveals Local and Domain-wide Mechanisms that Control Transcription Factor Binding and Function. Cell. 2018;173(7):1796-809 e17. Epub 20180517. doi: 10.1016/j.cell.2018.04.018. PubMed PMID: 29779944; PMCID: PMC6003872.

134. Waszak SM, Delaneau O, Gschwind AR, Kilpinen H, Raghav SK, Witwicki RM, Orioli A, Wiederkehr M, Panousis NI, Yurovsky A, Romano-Palumbo L, Planchon A, Bielser D, Padioleau I, Udin G, Thurnheer S, Hacker D, Hernandez N, Reymond A, Deplancke B, Dermitzakis ET. Population Variation and Genetic Control of Modular Chromatin Architecture in Humans. Cell. 2015;162(5):1039-50. Epub 20150820. doi: 10.1016/j.cell.2015.08.001. PubMed PMID: 26300124.

135. Madsen JGS, Madsen MS, Rauch A, Traynor S, Van Hauwaert EL, Haakonsson AK, Javierre BM, Hyldahl M, Fraser P, Mandrup S. Highly interconnected enhancer communities control lineage-determining genes in human mesenchymal stem cells. Nat Genet. 2020;52(11):1227-38. Epub 20201005. doi: 10.1038/s41588-020-0709-z. PubMed PMID: 33020665.

136. Brayer KJ, Kulshreshtha S, Segal DJ. The protein-binding potential of C2H2 zinc finger domains. Cell Biochem Biophys. 2008;51(1):9-19. Epub 20080220. doi: 10.1007/s12013-008-9007-6. PubMed PMID: 18286240.

137. Pantier R, Chhatbar K, Quante T, Skourti-Stathaki K, Cholewa-Waclaw J, Alston G, Alexander-Howden B, Lee HY, Cook AG, Spruijt CG, Vermeulen M, Selfridge J, Bird A. SALL4 controls cell fate in response to DNA base composition. Mol Cell. 2021;81(4):845-58 e8. Epub 20210105. doi: 10.1016/j.molcel.2020.11.046. PubMed PMID: 33406384; PMCID: PMC7895904.

138. Gerbi SA. Bundling up DNA. Elife. 2018;7. Epub 20180517. doi: 10.7554/eLife.37234. PubMed PMID: 29771237; PMCID: PMC5957526.

139. Saksouk N, Simboeck E, Dejardin J. Constitutive heterochromatin formation and transcription in mammals. Epigenetics Chromatin. 2015;8:3. Epub 20150115. doi: 10.1186/1756-8935-8-3. PubMed PMID: 25788984; PMCID: PMC4363358.

140. Askew K, Gomez-Nicola D. A story of birth and death: Insights into the formation and dynamics of the microglial population. Brain Behav Immun. 2018;69:9-17. doi: 10.1016/j.bbi.2017.03.009. PubMed PMID: WOS:000432905200002.

141. Li Q, Peterson KR, Fang X, Stamatoyannopoulos G. Locus control regions. Blood. 2002;100(9):3077-86. doi: 10.1182/blood-2002-04-1104. PubMed PMID: 12384402; PMCID: PMC2811695.

142. Guo Y, Hong W, Wang X, Zhang P, Korner H, Tu J, Wei W. MicroRNAs in Microglia: How do MicroRNAs Affect Activation, Inflammation, Polarization of Microglia and Mediate the Interaction Between Microglia and Glioma? Front Mol Neurosci. 2019;12:125. Epub 20190510. doi: 10.3389/fnmol.2019.00125. PubMed PMID: 31133802; PMCID: PMC6522842.

143. Guil S, Esteller M. Cis-acting noncoding RNAs: friends and foes. Nat Struct Mol Biol. 2012;19(11):1068-75. doi: 10.1038/nsmb.2428. PubMed PMID: 23132386.

144. Chellini L, Frezza V, Paronetto MP. Dissecting the transcriptional regulatory networks of promoter-associated noncoding RNAs in development and cancer. J Exp Clin Cancer Res. 2020;39(1):51. Epub 20200317. doi: 10.1186/s13046-020-01552-8. PubMed PMID: 32183847; PMCID: PMC7079525.

145. Yao RW, Wang Y, Chen LL. Cellular functions of long noncoding RNAs. Nat Cell Biol. 2019;21(5):542-51. Epub 20190502. doi: 10.1038/s41556-019-0311-8. PubMed PMID: 31048766.

146. Uesaka M, Nishimura O, Go Y, Nakashima K, Agata K, Imamura T. Bidirectional promoters are the major source of gene activation-associated non-coding RNAs in mammals. BMC Genomics. 2014;15:35. Epub 20140117. doi: 10.1186/1471-2164-15-35. PubMed PMID: 24438357; PMCID: PMC3898825.

147. Sayers EW, Bolton EE, Brister JR, Canese K, Chan J, Comeau DC, Connor R, Funk K, Kelly C, Kim S, Madej T, Marchler-Bauer A, Lanczycki C, Lathrop S, Lu Z, Thibaud-Nissen F, Murphy T, Phan L, Skripchenko Y, Tse T, Wang J, Williams R, Trawick BW, Pruitt KD, Sherry ST. Database resources of the national center for biotechnology information. Nucleic Acids Res. 2022;50(D1):D20-D6. doi: 10.1093/nar/gkab1112. PubMed PMID: 34850941; PMCID: PMC8728269.

148. Sweetman D, Smith T, Farrell ER, Chantry A, Munsterberg A. The conserved glutamine-rich region of chick csal1 and csal3 mediates protein interactions with other spalt family members - Implications for Townes-Brocks syndrome. Journal of Biological Chemistry. 2003;278(8):6560-6. doi: 10.1074/jbc.M209066200. PubMed PMID: WOS:000181129400133.

149. Yang X, Li C, Herrera PL, Deng CX. Generation of Smad4/Dpc4 conditional knockout mice. Genesis. 2002;32(2):80-1. doi: 10.1002/gene.10029. PubMed PMID: 11857783.

150. Schneider CA, Rasband WS, Eliceiri KW. NIH Image to ImageJ: 25 years of image analysis. Nat Methods. 2012;9(7):671-5. doi: 10.1038/nmeth.2089. PubMed PMID: 22930834; PMCID: PMC5554542.

151. Ma XL, Chen C, Veevers J, Zhou XM, Ross RS, Feng W, Chen J. CRISPR/Cas9-mediated gene manipulation to create single-amino-acid-substituted and floxed mice with a cloning-free method. Sci Rep-Uk. 2017;7. doi: ARTN 42244 10.1038/srep42244. PubMed PMID: WOS:000393576200001.

152. Sheets KG, Jun B, Zhou Y, Zhu M, Petasis NA, Gordon WC, Bazan NG. Microglial ramification and redistribution concomitant with the attenuation of choroidal neovascularization by neuroprotectin D1. Mol Vis. 2013;19:1747-59. Epub 20130804. PubMed PMID: 23922492; PMCID: PMC3733904.

153. Byun J, Verardo MR, Sumengen B, Lewis GP, Manjunath BS, Fisher SK. Automated tool for the detection of cell nuclei in digital microscopic images: application to retinal images. Mol Vis. 2006;12:949-60. Epub 20060816. PubMed PMID: 16943767.

154. Nott A, Schlachetzki JCM, Fixsen BR, Glass CK. Nuclei isolation of multiple brain cell types for omics interrogation. Nat Protoc. 2021;16(3):1629-46. Epub 20210125. doi: 10.1038/s41596-020-00472-3. PubMed PMID: 33495627; PMCID: PMC7969463.

155. Buenrostro JD, Giresi PG, Zaba LC, Chang HY, Greenleaf WJ. Transposition of native chromatin for fast and sensitive epigenomic profiling of open chromatin, DNA-binding proteins and nucleosome position. Nat Methods. 2013;10(12):1213-8. Epub 20131006. doi: 10.1038/nmeth.2688. PubMed PMID: 24097267; PMCID: PMC3959825.

156. Buenrostro JD, Wu B, Chang HY, Greenleaf WJ. ATAC-seq: A Method for Assaying Chromatin Accessibility Genome-Wide. Curr Protoc Mol Biol. 2015;109:21 9 1- 9 9. Epub 20150105. doi: 10.1002/0471142727.mb2129s109. PubMed PMID: 25559105; PMCID: PMC4374986.

157. Heinz S, Benner C, Spann N, Bertolino E, Lin YC, Laslo P, Cheng JX, Murre C, Singh H, Glass CK. Simple Combinations of Lineage-Determining Transcription Factors Prime cis-Regulatory Elements Required for Macrophage and B Cell Identities. Mol Cell. 2010;38(4):576-89. doi: 10.1016/j.molcel.2010.05.004. PubMed PMID: WOS:000278448100012.

158. Heinz S, Texari L, Hayes MGB, Urbanowski M, Chang MW, Givarkes N, Rialdi A, White KM, Albrecht RA, Pache L, Marazzi I, Garcia-Sastre A, Shaw ML, Benner C. Transcription Elongation Can Affect Genome 3D Structure. Cell. 2018;174(6):1522-+. doi: 10.1016/j.cell.2018.07.047. PubMed PMID: WOS:000443841000019.

159. Texari L, Spann NJ, Troutman TD, Sakai M, Seidman JS, Heinz S. An optimized protocol for rapid, sensitive and robust on-bead ChIP-seq from primary cells. STAR Protoc. 2021;2(1):100358. Epub 20210224. doi: 10.1016/j.xpro.2021.100358. PubMed PMID: 33718886; PMCID: PMC7921621.

160. Altschul SF, Gish W, Miller W, Myers EW, Lipman DJ. Basic local alignment search tool. J Mol Biol. 1990;215(3):403-10. doi: 10.1016/S0022-2836(05)80360-2. PubMed PMID: 2231712.

161. Fornes O, Castro-Mondragon JA, Khan A, van der Lee R, Zhang X, Richmond PA, Modi BP, Correard S, Gheorghe M, Baranasic D, Santana-Garcia W, Tan G, Cheneby J, Ballester B, Parcy F, Sandelin A, Lenhard B, Wasserman WW, Mathelier A. JASPAR 2020: update of the open-access database of transcription factor binding profiles. Nucleic Acids Res. 2020;48(D1):D87-D92. doi: 10.1093/nar/gkz1001. PubMed PMID: 31701148; PMCID: PMC7145627.

162. Stormo GD. DNA binding sites: representation and discovery. Bioinformatics. 2000;16(1):16-23. doi: 10.1093/bioinformatics/16.1.16. PubMed PMID: 10812473.

163. Shen Z, Hoeksema MA, Ouyang Z, Benner C, Glass CK. MAGGIE: leveraging genetic variation to identify DNA sequence motifs mediating transcription factor binding and function. Bioinformatics. 2020;36(Suppl_1):i84-i92. doi: 10.1093/bioinformatics/btaa476. PubMed PMID: 32657363; PMCID: PMC7355228.

164. Dobin A, Davis CA, Schlesinger F, Drenkow J, Zaleski C, Jha S, Batut P, Chaisson M, Gingeras TR. STAR: ultrafast universal RNA-seq aligner. Bioinformatics. 2013;29(1):15-21. Epub 20121025. doi: 10.1093/bioinformatics/bts635. PubMed PMID: 23104886; PMCID: PMC3530905.

165. Langmead B, Salzberg SL. Fast gapped-read alignment with Bowtie 2. Nat Methods. 2012;9(4):357-U54. doi: 10.1038/Nmeth.1923. PubMed PMID: WOS:000302218500017.

166. Love MI, Huber W, Anders S. Moderated estimation of fold change and dispersion for RNA-seq data with DESeq2. Genome Biol. 2014;15(12):550. doi: 10.1186/s13059-014-0550-8. PubMed PMID: 25516281; PMCID: PMC4302049.

167. Zhou Y, Zhou B, Pache L, Chang M, Khodabakhshi AH, Tanaseichuk O, Benner C, Chanda SK. Metascape provides a biologist-oriented resource for the analysis of systems-level datasets. Nat Commun. 2019;10(1):1523. Epub 20190403. doi: 10.1038/s41467-019-09234-6. PubMed PMID: 30944313; PMCID: PMC6447622.

168. Durand NC, Shamim MS, Machol I, Rao SSP, Huntley MH, Lander ES, Aiden EL. Juicer Provides a One-Click System for Analyzing Loop-Resolution Hi-C Experiments. Cell Syst. 2016;3(1):95-8. doi: 10.1016/j.cels.2016.07.002. PubMed PMID: WOS:000395772700014.

169. Durand NC, Robinson JT, Shamim MS, Machol I, Mesirov JP, Lander ES, Aiden EL. Juicebox Provides a Visualization System for Hi-C Contact Maps with Unlimited Zoom. Cell Syst. 2016;3(1):99-101. doi: 10.1016/j.cels.2015.07.012. PubMed PMID: WOS:000395772700015.

170. Lin YC, Benner C, Mansson R, Heinz S, Miyazaki K, Miyazaki M, Chandra V, Bossen C, Glass CK, Murre C. Global changes in the nuclear positioning of genes and intra- and interdomain genomic interactions that orchestrate B cell fate. Nat Immunol. 2012;13(12):1196-204. Epub 20121014. doi: 10.1038/ni.2432. PubMed PMID: 23064439; PMCID: PMC3501570.

171. Kent WJ, Sugnet CW, Furey TS, Roskin KM, Pringle TH, Zahler AM, Haussler D. The human genome browser at UCSC. Genome Res. 2002;12(6):996-1006. doi: 10.1101/gr.229102. PubMed PMID: WOS:000176433700017.

172. Li QH, Brown JB, Huang HY, Bickel PJ. Measuring Reproducibility of High-Throughput Experiments. Ann Appl Stat. 2011;5(3):1752-79. doi: 10.1214/11-Aoas466. PubMed PMID: WOS:000300382500003.

173. Juric I, Yu M, Abnousi A, Raviram R, Fang RX, Zhao Y, Zhang YX, Qiu YJ, Yang YC, Li Y, Ren B, Hu M. MAPS: Model-based analysis of long-range chromatin interactions from PLAC-seq and HiChIP experiments. Plos Comput Biol. 2019;15(4). doi: ARTN e1006982
10.1371/journal.pcbi.1006982. PubMed PMID: WOS:000467530600076.